2003 Fuel Cell Seminar

Special Session on Fuel Cell Power Conditioning
and International Future Energy Challenge

Proceedings

November 3, 2003
Miami, Florida

Sponsored by

U. S. DOE Office of Fossil Energy
U. S. DOE National Energy Technology Laboratory

Technical Co-Sponsored by

IEEE Power Electronics Society
IEEE Industry Applications Society

Forward

This first Special Session on Fuel Cell Power Conditioning and International Future Energy Challenge (IFEC) is organized in conjunction with the 2003 Fuel Cell Seminar. Dr. Samuel Biondo of the U.S. Department of Energy (DOE) Office of Fossil Energy started the idea of having the 2003 International Future Energy Challenge (IFEC) teams present their designs for the 5-kW solid oxide fuel cell power conditioning system. Dr. Mark Williams of DOE National Technology Laboratory (NETL) supported the idea and helped set up the Special Session within 2003 Fuel Cell Seminar program. With additional technical co-sponsorship from two Institute of Electrical and Electronics Engineering (IEEE) societies – Power Electronics and Industry Applications Societies, the Special Session was also able to include regular submissions to the 2003 Fuel Cell Seminar. Submissions from six out of twelve participating teams in the 2003 IFEC and one regular submission were selected by the organizing committee for presentation in this Special Session.

The Special Session not only provides the opportunity for the power electronics engineers to present their design ideas but also allows the interaction between them and fuel cell system developers. In these proceedings, it can be seen that there are many different designs for one common specification. The design variations are found in system architecture, dc/dc circuit topology, dc/ac circuit topology, and energy management. It should be pointed out that the work were predominately done by students with significant involvement from undergraduate students. Given limited time and resources, how the university students implement their ideas for a low-cost high efficiency inverter for fuel cell applications is quite interesting. Through their presentations in this Special Session, it is apparent that the design of fuel cell power conditioning systems is nontrivial, and the system aspects, especially fuel cell dynamics and the associated auxiliary energy management need to be considered as a whole. The organizing committee would like to see, through this Special Session, that the entire fuel cell system development takes the power conditioning system into account at an early stage to achieve the cost-effective design not only for the individual components, but also for the entire system.

Special Session Chair
Prasad Enjeti
Texas A&M University

Special Session Co-Chair
Jason Lai
Virginia Tech

2003 Fuel Cell Seminar Special Session on
Fuel Cell Power Conditioning and International Future Energy Challenge
Eden Roc Hotel, Miami Beach, Florida

Sponsors:	U.S. DOE Office of Fossil Energy U.S. DOE National Energy Technology Laboratory Fuel Cells Program
Technical Cosponsors:	IEEE Power Electronics Society IEEE Industry Application Society
Session Chairs:	Prasad Enjeti, Texas A&M University Jason Lai, Virginia Tech
Date:	Monday, November 3
Time:	1:00 -5:00 pm
Location:	Eden Roc Hotel, Palladium Room
On-site Coordinator:	Ronald H. Wolk, Wolk Integrated Technical Services

1:00 – 1:15pm	Registration and sign up
1:15 – 3:00pm	
1. Jin Wang, Fang Z. Peng, Joel Anderson, Alan Joseph and Ryan Buffenbarger, Michigan State University	A New Low Cost Inverter System for 5 kW Fuel Cell, pp. 1-7.
2. Chris Smith, Mike Gilliom, Damian Urciuoli, Andy McLandrich, Elton Pepa, and Jih-Sheng Lai, Virginia Tech	Low-Cost Solid Oxide Fuel Cell Power Conditioning with Bidirectional Charging, pp. 8-15.
3. Gang Wang, Pradeep Pant, Hasan Mohammad, Parviz Famouri* and Osman Demirci, West Virginia University	High Efficiency Low Cost Inverter System for Fuel Cell Application, pp. 16-20.
4. Y. R. Novaes, I. Barbi, Federal University of Santa Catarina – UFSC, Brazil	Low Frequency Ripple Current Elimination in Fuel Cell Systems, pp. 21-26.
3:00 – 3:30pm	Break
3:30 – 4:45pm	
5. Maja Harfman Todorovic, Leonardo Palma, Woojin Choi, Cody Dowling, Daniel Humphrey, David Tarbell, Prasad Enjeti, Jo Howze, Texas A&M University	Development of a Low Cost Fuel Cell Inverter System with DSP Control for Residential Use, pp. 27-32.
6. Jinhee Lee, Jinsang Jo, Sewan Choi, Soobin Han, Seoul National University of Technology	A 10kW SOFC-Low Voltage Battery Hybrid Power Processing Unit for Residential Use, pp. 33-40.
7. Ted P. Bohn and Robert D. Lorenz, University of Wisconsin	A Low-Cost Inverter for Domestic Fuel Cell Applications, pp. 41-48.

TABLE OF CONTENTS

A New Low Cost Inverter System for 5 kW Fuel Cell

Jin Wang, Fang Z. Peng, Joel Anderson, Alan Joseph and Ryan Buffenbarger
Department of Electrical and Computer Engineering
Michigan State University
2120 Engineering Building, East Lansing, MI 48824

***Abstract* – The high installation cost is the major obstacle of the commercialization of the Solid Oxide Fuel Cell (SOFC) for distributed power generation. This paper presents a new low cost 10 kW inverter system to overcome this obstacle. The proposed system consists of an isolated dc-dc converter to boost the fuel cell voltage to 400 V dc and a PWM inverter with filter to convert the dc voltage to two split-phase 120 V ac. The dc-dc converter uses phase shifting to control power flow through a transformer with a MOSFET full bridge on the low voltage side and a voltage doubler on the high voltage side. One IPM is used to realize the voltage doubler and the dc-ac inverter. Compared to the existing fuel cell inverter systems, the proposed circuit has low cost, less component count, smaller size, and reduced dc-dc converter peak current. Simulation and experimental results are demonstrated.**

***Index terms* –Solid Oxide Fuel Cell, dc-dc converter, two split-phase, voltage douler, IPM**

I. INTRODUCTION

The interest in distributed generation has increased significantly in recent years. It is believed that the distributed generation market will be between US$10 and 30 billion by the year 2010 [2]. Due to environmental concerns, more effort is now being put into the clean distributed power like geothermal, solar thermal, photovoltaic, and wind generation, as well as fuel cells that use hydrogen, propane, natural gas, or other fuels to generate electricity without increasing pollution [1-3].

There are five major types of the fuel cells in current technology. Among these five, Alkaline Fuel Cells (AFC) have been used in the NASA space program since 1960s. Polymer Electrolyte Membrane (PEM) fuel cells have very fast slew rates and low operating temperatures and are being used in electric vehicles. Phosphoric Acid Fuel Cells (PAFC) are very tolerant to impurities in the fuel steam and by far are the most mature in terms of system development and commercialization. Over 200 stationary units with typical capacity of 200 kW have been installed in the United States. Molten Carbonate Fuel Cells (MCFC) and Solid Oxide Fuel Cells (SOFC) both operate at high temperature 600-1,000°C, and are targeted at medium- and large-scale stationary power generation. In SOFC, other than some precious material, a solid ceramic material is used for the electrolyte, and viable fuels can be used without a separate reformer. The byproduct: hot water and heat can be used for heating. Much research has been done towards the residential application of SOFC. One of the major obstacles of its commercialization is the high cost of installation. In recent years, the production costs of fuel cells keep decreasing [2]. Reducing the price of the inverter of the fuel cell system to under $500 for a 10 kW system and at the same time achieving maximum power efficiency and quality now become more important and urgent [4].

This paper focuses on the development of a new low-cost inverter system that supports the commercialization of a 5 kW solid-oxide fuel cell (SOFC) power generation system to provide non-utility and ultra-clean residential electricity. The aimed fuel cell outputs 22 V to 41 V dc. For residential applications, the needed output is two split-phase 60 Hz, 120 V ac, the 5 kW SOFC is supplemented with a 5 kW battery pack to meet peak power-demand of 10 kW. The general inverter system configuration is shown in Fig. 1. The dc voltage from the fuel cell is first boost up to 350-450 V by a dc-dc converter then a dc-ac inverter with output filter is cascade-connected to produce ac voltage. The battery can be added to either the low voltage side or the high voltage side according to different topologies [4-8].

The dc-dc converter proposed in this paper uses phase shifting to control power flow through a transformer with a full bridge on the low voltage side and a controlled voltage doubler on the high voltage side. The transformer provides voltage isolation between the fuel cell and the ac output voltage improving overall safety of the system. A voltage doubler on the high voltage side decreases the turns ratio of the transformer, which reduces leakage inductance and makes the system more efficient and easier to control. And at the same time, the voltage and current stresses on the low voltage side are also minimized. A high voltage battery pack is added after the voltage doubler as transient power for load dynamics. Thus the capacitance of the high voltage side capacitors are minimized, which will significantly reduce the total cost of the system.

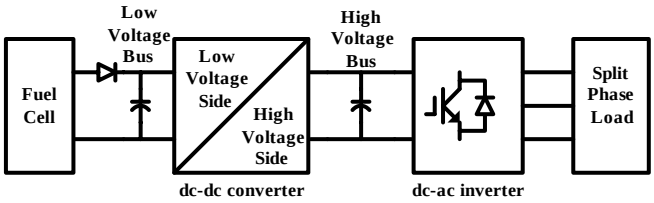

Fig. 1. Block diagram of the fuel cell inverter system

The dc-ac PWM inverter is constructed with a three phase IPM, in which one phase leg has dual function: voltage doubler and the neutral phase leg of the dc-ac inverter. Since the neutral phase leg switches at a high frequency, the equivalent switching frequency of the inverter may be increased by proper optimization and synchronization [4], [5]. Thus the size of the output filter can be greatly decreased and the cost of the inverter system can be further reduced.

II. TOPOLOGY ANALYSIS

Fig. 2 shows the proposed fuel cell inverter systems, which consists of an isolated dc-dc converter and a PWM inverter.

A. Dc-dc Converter

For isolation and high boost ratio, forward, push-pull, half bridge and full bridge can be considered as topology candidates [4-10]. The advantages and disadvantages of these topologies are fully discussed in [4], [5]. In general, forward and pull-push converter are not suitable for high power applications. Forward converters have restrained duty cycles and lossy resetting of excitation; in pull-push converters, the two halves of a center-tapped winding cannot be equal or symmetrically wound, and the power switch on/off times as well as their forward voltage drops are never equal. These irregularities, which exist in practice, can contribute to transformer core saturation and result in the converter failure [4]. In both forward and pull-push converters, the voltage rating of the device is two times that of the half and full bridge. Full bridge, which is used in this paper, compared to half bridge, though has more components, the current in device and transformer turns ratio can both be reduced to half. The voltage and current stresses of the devices in the full bridge are the smallest in all of the four topologies.

There are also several topology options for the high voltage side of the dc-dc converter like diode rectifier, controlled rectifier, voltage doubler and controlled voltage doubler. All these four topologies have the same device voltage rating. For the high voltage side, the current stress is much smaller than the low voltage side, so the major concerns for the topology selection should be:

1) The transformer turns ratio;
2) The control flexibility;
3) The current waveform of the low voltage side, and;
4) Coordination with the dc-ac inverter.

Voltage doubler circuits will give smaller transformer turns ratio. By using the active switches, there will be more flexibility in controlling the power flow and will create more possibility in control the current waveforms of the low voltage side, thus the current stress will be further depressed. So the controlled voltage doubler circuit is used in the proposed circuit.

B. PWM Inverter

For the two split-phase 120 V ac output inverter, there are two main topologies as shown in Fig. 3 [4-10]. For the four switch inverter as shown in Fig. 3(a), the neutral point is tapped from the center of the two capacitors. For the six switch inverter shown in Fig. 3(b), the neutral point is connected to the third phase leg. The two phase legs in four switch inverter are controlled by SPWM. The two sinusoidal control references have a 180° phase difference and the same amplitude. Two of the phase legs in the six switch inverter have the exact same control of the four switch inverter. The third phase leg in the six switch inverter usually is controlled to produce a square waveform to serve as the neutral phase and at same time achieve the maximum utilization of the DC bus voltage. The switching frequency of the third leg can be different from the other two phase legs. The comparison of the four switch and six switch inverters is shown in TABLE I. The six switch inverter is used in the proposed inverter system.

C. The Unique Phase Leg

One of the unique features of the topology proposed in this paper is that the voltage doubler phase leg and the neutral phase leg in the PWM inverter are actually combined together. In this way, by using just one phase leg, the voltage doubler function and all the advantages of the six switch inverters are achieved at the same time. Further more, in real circuit design, the voltage doubler and the

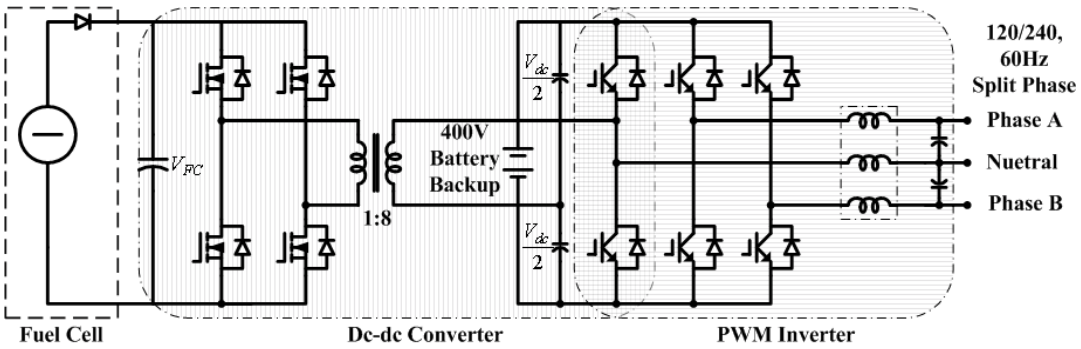

Fig. 2. Proposed fuel cell inverter system

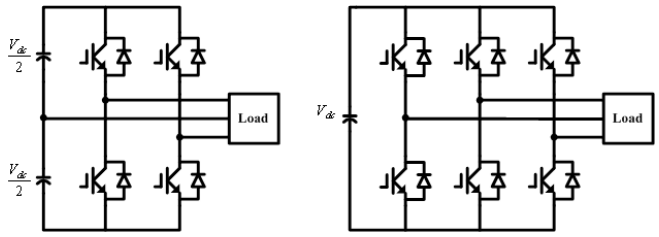

(a) Four switch inverter (b) Six switch inverter

Fig. 3. Split phase inverters

TABLE I
COMPARISON OF THE INVERTERS

	Four switch Inverter	Six switch Inverter
Switch Voltage/Current Rating	Same	
DC-link voltage balance	Active charge or discharge are needed in case of unbalanced load	No need to balance the capacitor voltage.
DC-link current ripple	Higher ripple amplitude. The lowest frequency component is 60 Hz.	Lower ripple amplitude. The lowest frequency component is 120 Hz.
Output filter size	Relatively larger	Relatively smaller

inverter can be realized by using just one IPM as shown in Fig. 2. A good coordination is achieved.

D. The Battery Pack

The battery pack supplies transient power up to 5 kW. It plays a key role in deciding the topology of the system.

There are several ways to connect the battery to the system [4-8]. Among those, two ways are most commonly used: 1) connect a 48 V battery to the low voltage side of dc-dc converter and 2) connect a 400 V battery pack to the high voltage side. The differences between these two are:

Case 1: 48 V battery at the low voltage side of dc-dc converter.

1) The fuel cell voltage changes from 22 V to 41 V, and the battery voltage usually changes from –20 % to 10 %, which is from 38.4 to 52.5 V, so boost function must be realized in the low voltage side. Because the isolation is desired in the dc-dc converter and high frequency transformers are often used in the design [4-10], the low voltage side of the dc-dc has two functions: to boost voltage and to invert the voltage from dc to high frequency ac;
2) The fuel cell and battery are both on the low voltage side, so the dc-dc converter must have 10 kW capacity;
3) To ensure safe operation, additional circuitry is needed to connect the low voltage battery.

Case 2: 400 V battery connected at the high voltage side of dc-dc converter.

1) The dc-dc converter only needs to handle 5 kW of power and the function of the low voltage side can be simplified;
2) The battery can be directly connected to the high voltage dc bus;
3) The capacitance of the high voltage dc-link capacitors can be greatly reduced;
4) A 400 V battery pack is often formed by connecting over thirty 12 V batteries in series and is believed to be expensive and easy to have voltage unbalance between the cells [4-5].

From the analysis above, it can be seen that different battery connections directly decides the function and power capacity of the dc-dc converter. In this paper, the high voltage side 400 V battery is adopted for the sake of low cost, simplicity and stability of the dc-dc converter.

The proposed topology of the inverter system as shown in Fig. 2, only has six main devices: 4 MOSFET for the low voltage side, one high frequency transformer and one IPM for high voltage side. It is low cost, reliable and easy to build, operate and control.

III. OPERATING PRINCIPLE AND CONTROL STRATEGY

A. Operating Principle Of Dc-dc Converter

The transformer primary side (low voltage side) referred equivalent circuit of the inverter system is shown in Fig. 4. In Fig. 4, Ls is the leakage inductance of the transformer. The full bridge and voltage doubler are controlled to switch at 20 kHz to produce two square waveforms with a phase shift, δ, as shown in Fig. 5. The two square-wave voltages impress across the both side of the transformer, respectively. So the current over the leakage inductance would look like the i_s as shown in the Fig. 5. As i_s can be seen as a function of ωt, where ω is the switching frequency, the current waveform can be analyzed as following:

At point 1 in Fig. 5, the low side voltage becomes positive while the high side voltage remains negative, creating a positive voltage across the leakage inductance making the current increase until point 2, where $\omega t = \delta$. The current at point 2 can be written as

$$i_s(\delta) = \frac{V_L + V_H}{\omega Ls}\delta + i_s(0),\ \omega t = \delta \qquad (1)$$

where V_L and V_H are the amplitudes of the transformer low side and high side voltage.

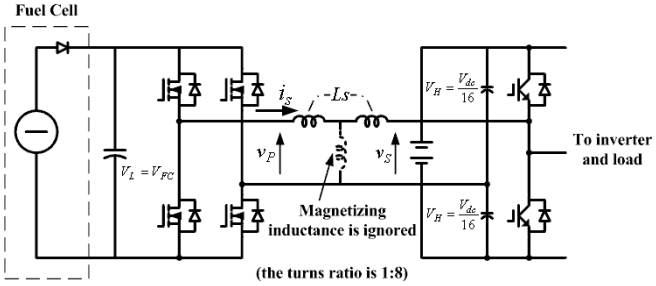

Fig. 4. Primary referred equivalent circuit of the dc-dc converter

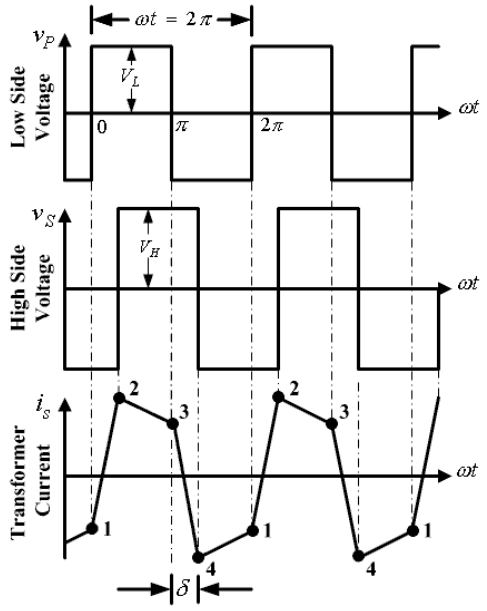

Fig. 5. Idealized voltage and current waveform of transformer

By proper control, V_L can be smaller, bigger or equal to V_H. The peak current will be minimized when $V_L = V_H$ is met. Fig. 5 shows the case of $V_L < V_H$. At point 2, the high side voltage becomes positive while the low side voltage remains positive, making the voltage across the leakage inductance negative allowing the current to decay to point 3, where $\omega t = \pi$,

$$i_s(\pi) = \frac{V_L - V_H}{\omega Ls}(\pi - \delta) + i_s(\delta),\ \omega t = \pi. \quad (2)$$

At point 3, the low side voltage becomes negative while the high side voltage remains positive, creating a negative voltage across the leakage inductance making the current decrease until point 4, where $\omega t = \pi + \delta$

$$i_s(\pi + \delta) = -\frac{V_L + V_H}{\omega Ls}(\pi - \delta) + i_s(\pi),\ \omega t = \pi + \delta. \quad (3)$$

Point 4 occurs when the low side voltage becomes negative while the high side voltage remains negative, making the voltage across the leakage inductance positive allowing the current to increase to point 1,

$$i_s(2\pi) = -\frac{V_L - V_H}{\omega Ls}(\pi - \delta) + i_s(\pi + \delta),\ \omega t = 2\pi. \quad (4)$$

Because $i_s(\delta) = -i_s(\pi + \delta)$ and $i_s(\pi) = -i_s(2\pi)$, the exact relationship between the current and voltages can be found as (5) and (6) by solving (1)-(4)

$$i_s(\delta) = \frac{2V_L\delta + (V_H - V_L)\pi}{2\omega Ls} \quad (5)$$

$$i_s(\pi) = \frac{2V_H\delta + (V_L - V_H)\pi}{2\omega Ls}. \quad (6)$$

From the representation of $i_s(\omega t)$, the power transferred through the transformer can be found as:

$$P = \frac{V_H V_L \delta(\pi - \delta)}{\omega Ls\pi}. \quad (7)$$

Three conclusions can be made based on the Fig. 5 and equations obtained above:

1) The power is transferred through the leakage inductance;
2) By controlling the phase shift of the voltages between the two sides of the transformer, the power transferred over the transformer as well as the high side dc voltage, V_{dc}, can be precisely controlled;
3) If the system is controlled to have $V_L \approx V_H$, the current wave form would be rather flat, which means the peak current can be smaller.

B. The Control Strategy

The system control diagram is shown in Fig. 6. For the dc-dc converter, the high dc link voltage (same as battery voltage), load phase voltage/current, together with the fuel cell voltage/current are used to calculate the output power and the phase shift angle, δ, and at the same time decide the charge and discharge of the battery. For the inverter part, the close loop voltage control is implemented to keep the amplitude and power quality of the output voltage.

IV. DESIGN GUIDE AND PROTOTYPE

A. Transformer

The transformer has three functions in the proposed converter: (1) It isolates the low voltage side and high voltage side, (2) it boosts voltage, and (3) the leakage inductance of the transformer is used as an energy storage and transfer element [7].

1. Turns ratio:

The fuel cell voltage changes according to load current as shown in Fig. 7. At full load, the fuel cell outputs its lowest voltage, thus at that time, the low voltage side devices will have the maximum current stress. According to this, the turns ratio of the transformer should be designed to satisfy the following criteria:

1) at the lowest fuel cell voltage, with very small phase shifting, the high voltage side dc voltage V_{dc} should be at least 350 V, because the operating voltage range is 350-450 V;

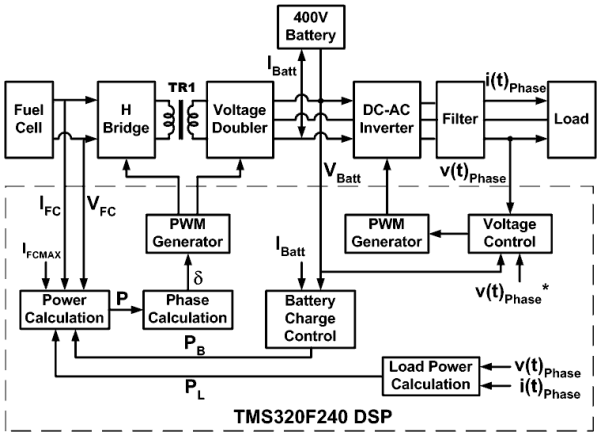

Fig. 6. Control block diagram

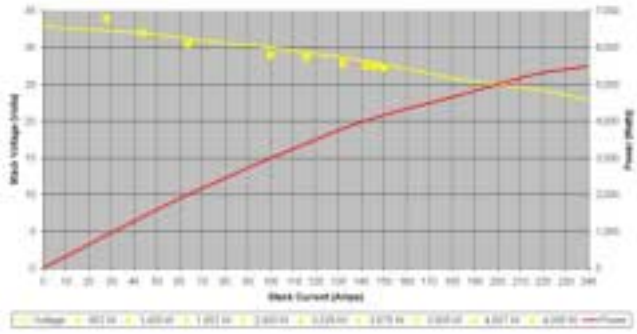

Fig. 7. The relationship between fuel cell voltage, current and power

2) as the high voltage side voltage is controlled to charge or discharge the battery according load demand and battery voltage, the voltage value can be anything between 350-450 V. When referred to the transformer primary side, the voltage of both sides of the transformer should be kept as close as possible to make the shape of the current waveform at full load flat and have the smallest peak.

Since the fuel cell voltage changes from 22 V to 41 V, the turns ratio of the transformer in the prototype is chosen 1:8.

2. Leakage inductance:

From (7), it can be seen that the smaller the leakage inductance, the higher the power that can be transferred through the transformer. So in the design, the leakage inductance should be kept as small as possible. Fig. 8 shows the power curves at $Ls = 0.5\ \mu H$ and $V_{dc} = 400$ V as the fuel cell voltage changes from 22 V to 41 V. The curves can be concluded as following:

1) when the phase shifting changes from 0 to $\pi/2$, the power that can be transferred peaks;
2) the higher the fuel cell voltage, the larger the power that can be transferred;
3) when $Ls = 0.5\ \mu H$, very small phase shifting is needed for 5 kW at all fuel cell voltages.

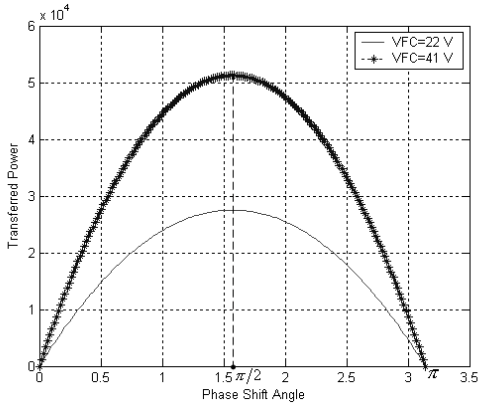

Fig. 8. The output power vs. phase shift angle when leakage inductance is 0.5 μH at different fuel cell voltage

In the prototype, a 5 kW high frequency transformer is made with ferrite cores, copper sheets and magnet wires. The primary winding has two turns and is made of copper sheets; the secondary winding has 16 turns and is made of 4 parallel 16 AWG magnet wires.

B. Power Devices

From Fig. 5 and the analysis above, it can be concluded that at full load, the peak current occurs at point 2. So for the low voltage side, the peak current goes through the switch is

$$I_{peak} = \frac{2V_L\delta + (V_H - V_L)\pi}{2\omega Ls}. \quad (8)$$

The peak voltage on the same switch is the fuel cell voltage,

$$V_{peak} = V_{FC}. \quad (9)$$

At the high voltage side, the peak voltage for all the switches is the dc link voltage V_{dc}. The peak current of the voltage doubler is eight times smaller than the low voltage side; the peak currents in the other two phase legs of the inverter are decided by the load.

For the low voltage side, MOSFETs are used. The major concern is the on resistance. In the prototype, ten MOSFETs are paralleled per switch. The rated voltage is 75 V and the rated current is 75 A. The equivalent on resistance per switch is 0.8 $m\Omega$. For the high voltage side, a six pack 600 V/200 A IPM is used. The saturation voltage of the IGBT is 2.8 V.

C. Efficiency Analysis

The power loss of the low voltage side mainly comes from the power loss on the MOSFETs. At 5 kW load, the turn on loss of the low voltage side switches is calculated as following:

$$P_{ll} = 2 \times I_l^2 R_{on} \approx 2 \times 230^2 \times 0.001 = 105.8 \text{ W}, \quad (10)$$

where P_{ll} is the power loss, I_l is the R.M.S current goes through the switch, which is around 230 A at 5 kW, and R_{on} is the on resistance of the switch.

At the high voltage side, at 5 kW, the R.M.S value of the current that goes through the voltage doubler switch is around 25 A. The current going through the other two phase legs at balanced load is around 21 A.

So the main power loss on the IGBTs at 5 kW balanced load can be approximately calculated as following:

$$P_{lh} = 2 \times I_i V_{sat} + I_d V_{sat} = 2 \times 21 \times 2.8 + 25 \times 2.8 \approx 188 \text{ W}, \quad (11)$$

where P_{lh} stands for the power loss in the high voltage side switches, I_i is the R.M.S of inverter current, I_d is the R.M.S of the voltage doubler current, and V_{sat} is the IGBT saturation voltage.

Considering the switching loss, capacitor loss, and transformer efficiency, the estimated overall efficiency of the system is around 92 % at 5 kW.

V. SIMULATION AND EXPERIMENTAL RESULTS

Simulation of the proposed system has been carried out with Saber. The prototype is fully built and tested. The picture of the prototype is shown in Fig. 9. In simulation and experiments, a resistive load is used, the dc-dc converter is operating at 20 kHz, and the two phase legs in the inverter are operating at 10 kHz. The dc-dc converter simulation and experimental results are shown in Fig. 10 and Fig. 11. The ac-dc simulation and experimental results are shown in Fig. 12. Simulation and experimental results both verified the system operation principle.

In Fig. 10 and Fig. 11, the phase shifting of the voltages over the transformer is clearly shown; the low voltage side voltage is smaller than the primary referred high voltage side voltage, it verifies that V_{dc} can be fully controlled by doing the phase shifting; the transformer current is quite flat. In the experiments, there is some voltage oscillation on the low voltage side. This is due to the leakage inductance of the low voltage bus bar.

In the simulation and experimental results of the dc-ac inverter as shown in Fig. 12, two split-phase 60 Hz, 120 V outputs are realized and the voltage waveforms are quite sinusoidal.

VI. CONCLUSION

A new low cost fuel cell inverter system for residential application has been presented in this paper. The operation, analysis, features, and design considerations were illustrated. Simulation and experimental results for the 5 kW prototype are shown to verify the operation and control principle.

It is shown that the peak current of the dc-dc converter is controlled. Thanks to the dual function (voltage doubler and neutral phase leg) provided by one phase leg of the IPM, the size of the converter and number of the circuit components are minimal.

As a result, the advantages of the new circuit including decreased voltage/current stress and device count, high efficiency, more reliability, and simplified control as well as low cost, make the proposed inverter system very promising for fuel cell residential power generation.

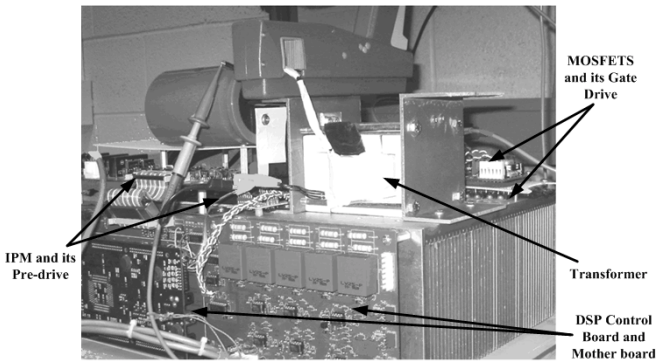

Fig. 9. The prototype during the test

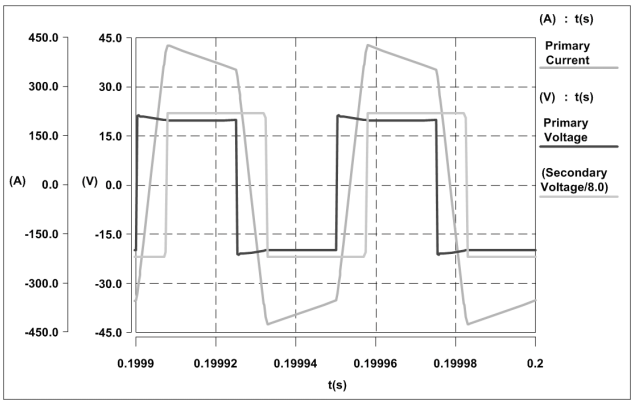

(a) The simulation results of the dc-dc converter

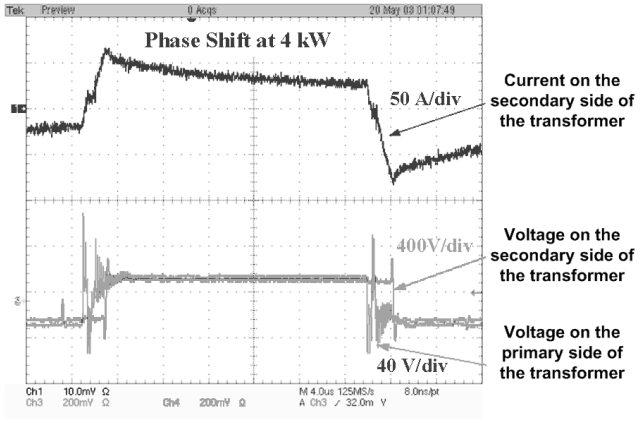

(b) The experimental result of the dc-dc converter

Fig. 10. The simulation and experimental result of the dc-dc converter

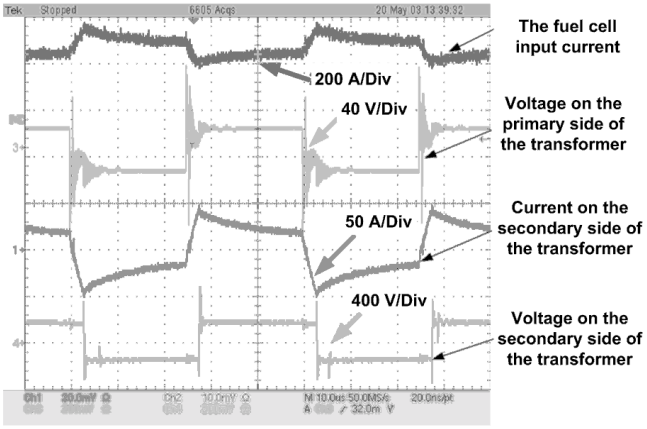

Fig. 11. The experimental verification at 5 kW

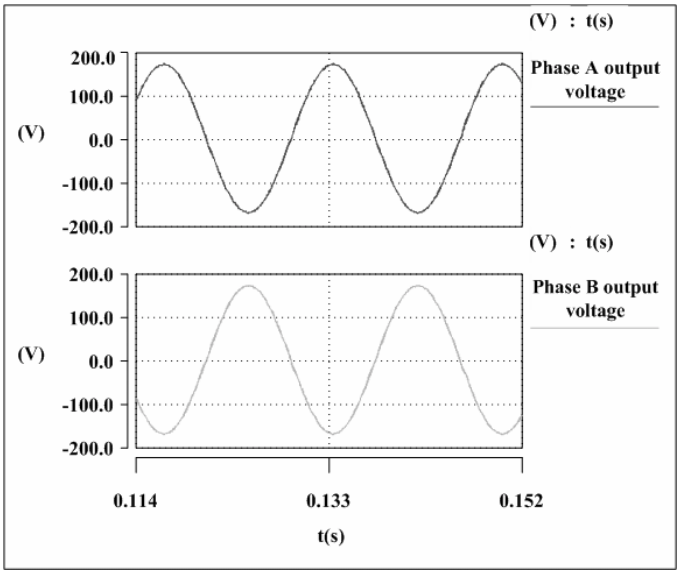

(a) simulation result of the inverter

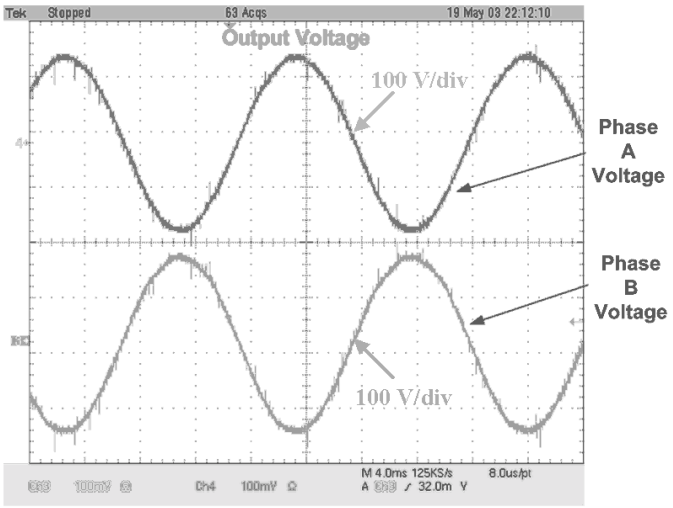

(b) experimental result of the inverter

Fig. 12. The simulation and experimental result of the inverter

Reference

[1] R. C. Dugan, T. E. McDermott, "Distributed generation," *Industry Applications Magazine, IEEE, Volume: 8 Issue: 2, March-April 2002,* pp. 19 –25.

[2] H. B. Puttgen, P. R. MacGrego, F. C. Lambert, "Distributed generation: semantic hype or the dawn of a new era," *Power and Energy Magazine, IEEE , Volume: 1 Issue: 1 , Jan.*-Feb. 2003, pp. 22 –29.

[3] G. J. Miranda, "Be prepared! [power industry deregulation]," *Industry Applications Magazine, IEEE , Volume: 9 Issue: 2 , March-April 2003*, pp. 12 –20.

[4] Fuel Cell Handbook (Sixth Edition) DOE/NETL, 2002

[5] T. A. Nergaard, J. F. Ferrell, L. G. Leslie, Jih-Sheng Lai, "Design considerations for a 48 V fuel cell to split single phase inverter system with ultracapacitor energy storage," *in Conf. Rec. Power Electronics Specialists Conference, 2002. pesc 02. 2002 IEEE 33rd Annual , Volume: 4 , 23-27 June 2002* pp. 2007 –2012

[6] R. Gopinath, et al, "Development of a low cost fuel cell inverter system with DSP control," *in Conf. Rec. Power Electronics Specialists Conference, 2002. pesc 02. 2002 IEEE 33rd Annual , Volume: 1 , 23-27 June 2002* pp. 309 -314 vol.1

[7] Hui Li, Fang Zheng Peng, J. S. Lawler, "A natural ZVS medium-power bidirectional DC-DC converter with minimum number of devices" *IEEE Trans. Industry Applications*, Volume: 39 Issue: 2, pp. 525-535 March-April 2003

[8] A. M. Tuckey, J. N. Krase, "A low-cost inverter for domestic fuel cell applications," *in Conf. Rec. Power Electronics Specialists Conference, 2002. pesc 02. 2002 IEEE 33rd Annual , Volume: 1 , 23-27 June 2002* pp. 339 -346 vol.1

[9] G. K. Anderson, C. Klumpner, S. B. Kjaer, F. Blaabjerg, "A new green power inverter for fuel cells," *in Conf. Rec. Power Electronics Specialists Conference, 2002. pesc 02. 2002 IEEE 33rd Annual , Volume: 1 , 23-27 June 2002* pp. 727 -733 vol.2

[10] Mazumdar, et al, "High frequency low cost DC-AC inverter design with fuel cell source for home applications," *in Conf. Rec. Industry Applications Conference, 2002. 37th IAS Annual Meeting. Conference Record of the, Volume: 2, 13-18 Oct. 2002*, pp. 789 -794 vol.2

Low-Cost Solid Oxide Fuel Cell Power Conditioning with Bidirectional Charging

Chris Smith, Mike Gilliom, Damian Urciuoli, Andy McLandrich, Elton Pepa, and Jih-Sheng Lai
Virginia Polytechnic Institute and State University
Future Energy Electronics Center
676B Whittemore Hall
Blacksburg, VA 24061-0111

ABSTRACT-For the 2002-2003 Future Energy Challenge, this paper suggests a power conditioning system architecture that is potentially low cost and high efficiency for the low input voltage solid oxide fuel cell (SOFC). In order to maintain high efficiency, a two-stage power conversion system including a dc-dc converter and a dc-ac inverter is used for the main power flow path from fuel cell to the load, and an auxiliary energy management system is attached to handle load transients. Since the transient load power comes from the auxiliary battery, the dc-dc converter and thus the fuel cell only need to provide 50% of the peak power, and the inverter can be designed to handle 100% peak power for a period long enough that SOFC can adjust the fuel flow and power output. The complete system is controlled by the TMS320F2407 digital signal processor for predictive control implementation. Different operating modes have been tested to verify the performance of proposed designs.

I. Introduction

The 2002-2003 Future Energy Challenge calls for a design to have 5-kW power conversion system that takes low-voltage 22 to 35-V SOFC output and converts it to 60-Hz ac 120/240V output that is capable of 5-kW continuous rating and 10-kW transient capability for 1 minute. The efficiency of the entire system from fuel cell to load needs to be greater than 90% [1].

To design a power conditioning system with low cost high efficiency, all the system components should be taken into account. Although the most crucial components are the conventional dc-dc converter and dc-ac inverter that are connected in between SOFC and the load, a less-known auxiliary component that is to assist slow fuel cell dynamic and to supplement energy needed during load transient is in fact the detrimental factor to the entire system cost [2–3]. This auxiliary component is to have an auxiliary energy, typically a battery bank, and its associated energy management system to deal with transient and dynamic load changes.

The auxiliary energy source can be ultra capacitors, low-voltage batteries, and high-voltage batteries. The ultra capacitors typically have a lower energy density than that of batteries, but they allow flexible voltage level and can be paralleled with any voltage source. However, their cost today is too high to be practical. The problems with high-voltage batteries are not just higher cost, but also difficult to balance individual cells. Thus, low-voltage batteries with voltage level 48 V or lower make more sense. However, the location to place the low-voltage battery is quite questionable. Since the battery voltage range is not compatible with fuel cell, it is not possible to parallel them. If the battery is charged with fuel cell through a boost converter, and the rest of the system is added after the battery, then there is an additional power conversion loss in the main power flow path, and the dc-dc converter needs to be designed to handle the peak power, a major cost penalty. Thus, the proposed system is to adopt a low-voltage battery bank along with a bidirectional dc-dc charging system to allow energy flow in between high-voltage dc bus and the battery.

The entire power conditioning system is divided into three main sections: (1) the dc-dc converter that boosts from the fuel cell to the high voltage bus, (2) the dc-ac inverter produces two 60 Hz, 120 volt RMS outputs, with 180° out of phase to produce 240 volts RMS across the two phases, and (3) the auxiliary energy management system that consists of a battery bank and a bi-directional dc-dc converter to provide power during load transients. Fig. 1 shows the block diagram of the proposed power conditioning system.

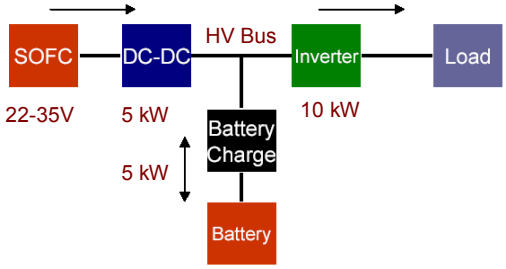

Fig. The proposed power conditioning system block diagram.

II. Three-Phase DC-DC Converter

There are several possible topologies for a system of this nature. The conventional dc-dc converter topologies that are well understood by practicing engineers include forward, push-pull, half-bridge, and full-bridge converters [4–6]. Neither the forward nor the push-pull circuits work well for higher power applications. The half bridge topology requires a split capacitor bus and twice the device current. The push-

pull converter works well for low-voltage low-power systems. Its major problem is the center tap termination, which is difficult to be centered in high current transformers, and the transformer tends to be saturated with slight unbalanced excitation. The full bridge is considered the best choice among conventional converter because its devices are fully utilized, and the switching losses can be eliminated by adopting the soft-switching technique. Because the input current rating is more than 200 A at the full load, each leg of the full bridge converter would need to handle more than 100 A, which not only is difficult to find proper low-voltage power devices, but also introduces substantial interconnect parasitic losses. One may argue that the device problem can be achieved with paralleling multiple devices, but the additional interconnect parasitic components will apparently worsen the efficiency. Thus a three-phase dc-dc converter is proposed to reduce the device current on each phase leg. Fig. 2 shows the proposed three-phase dc-dc converter. Although more phase legs appear to be better of current sharing, the gate drive circuit and control design for more legs becomes troublesome when the phase number increases further.

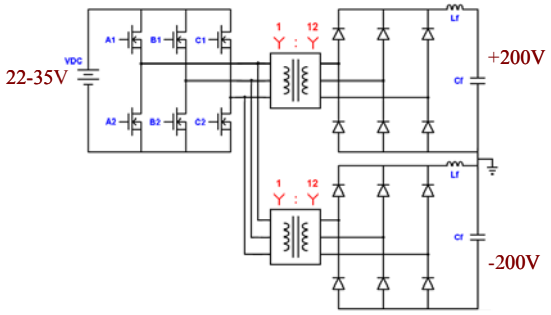

Fig. 2. Circuit diagram of the proposed three-phase dc-dc converter.

In order to meet the overall system efficiency of 90% requirement, the dc-dc stage should have at least 95% efficiency. Based on conduction loss calculation, it is found that at least four 75-V, 4.8-Ω rated power MOSFETs need to be paralleled for each switch to achieve the desired efficiency. With such a high number of devices connected, the interconnect parasitic is a concern. Thus, the TO-263 surface-mount devices along with the insulated metal substrate (IMS) board, shown in Fig. 3, are adopted for the power circuit board assembly.

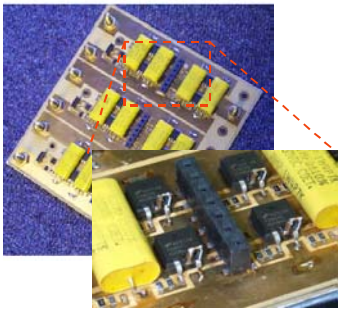

Fig. 3. Power circuit board assembly.

The gate drive pins are located in the center to avoid big difference in switching delay among devices. High frequency capacitors are placed right on top of the devices to minimize the parasitic induced voltage spike during turn-off.

By assuming a maximum duty cycle of 90% and a minimum input voltage of 22 V, the minimum turns ratio was found in (1).

$$n_{\min} = \frac{V_{out}}{0.9 \cdot V_{in,\min}} = \frac{200V}{0.9 \cdot 22V} = 10.1 \qquad (1)$$

Since the planar transformer is used, the secondary is constructed with copper bars, which occupy four layers. In order to reduce leakage and associated duty cycle loss, the turns ratio is thus increased to 1:12 so the output voltage can be maintained at proper level even if the fuel cell voltage drops below at V_{min}. Fig. 4 shows the final assembly of the planar three-phase transformer.

Fig. 4. Three-phase transformer.

This slightly more complex converter design offers benefits over the full-bridge. The converter switching frequency was chosen to be 50kHz. However, in the case of the three-phase converter, phase shifting and rectification increase the ripple frequency seen by the load by a factor of 6. Thus the load sees an equivalent switching frequency of 300 kHz. The converter's operation was first verified at both input voltage boundary conditions. With a 1:12 transformer turns ratio, it was seen that 200-volt outputs could be achieved for minimum and maximum input voltage without exceeding duty cycle boundary limitations. It is important to note that for the phase-shifted topology the input voltage was modeled as 12 times the actual DC input voltage.

The output filter capacitor needs to handle 120 Hz, 25 A ripple current generated from the next stage inverter. The voltage ripple is limited to 5%. Therefore, the capacitance can be calculated as (2).

$$C = \frac{\Delta I}{8 \cdot f_{ripple} \cdot \Delta V} = \frac{12.5A}{8 \cdot 120 \cdot 200 \cdot 0.05} = 1.3mF \qquad (2)$$

After simulating the converter, the capacitor value was adjusted to a standard value and to meet the actual specification. However to further reduce the ripple reflecting back to the fuel cell, the final capacitor value was increased to 6.8 mF.

The output filter for the three-phase converter was designed for an equivalent switching frequency of 300kHz. As a starting point, the inductor was designed for a 20%

inductor ripple and a 90% maximum duty cycle, the inductance was calculated as (3).

$$L = \frac{n \cdot V_{in} - V_o}{0.2 \cdot I_L} \cdot \frac{D}{6 f_s} = \frac{12 \cdot 22 - 200}{0.2 \cdot 15} \cdot \frac{0.9}{300k} = 64 \mu H \quad (3)$$

This inductor size is significant reduced over what has been used in the full bridge converters. As compred in Fig. 5, the newly constructed inductor uses only one small Koo-Mu core rather than four large MPP core, an equivalent 12 times size and weight reduction.

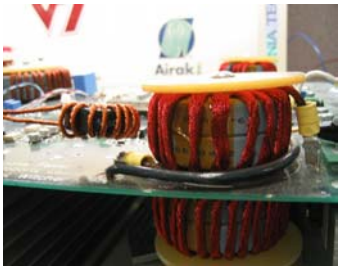

Fig. 5. Inductor size reduction with the proposed scheme.

It should be noticed that the dc output right after the diode bridge and before the inductor has a high voltage swing due to parasitic ringing, which is harmful to the diodes under light load high input voltage conditions. It will also cause electromagnetic interference (EMI) problem. A lossless voltage clamp circuit [7] is thus adopted, as shown in Fig. 6.

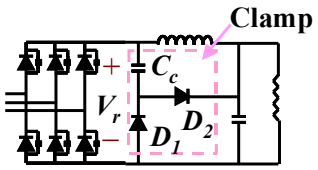

Fig. 6. Lossless clamping circuit

Fig. 7 shows device voltage and its corresponding gate signal for an output power of 3.8kW. With input at 29 V, the voltage across drain and source pins during switching is about 43 V, and is much lower than the device rating.

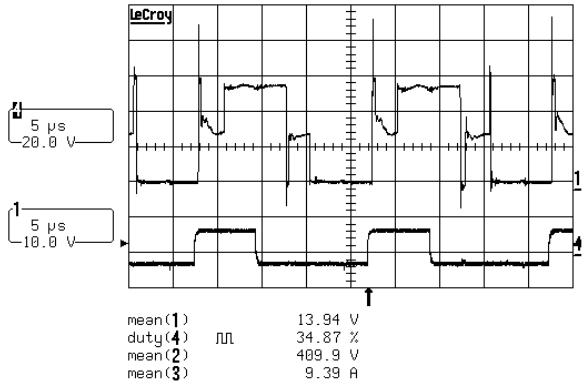

Fig. 7. Device waveforms operating at 3.8-kW under zero-current turn-on condition.

The device turn-on duty cycle for the operating condition shown in Fig. 7 is only 33%, and the device is always turned on at zero current. Under low input voltage condition, the device conduction duty reaches 50%, and the soft switching can be achieved with zero voltage overshoot. Fig. 8 shows the device voltage, inductor current, and the voltage before LC filter under soft-switching condition.

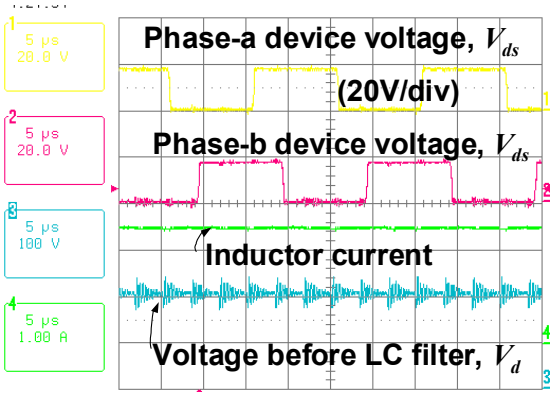

Fig. 8. Device waveforms operating under soft-switched condition.

III. The Split-Phase DC-AC Inverter

There are several possible choices for the inverter [6,8]. The selection criteria can be determined by voltage level, passive component size, and ease of control, etc. The selected design uses two half bridges connected as a full H-bridge. Because the dc-dc converter uses two transformer taps, two well-regulated output buses are available to avoid unbalance. Fig, 9 shows the inverter circuit and its photograph.

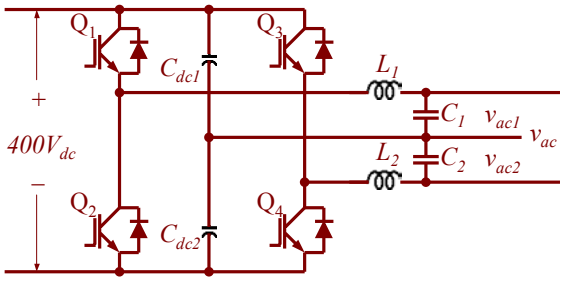

(a)

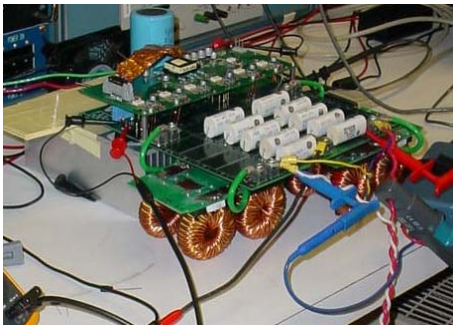

(b)

Fig. 9. The split-phase inverter: (a) circuit diagram, and (b). photograph.

The output filter was sized by choosing a cut-off frequency of 10 times less than the switching frequency of 20kHz, i.e., $f_c = 2\pi(LC)^{1/2} = 2{,}000$. Also, the inductor was selected to have a predetermined ripple current. The resulted LC values are 240 μH and 27 μF, respectively.

Shown in Fig. 10, the inverter controller for the full-bridge can be modeled in controlled voltage and current sources [9].

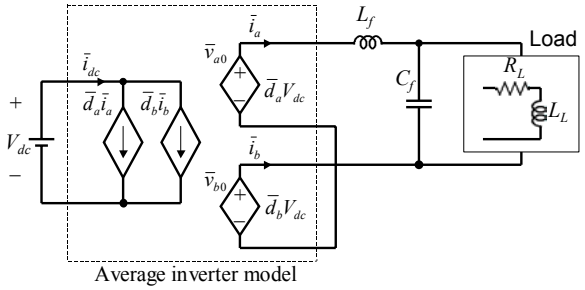

Fig. 10. Average inverter model.

For the split-phase full-bridge inverter with 120/240V outputs, the individual phase legs are controlled with 180° out of phase, and the average duty cycles as a function of the modulation index, d_m, can be expressed in (4a) and (4b).

$$d_a = \text{average}(d_a) = 0.5(1 + d_m \sin\omega t) \quad (4a)$$

$$d_b = \text{average}\,(d_b) = 0.5(1 + d_m \sin(\omega t - 180°)) \quad (4b)$$

Current-Loop Controller Design

The Bode plots for d to i_L are shown in Fig. 11. A current mode controller can be closed inside the voltage loop in order to speed up the transients, and since d to i_L has a zero that makes the frequency response look like a first order system, it should be easy to control.

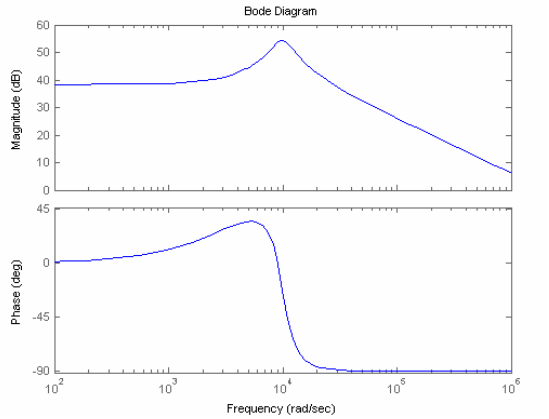

Fig. 11. Bode plots of open loop duty cycle to current transfer function.

The controller selected is a zero at the resonance and an integrator, shown in (5), and the Bode plots of the closed loop system are shown in Fig. 12.

$$G_c(s) = \frac{s + 10000}{s} \quad (5)$$

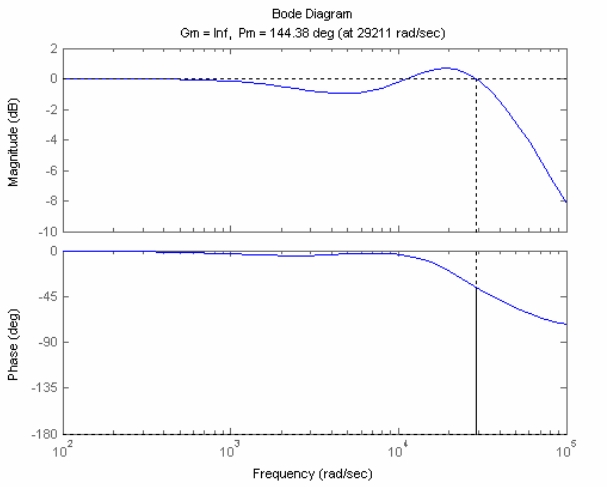

Fig. 12. Bode plots of the closed-loop duty cycle to current transfer function.

Voltage-Loop Controller Design

The voltage loop (d to v_C) transfer function Bode plots for the new system with the current loop closed are shown in Fig. 13.

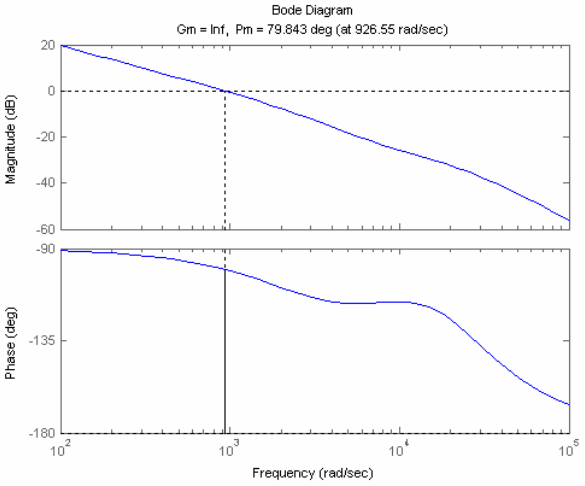

Fig. 13. Open loop duty cycle to output voltage transfer function.

Since the system is over-damped, a double zero at the natural frequency and an integrator with a high frequency pole will control the voltage loop. The controller transfer function is shown in (6), and the closed loop Bode plots for the system can be found in Fig. 14. The results indicate a sufficient phase margin is obtained to ensure the stability during load transient.

$$G_v(s) = \frac{28(s^2 + 39000s + 380250000)}{s^2 + 1000000s} \quad (6)$$

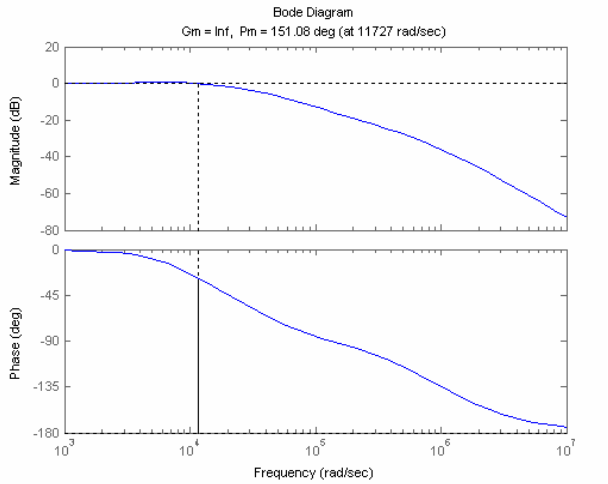

Fig. 14. Closed Loop Duty Cycle to Output Voltage Transfer Function

Fig. 15 shows two-phase inverter output voltage and load current waveforms. With dual modulation scheme, the voltage and current ripples are negligible.

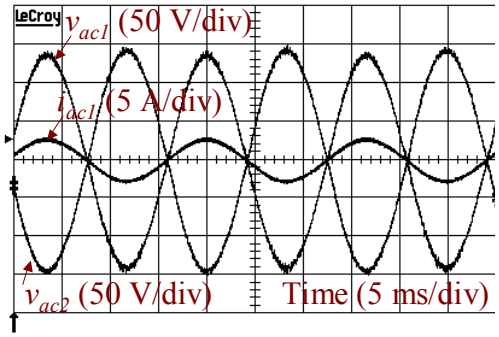

Fig. 15. Experimental results with the plit-phase inverter.

IV. The Bidirectional DC-DC Converter

The bidirectional dc-dc converter has been proposed for fuel cell energy management in [10]. As described before, it makes more sense to have low-voltage battery managing the high-voltage dc bus to allow small dc-dc converter size. Although the isolated bidirectional dc-dc converter suits the application well, it requires two sets of converters and associated controls. Since our voltage levels between low voltage and high voltage is not unacceptably high, it is possible to adopt non-isolated version with two sets of 48 V low-voltage battery bank to interact with individual 200 V high-voltage dc buses.

Fig. 16 shows the proposed bidirectional dc-dc converter circuit and photograph. When the power flow is from battery to dc bus, the circuit operates in "discharging" or "boost" mode. On the other hand, when the power flow is from dc bus to battery, the circuit is operating in "charging" or "buck" mode. The disadvantage of the proposed circuit is that high device voltage and current ratings are required. Thus, each converter contains two phase legs with 180° phase-shift operating in an interleaved fashion to reduce the current magnitude of each phase leg and to reduce the current ripple. Two avoid diode reverse recovery problem with power MOSFET, the 600-V discrete IGBTs co-packaged with ultra fast reverse recovery diodes are selected as the switching device. In order to reduce the inductor size, discontinuous conducting mode (DCM) was designed for all switch operating conditions either under charging or discharging mode.

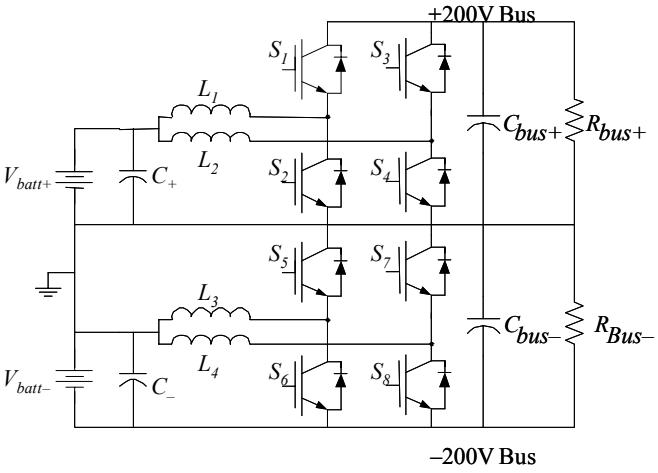

(a)

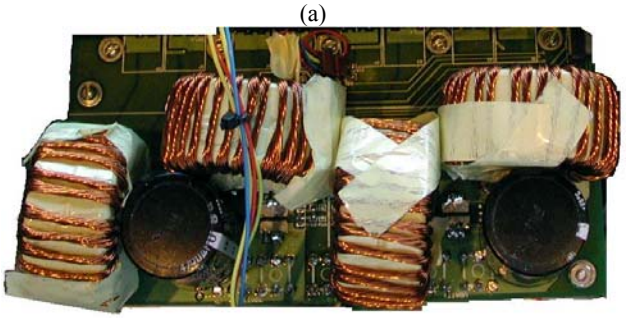

(b)

Fig. 16. The bidirectional converter for energy management: (a) circuit diagram, and (b) photograph.

Based on the selected IGBT device current limit of 37-A, the switching frequency was selected to be 10 kHz, and the inductor was designed to have circuit operating under DCM and CCM boundary condition, which yields a value of 59μH. After substantial cost comparison, the Kool-Mu material model 77111-A2 with A_L = 30 nH/turn was selected for implementation. With two cores stacked together, the A_L becomes 60 nH/turn, and a total of 31 turns will achieve the design.

Fig. 17 shows the experimental device voltage and inductor current waveforms. It should be noticed that the inductor current maintained linear over full-load range, and current run away condition under inductor saturation condition was avoided. The gate signal

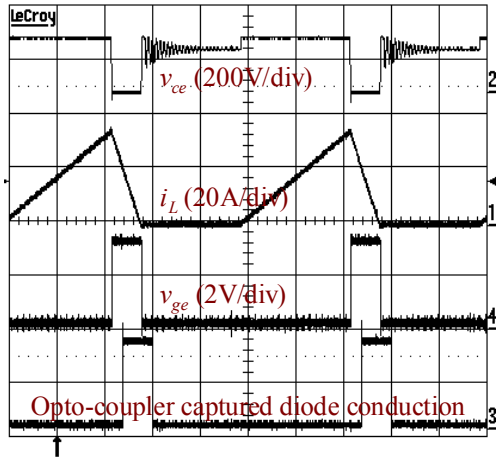

Fig. 17. Experimental device voltage and inductor current waveforms.

Digital Controller Design

With all of the pertinent plant information converted to the digital domain, the current and voltage compensators can be designed. The controller can be designed with proper stability margins for both boost and buck mode operations. The boost mode controller is a dual-loop system with an inner current loop and an outer voltage loop. The buck controller has two loops, a current loop and a voltage loop. The converter will run in current mode until the voltage reaches the proper charging voltage and then switch to voltage mode for the remainder of charging. Since the DSP is sampling at 10 kHz, the bandwidth of the system will be limited to 5 kHz and there will be an inherent one-cycle delay that will be modeled accordingly.

To develop effective compensators for both the voltage and current loops, it is necessary to have accurate small-signal models of the plant. Of the many possible transfer functions, control-to-output voltage G_{vd}, and control-to-inductor current G_{id} are the most important to the control. For the modeling of these transfer functions, the procedure outlined in [4] will be used, and the boost mode transfer function can be expressed in (7).

$$Gvd_{boost} = H_d \frac{\left(1+\frac{s}{s_{z1}}\right)\left(1-\frac{s}{s_{z2}}\right)}{\left(1+\frac{s}{s_{p1}}\right)\left(1+\frac{s}{sp2}\right)} \tag{7}$$

where $H_d = \frac{2V_o}{D}\frac{M-1}{2M-1}$, $s_{p1} = \frac{2M-1}{M-1}\frac{1}{RC_o}$, $s_{z1} = \frac{1}{r_{ESR}C_o}$, $s_{z2} = \frac{R}{M^2L}$, $s_{p2} = 2f_s\left(\frac{1-1/M}{D}\right)^2$.

The derivation of G_{id} is performed using the same method. The control-to-output transfer function shown in (8) for buck mode was given in [4] and can be checked with Pspice simulation.

$$Gvd_{Buck} = H_d \frac{\left(1+\frac{s}{s_{z1}}\right)}{\left(1+\frac{s}{s_{p1}}\right)\left(1+\frac{s}{sp2}\right)} \tag{7}$$

where $H_d = \frac{2I_o}{D}\frac{rR}{r+R+r_L}$, $s_{p1} = \frac{1}{RC}\frac{2-M}{1-M}$, $s_{z1} = \frac{1}{r_{ESR}C_o}$, $s_{p2} = 2f_s\left(\frac{M}{D}\right)^2$, $r = R(1-M)$, $I_o = \frac{V_o}{R}$.

As with the boost converter, the control-to-inductor transfer function G_{id} was derived and verified using the same method and is shown in (8).

$$Gid_{buck} = \frac{2I_o}{D}\frac{r}{r+Z_{equ}} \tag{8}$$

where $I_o = \frac{V_o}{R}$, $Z_{equ} = R\left(r_c+\frac{1}{sC}\right)\frac{1}{R+r_c+\frac{1}{sC}} + r_L + sL$, and $r = R(1-M)$.

These transfer functions can be plotted in frequency domain for the controller design. The design approach adopted here is to use MATLAB c2d() command and RLTOOL for digital compensator implementation. The IIR filter in Direct Form II is implemented. This form only represents the poles and zeros of the compensator. The difference equation and transfer function in z-domain can be represented in (9) and (10), respectively.

$$\begin{aligned} v(n) &= -a_1v(n-1) - a_2v(n-2) + x(n) \\ y(n) &= b_0v(n) + b_1v(n-1) + b_2v(n-2) \end{aligned} \tag{9}$$

$$H(z) = \frac{b_0 + b_1z^{-1} + b_2z^{-2}}{1 + a_1z^{-1} + a_2z^{-2}} \tag{10}$$

The integrator is implemented independently to allow for an anti-windup scheme. The structure of the integrator is shown in (11).

$$y(n) = x(n) + y(n-1) \tag{11}$$

One of the main concerns is to not change the value of the feedback coefficients, a_1 and a_2. These directly affect the response of the filter and cannot be scaled but the output coefficients, b_o-b_2 can be scaled as needed. In an analog system, the gain of the integrator can be placed on either side, but due to the limitations of the digital system, the integrator gain must be placed before the storage element. Combining these different parts yields the full-scaled system as it is implemented in the DSP and is shown in Fig. 18.

The current loop is designed to have a large bandwidth and high DC gain. Since the sampling frequency is 10 kHz and there is the inherent one-cycle delay, the phase drops off sharply as it approaches the Nyquist frequency of 5 kHz. This limits the amount of gain that is achievable due to the low phase margin at high frequencies.

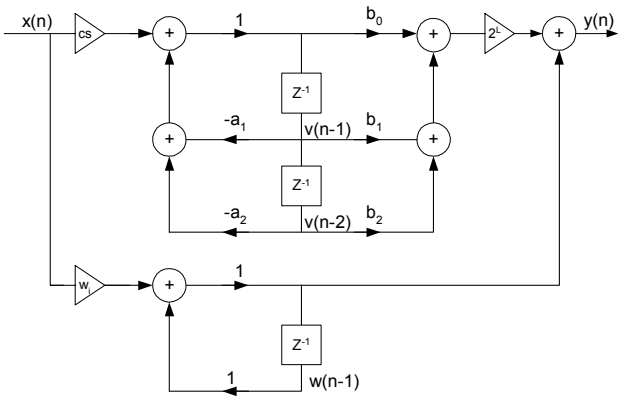

Fig. 18. Complete digital compensator implementation.

The placement of the poles and zeros not only depends on the desired system response but also the achievable gain of the DSP. It was found that due to the resolution of the limited sampling frequency, if the zero were moved to lower frequencies, it would result in canceling the integrator. Also, the closer the pole and zero are together, the larger the necessary scaling. After several iterations of poles, zeros and integrator gains, the compensator was designed as shown in (12).

$$Ci_z = 0.08614\frac{(z-0.9987)}{(z-1)(z-0.9254)} \qquad (12)$$

The compensator has a bandwidth of f_c = 355 Hz and a phase margin of φ = 63.9° at 1500 W as shown in Fig. 19.

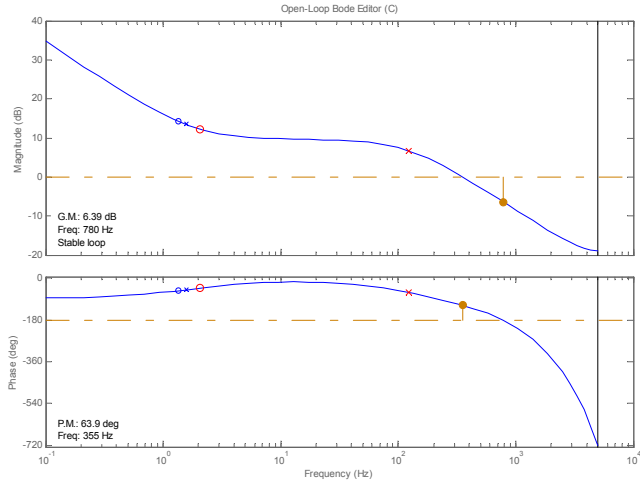

Fig. 19. Boost Open Loop Current Response

To determine if the loop is stable over the full power range, additional loop responses were calculated for 160 W and 2.5kW. Table 1 indicates that at high power, there is a possibility for the loop to become unstable due to the reduced gain and phase margins. On the opposite end of the power spectrum, the loop becomes very stable at low power levels but has a very slow response.

Table 1. Boost Current Compensator Response Summary

Power Level	Crossover Frequency	Gain Margin	Phase Margin
160 W	12.8 Hz	15.8 dB	164.7°
1500 W	355 Hz	6.39 dB	63.9°
2500 W	478 Hz	3.9 dB	43°

For the voltage compensator, it is desirable to have large dc gain and to fall off as quickly as possible. Through many design iterations, it was found that the zero could not be pulled too far in as it would create a large bump in the gain. Again the pole and zero must be separated so the resulting compensator could be scaled within the limits of the DSP. Due to the scaling constraints of the current method, this compensator was implemented and tested regardless of the predicted potential instability. The resulting compensator in the digital domain is shown in (13).

$$Cv_z = 2.7232\frac{(z-0.992)}{(z-1)(z-0.4053)} \qquad (13)$$

The compensated outer loop has a bandwidth of f_c = 18 Hz and a phase margin of φ = 74° at 1500 W as shown in Fig. 20.

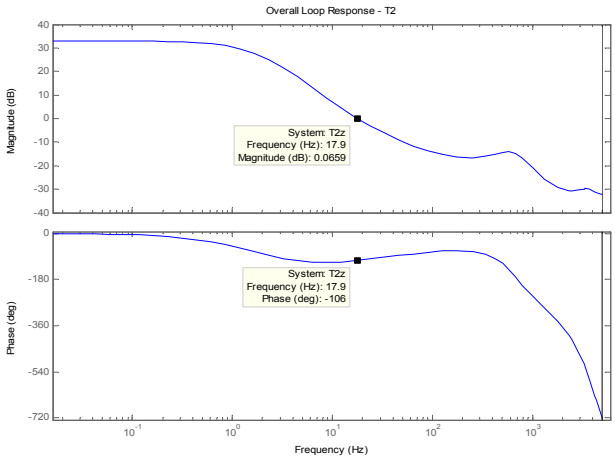

Fig. 20. Boost Overall Loop Gain at 1500 W

The buck converter can be designed using the same procedure. With the pole placed at the ESR zero of the output capacitor and the zero placed to cancel the plant pole, the final compensator is shown in (14).

$$Cv_z = 0.6404\frac{(z-0.994)}{(z-1)(z-0.395)} \qquad (14)$$

The frequency domain performance of the compensated system under different load condition can be summarized in Table 2. It can be seen that the system is stable throughout the entire load range.

Table 2. Buck Voltage Compensator Response Summary

Power Level	Crossover Frequency	Gain Margin	Phase Margin
50 W	0.358 Hz	84 dB	75°
400W	1.03 Hz	57 dB	89.8°
1800 W	2.28 Hz	37 dB	100°

The bidirectional dc-dc converter has been tested extensively in both boost and buck mode under load dump and load step conditions. Fig. 21 shows the test results under (a) boost voltage mode during 800-W load dump, (b) boost voltage mode during 800-W load step, (c) buck current mode during 6-A load dump, and (d) buck current mode during 6-A load step. The controller operation is proven to be stable in any operating mode.

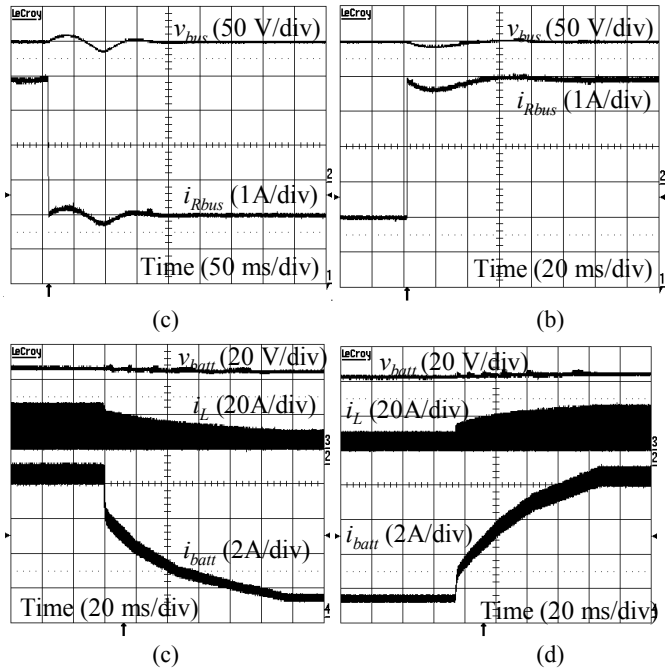

Fig. 21. Test results with the bidirectional dc-dc converter: (a) boost voltage mode during load dump, (b) boost voltage mode during load step, (c) buck current mode during load dump, and (d) buck current mode during load step.

It should be noticed that with DSP implementation, the current loop control was implemented with current estimation to eliminate the expensive current sensor and thus reducing the system cost. Fig. 22 shows the DCM current and its timing relationship with the supply voltage.

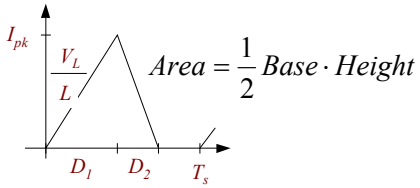

Fig. 22. Current estimation technique with DCM operation.

V. CONCLUSION

A low-cost high-efficiency SOFC power conditioning system has been proposed and implemented. The overall design philosophy is focused on cost reduction while maintaining high efficiency in power stage design and high dynamic performance in control loop design.

Key features of the proposed system are: (1) soft-switched 3-phase dc-dc converter to reduce the device current stress, switching loss, and passive component size and weight, and thus improving the efficiency and reducing the cost, (2) bidirectional dc-dc converter based energy management system that allows power flow between low-voltage battery and high-voltage dc bus with a simple non-isolated circuit structure, and (3) sensorless current controller design for the bidirectional dc-dc converter with DSP implementation to eliminate expensive current sensors.

Future work should be directed to actual SOFC testing to see the fuel cell and converter interactions.

REFERENCES

[1] Future Energy Competition Updated Specifications, March 2003.

[2] Department of Energy (DOE) SOFC Webpage, http://www.fe.doe.gov/coal_power/fuelcells/fuelcells_sofc.shtml.

[3] I.N. Varakin, et al in Proc. of *The 8th International Seminar on Double Layer Capacitors and Similar Energy Storage Devices,* December 7-9, 1998.

[4] Erickson, Robert W.; Maksimović, Dragan, Fundamentals of Power Electronics, 2nd ed, Kluwer Academic Publishers, 2001.

[5] L. H. Mweene, C. A. Wright, and M. F. Schlecht, "A 1 kW 500 kHz Front-End Converter for a Distributed Power Supply System," *IEEE Trans. on Power Electronics*, Vol 6, No. 3, July 1991, pg. 398-405.

[6] T. A. Nergaard, J. F. Ferrell, L. G. Leslie, and J. S. Lai, "Design considerations for a 48 V fuel cell to split single phase inverter system with ultracapacitor energy storage," in *Proc. IEEE Power Electronics Specialist Conference*, Cairns, Australia, June, 2002.

[7] F. Canales, P. Barbosa, and F. C. Lee, "A Zero-Voltage and Zero-current Switching Three-Level DC/DC Converter," *IEEE Trans. on Power Electronics*, Vol. 17, No. 6, Nov. 2002, pp. 898-904.

[8] G. K. Andersen, C. Klumpner, K. Christian, B. Søren Bækhøj, and F. Blaabjerg, "A New Green Power Inverter for Fuel Cells," in *Conf. Rec. of Power Electronics Specialists Conference*, Vol 2, June 2002, pg. 727-733.

[9] J. S. Lai, ECE 5334 Class Note, Virginia Tech, Blacksburg, VA.

[10] K. Wang, F. C. Lee, and J. Lai, "Operational Principles of Bi-directional Full-bridge DC/DC Converter with Unified Soft-switching Scheme and Soft-starting Capability," in *Proc. of IEEE Applied Power Electronics Conference*, 2000, pp. 111-118.

High Efficiency Low Cost Inverter System for Fuel Cell Application

Gang Wang, Pradeep Pant, Hasan Mohammad, Parviz Famouri* and Osman Demirci **

* Lane Department of Computer Science and Electrical Engineering
West Virginia University
Morgantown, WV 26506-6109

** America Electric Power
1 Riverside Plaza
Columbus, Ohio, 43215

Abstract—**This paper presents a new high-efficiency, low cost inverter system suitable for fuel cell applications. The proposed inverter provides a solution for the low-voltage/high-current fuel cell source by using power modules that are parallel connected input and series connected output in DC-DC boost stage. The inverter topology is analyzed and outlined in this paper. A prototype has been developed and experimental results have been presented.**

Keywords: Fuel Cell, Inverter, PWM, Converter, Parallel, Series

I. INTRODUCTION

Environmental concerns are a major issue in the United States. A major source of atmospheric pollution in the U.S and other countries is fossil fuel combustion for thermal power generation. To obtain a cleaner method of power generation, a search for alternative power sources has taken place during last thirty years. Currently, the most prevalent alternative source of electric power is fuel cells. By using hydrogen as a fuel source and producing water as a byproduct, these devices offer an environmentally friendly answer to the pollution problem. Also the electric energy demands are ever increasing, yet with limited transmission lines and many obstacles for right-of-way of new lines, distributed generation (DG) is becoming a reality. Demand for energy efficiency will drive the future residential homes and small businesses to operate through integrated heat/electricity (cogeneration) systems.

Because a fuel cell generates a low voltage DC power, the design of the power inverter system used to interface fuel cell power systems to electric utilities, as well as stand-alone loads, is a major challenge. Unlike the common DC-AC inverter, the fuel cell inverter has its own requirements in order to meet the particular characteristics of fuel cell power generation systems, such as the relatively low output DC voltage, and a relatively slow response to sudden load change. The challenge for the fuel cell inverter is to maximize the fuel cell overall performance, power output, quality and efficiency from a low-voltage, high-current, slow responding DC source. [1]

In this paper, the design and implementation of a fuel cell inverter system designed at West Virginia University for the 2003 International Future Energy Challenge fuel cell conversion topic is presented. The theme of this competition is "Energy Challenge in the Home", and the main goal of the competition is to develop low-cost power processing systems that support the commercialization of a solid-oxide fuel cell (SOFC) power generation system used to provide non-utility and ultra-clean residential electricity. The total rating for the inverter is 10 kW, divided into 5 kW for the solid-oxide fuel cell (SOFC), and a 5 kW battery set. The battery set is required to meet extended-duration power-demand periods exceeding 5 kW, as well as short-duration transient high power loads [2]. To meet inverter specifications, the proposed fuel cell inverter adopts the novel idea of "parallel-input, series-output " in push-pull DC-DC boost stage, providing a solution to the challenge of low-voltage/high-current operation while improving efficiency and reducing the cost. By arranging the power modules in this manner, each module will carry a lower load and share the high input current from the power source, reducing the conduction and switching losses at high current levels and reducing the need for high power rating components**.** In addition, the proposed inverter takes advantage of a digital controller to provide the advanced and complex control algorithm needed to meet the requirements of the fuel cell system, as well as the power management of the overall system. The prototype of proposed inverter has been tested and the experimental result of DC-DC booster open-loop and closed-loop operation, load current sharing and limiting among booster modules are presented.

II. SYSTEM DESCRIPTION

A. Operation and Topology

The system involves three linked subsystems, the inverter, a 3-unit booster module, and a digital controller, illustrated in Figure 1. The booster block will convert and combine low DC voltage (29V DC from the solid- oxide fuel cell (SOFC) and 48 VDC from the battery) to high DC link voltage (400 VDC) suitable for use by the inverter. The PWM driven inverter will take the high DC boost voltage and convert it to 120V/240V, 60Hz, single-phase AC. The digital controller will provide all the PWM control signals to the booster and the inverter, and communicate with the fuel cell computer. The specification of the fuel cell power generation system is 5kW output power with 29VDC output voltage. A 5 kW

lea d-acid battery set with output 48VDC is employed as an energy buffer to meet extended-duration power-demand periods exceeding 5kW and short-duration transient high power loads, thus giving the fuel cell system time to respond to the load demand.

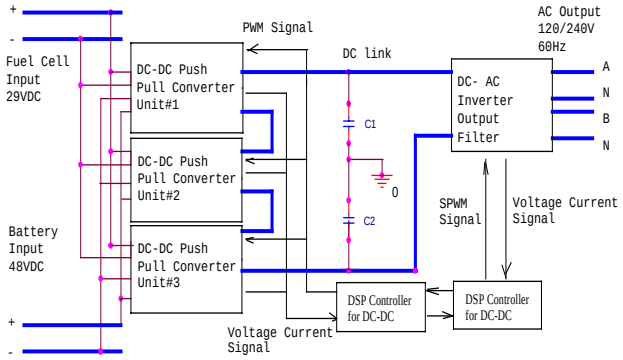

Fig.1. Fuel cell inverter block diagram.

B. DC-DC booster module

For the DC-DC booster stage, several topologies of PWM Switching Power Supply have been studied. Considering the factors of power, voltage level, input/output isolation, and relative parts cost, the push pull topology has been adopted [3]. The switching frequency is 25 kHz. In order to handle 5kW power output and the 275 A maximum current output of the fuel cell, a cost effective, flexible, three-unit design has been utilized. With the idea of parallel-input, series-output, high fuel cell and battery output current are distributed into each booster board connected in parallel, reducing the input current in each board, as well as conduction and switching losses at high current levels. The outputs of each booster board are connected in series to achieve the relatively high voltage level required by the output. Also, by modulating booster boards to a lower power with lower VA rating switching device, mass production costs would drop considerably. In mass production, the size, symmetry, and low-power components of the units would lower the production cost in comparison to a high-power single circuit design. The modular design also allows for additional units to be added for fuel cells with higher output current and power rating. Output voltage of each booster board is regulated independently, and the booster topology makes DC link voltage regulation easier and more precise since the voltage boost level is lower for each board. In the design of each individual booster circuit, conventional isolated push-pull topology has been adopted. Figure 2 shows the schematic of a single booster unit.

A digital controller is employed in the DC-DC booster stage. The advantages are: high degree of programmability, high flexibility, reduced sensitivity to environmental noise, implementation of complex and advanced control algorithm and additional processing options. Some digital controllers for power supply design have been presented in the reference [4-6]. The controller provides an advanced PI closed-loop control to achieve the desired regulated output voltage for each board. The digital controller also implements such functions as soft start, dead band adjustment, including the over current, over voltage, low voltage and short circuit protections.

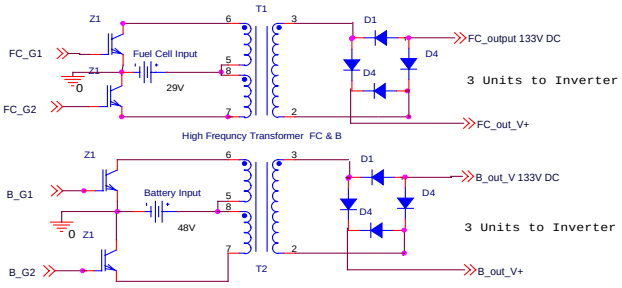

Figure 2. Single Unit schematic

C. Current Sharing and optimal number of modules

Load current sharing in booster modules is the key to proper operation of this design. For high current and high power applications, it is economical to make standard module power supplies work in parallel. If special methods are not made to equally distribute the load current among the operated power modules, one or more module will carry more current while leaving other units essentially idle. This unbalance current distribution will result in greater thermal stresses on specific modules and lead to a reduction in system reliability. To achieve equal current sharing, several approaches have been explored [7]. For fuel cell power generation applications, the challenge also lies in the relatively low input voltage that the booster must convert to a high output voltage. The proposed DC-DC topology provides a straightforward scheme to achieve balanced current sharing while regulating the output voltage to a desire level. As shown in Figure 3, the three modules share the same output current because they are connected in series. Since the output voltages of the three boards are regulated independently to the same level (in this case 133VDC), the output power of each board is approximately the same. Therefore, by regulating the output voltage, the input current can be shared by each board; hence the parallel-input, series-output configuration operates stably for high-current/low-voltage fuel cell application.

The optimal number of modules is a balance between advantages of this configuration (cost/efficiency) and reliability. The higher the number of modules, the higher the efficiency and lower the cost, however, having the outputs of many modules in series would lower the reliability since failure of one results in the failure of the

system. Three modules are used in the proposed design, and each module will carry a third of 5kW at full load.

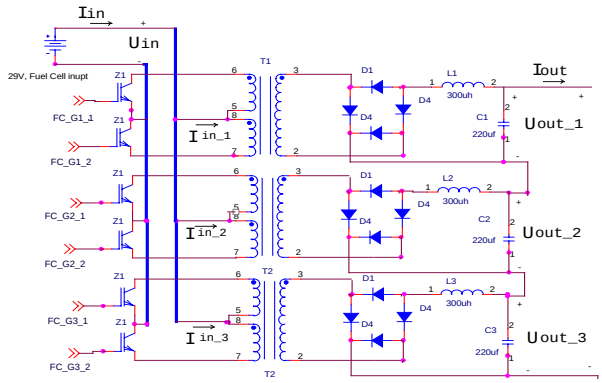

Fig. 3. Current sharing in DC-DC modules

D. Inverter

The inverter converts high DC voltage from the booster to AC. The schematic of the DC-AC inverter circuit is shown in Figure 4. To obtain independent single phase AC output, two half-bridge inverters are used, each supplying a separate single-phase load at 120VAC, 60Hz. The modulating frequency is 20 kHz. A TMS320F2812 DSP is used to control the inverter to achieve high efficiency operation while generating sine waves that have a THD value less than 5%.

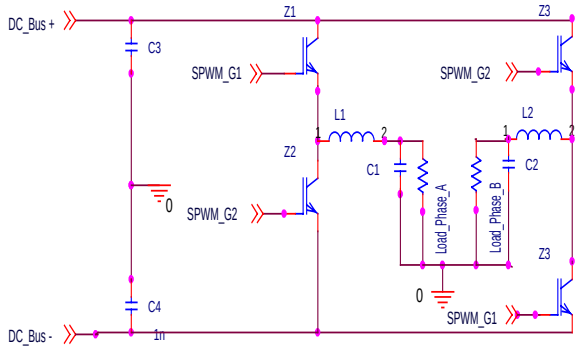

Fig.4. DC-AC inverter schematic.

III. EXPERIMENTAL RESULTS

To verify the proposed topology and design, a 10 kW experimental prototype was constructed for the competition with specifications given below:

- 88 liters in volume (17”x19.25”x16”)
- 45 lbs total weight
- Each boost converter measured to be 90% efficient
- 50 dB audible noise level
- Overall low cost design

Before system integration, the three DC-DC booster boards were tested independently on both the fuel cell side and the battery side with different loads and different duty cycles during open loop and closed-loop operation. Figure 5 shows the switching dynamic of one push pull booster on a fuel cell side. From Figure 5 (a) to (d), the duty cycle increases from 10% to 40%, and the output voltage reaches the desired level, 133V. The input current from the power supply is 3A, 6A, 12A and 22A respectively.

A passive snubber circuit was designed to protect the switching device. Suitable values for capacitor and resistor were chosen based on experimental results. Figure 6 shows that the snubber capacitor discharges completely within 10% of the maximum turn on time. The figure 6 (a) shows at 10% duty cycle, and figure 6 (b) shows at 40% duty cycle.

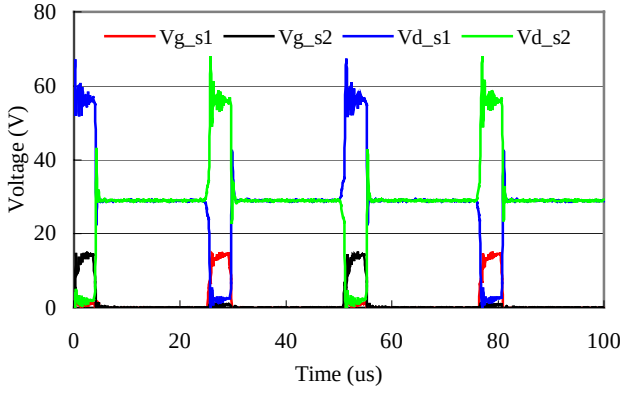

(a)

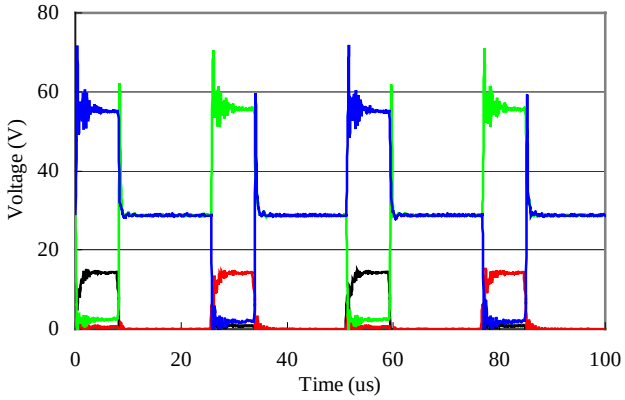

(b)

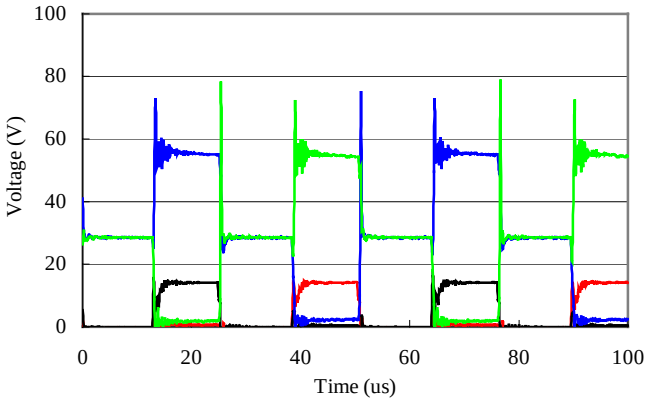

(c)

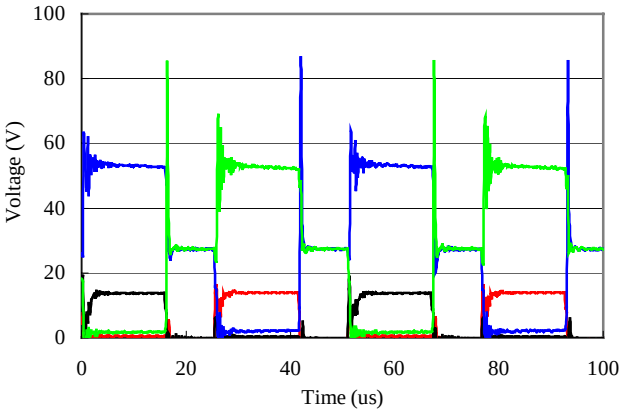

(d)

Fig .5. Switching procedure with different duty cycles. (a) 10% duty, input current 3 A (b) 20% duty cycle, input current 6 A (c) 30% duty cycle, input current 12 A (d) 39% duty cycle, input current 22A

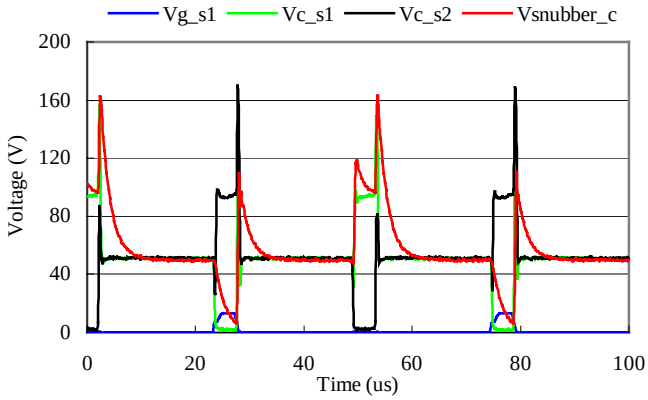

(a) 10% duty cycle

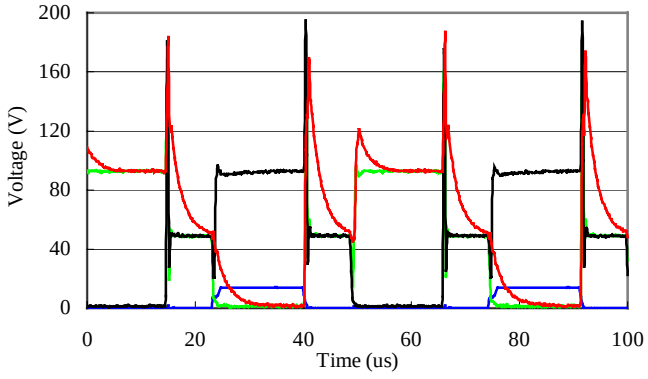

(b) 40% duty cycle

Fig.6. Experiments on snubber circuit with different duty cycle

Figure 7 shows the close loop operation at start up. A digital controller is used at DC-DC booster stage, providing PI close loop control to regulate the output voltage of each board. Increasing the proportional gain decreases the rise time however over shoot would occur. Increasing the integral gain would decreases the steady state error. Suitable gains are selected by trial and error, and as seen in Figure 7, transient response at start up is quite satisfactory.

Figure 8 shows the practical start operation of one board. The fuel cell PWM signal uses a different algorithm than the battery PWM signal. When the power is turned on, it takes more than 1 minute for fuel cell source to respond to the load. In this case, the battery initially takes most of the load, while the fuel cell will eventually take over the load.

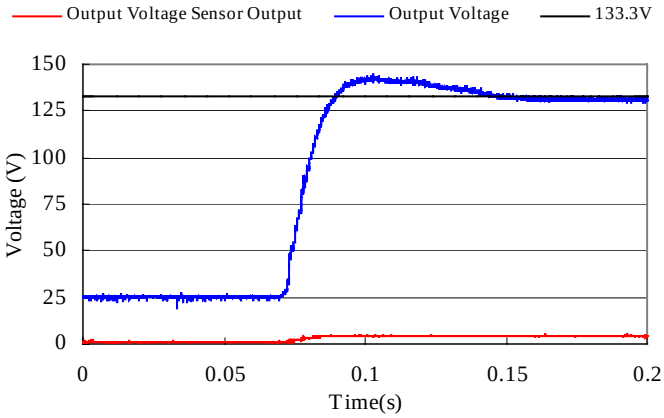

Fig.7. Close loop operation at start-up

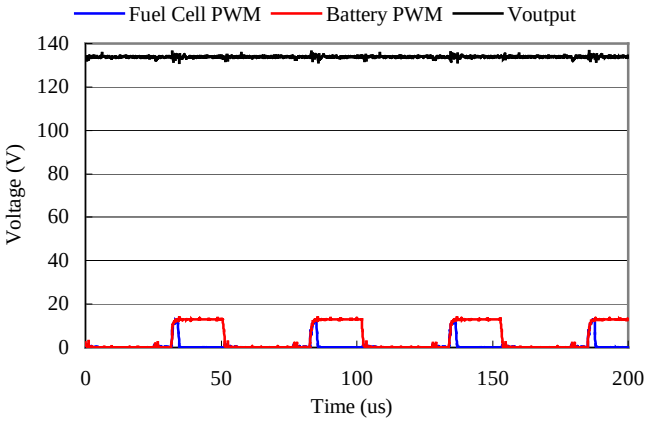

Fig .8 . Fuel cell and battery PWM signal in start procedure

To verify load current sharing, the modules' currents are monitored during the start up and steady state operation in open loop. Figure 9 shows the experimental result. Current sharing activity at start-up is shown in Figure 9(a). *Voutput_#1* is the output voltage of board 1, and *Iinput_#1* is the input current of board 1 while *Voutput_#2* and *Iinput_#2* are the same parameters in board 2. The Figure 9(b) shows steady state operation. As shown in this figure, when the output voltages of two boards are regulated to same level, balance input current can be achieved simultaneously.

Figure 10 shows inverter output. The system was integrated, and experiment measurements were taken at both the battery and fuel cell sides.

VI. CONCLUSION

A high-efficiency, low-cost inverter system for fuel cell applications has been designed and implemented. This paper outlines the topology and the novel approach adopted in DC-DC booster stage. The proposed inverter system provides a solution for relative high current/low voltage fuel cell power source applications. Experimental results are also presented, which verify the theoretical analysis and demonstrate the feasibility of the approach.

Acknowledgments:

The authors would like to thank the students in West Virginia University 2003 spring semester "future energy challenge" senior design group, especially Mr. Kush Scott, for their assistance with the prototyping and experiments. They would also like to thank American Electric Power for sponsoring this project.

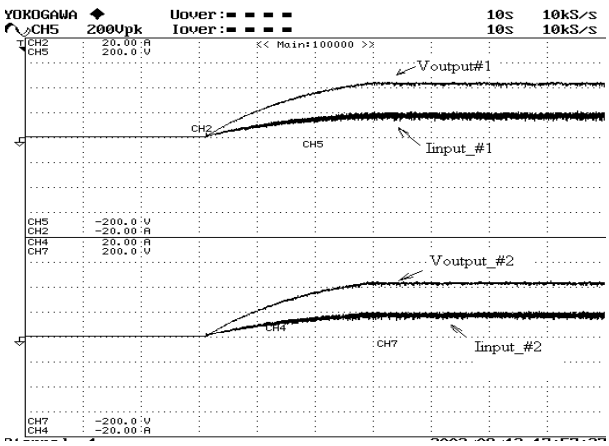

(a) Current sharing at start up

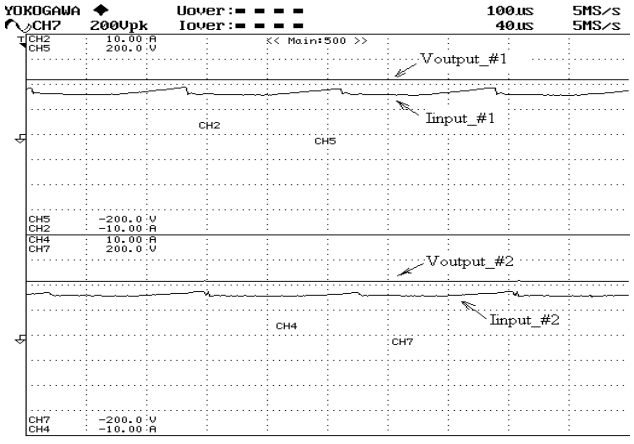

(b)Current sharing at steady state

Fig .9 Load current sharing

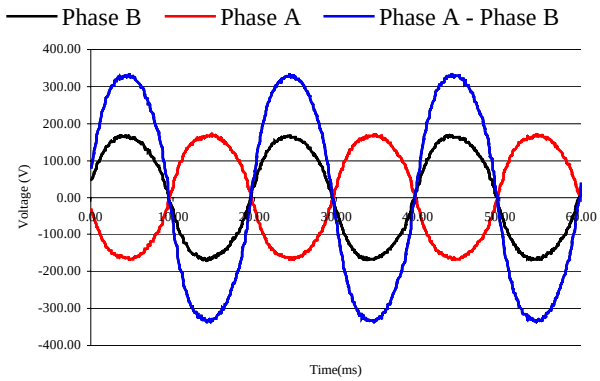

Fig .10 Inverter output at 0.5 kW

REFERENCES

[1] Bill Scheweber, "Inverter is key to fuel cell success ", EDN, July 6, 2000, pp. 48-52.

[2] http://www.energychallenge.org/

[3] Marty Brown, 'Power Supply Cookbook,' Second Edition. pp. 29.

[4] H. Matsuo, Y. Mimura, Y. Nakao, F. Kurokawa and M. Sasaki, 'Novel digital controller for the PWM and/or PFM controlled switching dc-dc converters', *INTELEC-20 the International Telecommunications Energy Conferenc*e, IEEE, Piscataway, USA, 1999, pp. 225-230.

[5] L. Rossetto and S. Buso, 'Digitally controlled single-phase AC/DC integrated PWM Converter', *2001 IEEE Industry Applications Conference Record*, vol.4, pp. 2157-2166.

[6] S. Bibian and H. Jin, 'Time delay compensation of digital control for DC switch mode power supplies using prediction techniques', *IEEE Transactions on Power Electronic*s, vol.15, no.5, September 2000, pp. 835-842.

[7] Mark Jordan, 'UC3907 load Share IC simplifies parallel power supply design', *Unitrode Application Note*, U-129, pp. 3-203-212.

Low Frequency Ripple Current Elimination in Fuel Cell Systems

Y. R. Novaes, I. Barbi, Senior Member, IEEE
Federal University of Santa Catarina - UFSC
Power Electronics Institute - INEP
P. O. Box. 5119 - 88.040-970 - Florianópolis - SC - Brazil
Tel.: (55)48-331.9204 - Fax: (55) 48-234.5422
E-mail: yales@inep.ufsc.br - ivobarbi@inep.ufsc.br

***Abstract* – This paper describes an analysis of the low frequency ripple current generation, distribution and reduction in a fuel cell system. A case study provides a methodology that can be easily used in some architectures powered by fuel cells. The internal resistance of a fuel cell was taken into account to explain a natural reduction of the ripple current in a system. At the end of the paper, an active filter was added to the system, draining the low frequency ripple.**

***Index Terms*- fuel cells, power conditioning, active filter, ripple current.**

I. NOMENCLATURE

ω	Angular freq. of the output voltage of the inverter/ripple current
η	Efficiency
D	DC-DC converter duty cycle
H_R	Reactive power (CA current)
Ib	Ripple current caused by the DC-AC conversion
ICo	Output capacitor current
Ii_{inv}	Inverter input current
ILi	Input inductor current
ILo	Output inductor current
INp	Primary side transformer current
Io	Inverter output current
Io_{conv}	DC-DC converter output current
Ip	Inductor ILf peak current
Ip	Inverter output peak current
IZbat	Battery ripple current
IZbat	Battery ripple current
IZCi	Input capacitor ripple current
IZfc	Fuel cell ripple current
IZfc	Input inductor ripple current
IZLi	Input inductor ripple current
Mi	Modulation index
n	DC-DC transformer turns ratio
PF	Power factor
PI_{conv}	DC-DC active power input
Poinv	Inverter output power
Rx	Fuel cell and battery equivalent resistance
Rxeq	Effective resistance
SI_{conv}	Volt-ampere power (rms values)
Vb	Battery/fuel cell voltage
VCf	Capacitor Cf voltage
VCi	Input capacitor voltage
Vo	Inverter output voltage
Vo_{conv}	DC-DC converter output voltage
Vp	Inverter output peak voltage
Zbat	Battery impedance
ZCi	DC-DC converter input capacitor impedance
ZCo	DC-DC converter output capacitor impedance
Zfc	Fuel cell impedance
ZLi	DC-DC converter input inductor impedance
ZLo	DC-DC converter input inductor impedance
Zx	Primary side impedance

II. INTRODUCTION

Fuel cells have an application potential fairly diversified [1-3]. It could be said that where there is electrical energy consumption, fuel cell technology could contribute towards generate this energy. Proved its contribution towards sustainable development, only scientific progress and economical interests will determine if fuel cell technology will become a standard solution for several application areas or will assist only some application niches. Either way, its high efficiency and reduced environmental impact, and the eminent problems with oil, invite researchers to invest their efforts in this new and promising research area.

Fuel cells are usually stacked at low voltages due to some difficulties in building them safely and reliably at large voltages (>400V) [4]. Nowadays, the standard voltages are around 48 VDC. Nevertheless, the fuel cell regulation is very poor, and especially when fueled by reformers, some dynamic requirements must be attended to. These are some reasons for using power electronics to process the electrical power drained from fuel cells. Fortunately however, the application of electronic techniques in these types of sources brings new phenomena and challenges to be solved. One of them is when the fuel cell system feeds an AC single-phase load. The instantaneous power processed will be pulsed, generating large ripple currents at a low frequency. Since fuel cells are DC sources, the drained current should be continuous and with a minimal ripple, to avoid wasting fuel and reducing their lives. Motivated by these reasons, this work presents a case study and an analysis of the low frequency ripple current distribution in a fuel cell system, including a discussion about the ways to reduce this ripple current.

III. THIS WORK IN THE FUEL CELL WORLD

To perform the ripple current distribution analysis, an extensive research was performed in literature [5-14] to find

what architectures have been used to process electrical power in fuel cell systems, also called power conditioning systems. This research shows that the most common application areas of fuel cells can be classified in five main groups, as shows in Fig. 1. Based on this information, the stand-alone sources group was chosen to be the focus of this work. This distinction was made because in DC systems or in transportation systems, the behavior and origin of the ripple current is different. In all of these groups, some fuel cell architectures were found and one of them was chosen to be detailed here, regarding the ripple current generation.

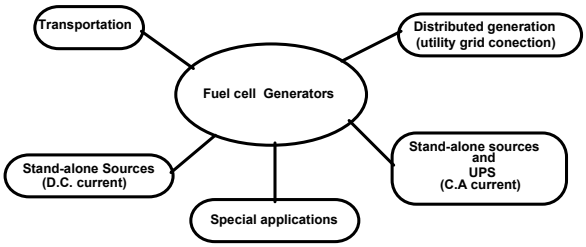

Fig. 1 - Classification of fuel cell applications.

Figure 2 shows the architecture chosen, it uses a battery bank to supply the energy during load variations. It was chosen because this architecture is the simplest and some industries of fuel cells are using it in their systems. The advantages and disadvantages of this architecture and others will not be discussed in this paper.

IV. The Ripple Current Origin and Reactive Energy Circulation

As shown in Fig. 2, a battery charger manages the energy drained from the fuel cell to charge the battery. This battery charger is only a static switch that limits the current when necessary. Now, declared the considerations, the ripple current generation is quantified as follows.

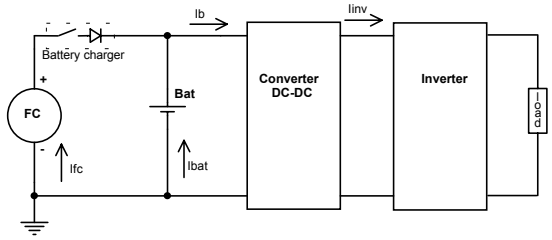

Fig. 2 - Architecture chosen as an example.

The instantaneous power of the output inverter can be expressed as (1) and (2).

$$Po_{inv}(t) = 2 \cdot Vo_{rms} \cdot Io_{rms} \cdot \sin^2(\omega \cdot t) \quad (1)$$

$$Po_{inv}(t) = Vp \cdot \sin(\omega \cdot t) \cdot Ip \cdot \sin(\omega \cdot t) \quad (2)$$

Considering the efficiency and the modulation index, Mi, of the inverter, its input current can be expressed by (3) and the DC-DC converter output current can be expressed by (4).

$$Ii_{inv}(t) = Io_{conv}(t) = \frac{2 \cdot Vo_{rms} \cdot Io_{rms}}{Vo_{conv} \cdot \eta_{inv}} \cdot \sin^2(\omega \cdot t) \quad (3)$$

$$\frac{Io_{conv}}{Io_{rms}} = \overline{Io_{conv}} = \frac{2\sqrt{2} \cdot Mi}{\eta_{inv}} \cdot \sin^2(\omega \cdot t) \quad (4)$$

Figure 3 shows the instantaneous power drained by the inverter, represented by a DC component and an AC component. The peak power processed by the DC-DC converter is twice the nominal power of the inverter.

Considering the FC as an ideal power source, all of this low frequency ripple current could circulate through the FC and the battery. Therefore, the power factor of this system is not unity, and can be calculated using (5) through (9).

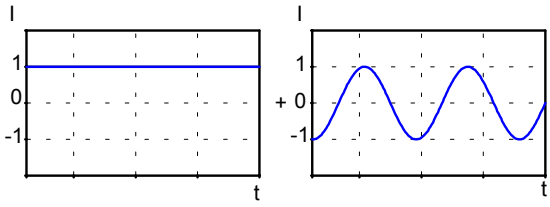

Fig. 3 - DC-DC converter's instantaneous input power.

$$PF = \frac{P_{Iconv}}{S_{Iconv}} \quad (5)$$

$$PF = \frac{\frac{1}{2\pi}\int_0^{2\pi} 2 \cdot Vo_{rms} \cdot Io_{rms} \cdot \sin^2(\omega t)\, d\omega t}{\sqrt{\frac{1}{2\pi}\cdot\int_0^{2\pi}(Vo_{conv}(t))^2\, d\omega t}\cdot\sqrt{\frac{1}{2\pi}\int_0^{2\pi}\left(\frac{2 \cdot Vo_{rms} \cdot Io_{rms}}{Vo_{conv}} \cdot \sin^2(\omega t)\right)^2 d\omega t}} \quad (6)$$

$$P_{Iconv} = V_{O_{rms}} \cdot I_{O_{rms}} \quad (7)$$

$$S_{Iconv} = \frac{\sqrt{6}}{2} \cdot V_{O_{rms}} \cdot I_{O_{rms}} \quad (8)$$

$$FP = \frac{\sqrt{6}}{3} = 0.816 \quad (9)$$

The reactive power that would circulate through the FC and battery terminals, can be determined by (10) and (11).

$$H_R = \sqrt{Si_{conv}^{\ 2} - Pi_{conv}^{\ 2}} \quad (10)$$

$$H_R = \frac{1}{\sqrt{2}} \cdot P_{Iconv} \quad (11)$$

If all the ripple current were eliminated from the circuit by creating and alternative path for circulation, a reduction of 22.5% in the RMS current would be reached, as determined by (12).

$$\frac{Io_{conv\ AVG}}{Io_{conv\ RMS}} = \frac{\sqrt{6}}{2} \rightarrow 22.5\% \quad (12)$$

These calculations represent a merit factor of a power conditioning system performance based on FC's. An observation needs to be made about the DC-DC converter voltage control. If the DC-DC voltage control loop is designed to eliminate any low frequency disturbance, like 120Hz, the previous calculations are correct. Otherwise, if a low frequency ripple voltage is admitted at the DC-DC output, which can be reduced by the output capacitor, only a part of that ripple current will circulate through the

primary and secondary sources. Thus, a natural reduction in the FC and battery ripple currents will be noted by taking into consideration the impedances of these sources, as follows.

A. Ripple Current Distribution

Taking as an example a voltage-sourced converter, the fuel cell system can be simplified and represented by

Fig. ***4***. The current sources in the right side of this figure represent the current drained by a voltage source inverter using PWM modulation and a resistive load. Components Li, Ci, Lo and Co are the high frequency filter elements. In this figure, Zfc and Zbat are the Fuel Cell and battery impedances.

Eliminating the DC sources and taking into consideration the impedances, the transformer and the switch cell, a model of the system is defined and presented in Fig. 5.

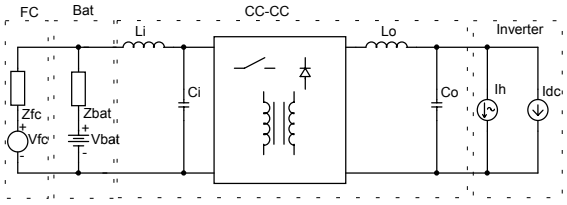

Fig. 4 - DC-DC converter's instantaneous input power

This model will help to determine how much low frequency current will circulate through the sources, taking into consideration the influence of the converter duty cycle and the transformer turns ratio.

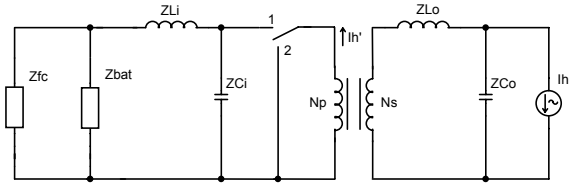

Fig. 5 - Model of the system susceptible to the low frequency current.

First of all, the influence of the duty cycle will be calculated. To do this, a resistor substitutes the impedance and the converter operation characteristic is considered. In the Fig. 6, the equivalent circuit is shown.

Looking for an equivalent resistance seen by source Ih', using active power equivalence, the duty cycle influence was found, and is shown in (18). The capacitor input voltage, VCi, and the reflected current, Ih', were considered constant.

Thus, reflecting the equivalent impedance, Zx, through the switch cell and the transformer, a new equivalent circuit can be drawn, which is shown in Fig. 7 (a), where Zx is the primary side impedance, as shown in (19). Hence, current ILo can be easily determined, as shown in (21).

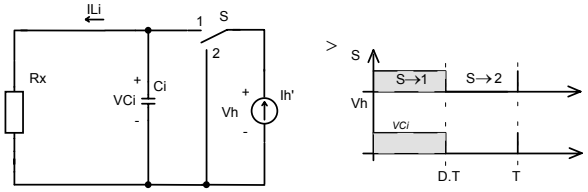

Fig. 6 - Equivalent circuit used to determined the influence of the duty cycle.

$$VCi = Rx \cdot ILi_{avg} \tag{13}$$

$$ILi_{avg} = Ih' \cdot D \tag{14}$$

$$Vh_{avg} = VCi \cdot D \tag{15}$$

$$Vh_{avg} = R \cdot Ih' \cdot D^2 \tag{16}$$

$$R\,x\,eq = \frac{Vh_{avg}}{Ih'_{avg}} = R \cdot D^2 \tag{17}$$

$$\frac{R\,x\,eq}{R} = D^2 \quad \rightarrow \quad \frac{Zxeq}{Zx} = D^2 \tag{18}$$

As fuel cell stacks arrangements are usually at a low voltage or at least smaller than the output voltage required by the load, a pull-up converter is necessary. If a transformer is used to achieve this voltage increase, a benefic effect occurs, because the fuel cell impedance, which imposes a natural barrier against the ripple current circulation, will be amplified by a quadratic factor (transformer turns ratio).

$$Zx = \frac{ZCi \cdot \left[Zfc \cdot \left(Zbat + ZLi \right) + ZLi \cdot Zbat \right]}{Zfc \cdot \left(Zbat + ZLi + ZCi \right) + Zbat \cdot \left(ZLi + ZCi \right)} \tag{19}$$

$$n = \frac{Ns}{Np} \tag{20}$$

$$ILo = \frac{ZCo}{Zx \cdot D^2 \cdot n^2 + ZLo + ZCo} \cdot Ih \tag{21}$$

$$ICo = \frac{Zx \cdot D^2 \cdot n^2 + ZLo}{Zx \cdot D^2 \cdot n^2 + ZLo + ZCo} \cdot Ih \tag{22}$$

Knowing how the current (in a switching period) circulates through inductor Lo, the average value of the primary transformer current is determined by (23).

$$INp = \frac{ZCo \cdot n \cdot D}{Zx \cdot D^2 \cdot n^2 + ZLo + ZCo} \cdot Ih \tag{23}$$

Using Fig. 7(b), the distribution of the ripple current between both, fuel cell and battery, is calculated by (24) through (27).

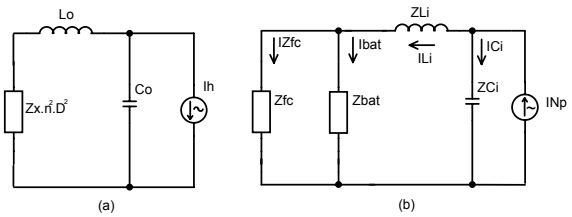

Fig. 7 - Equivalent circuits, (a) Impedance Zx transferred to the primary side; (b) Current distribution.

Searching for a limited ripple current circulation

through the sources those equations can be used to determine the DC-DC component filters, resulting in a dedicated design for fuel cells.

$$IZCi = \frac{INp \cdot \left(ZLi + \frac{Zfc \cdot Zbat}{Zfc + Zbat} \right)}{ZCi + ZLi + \frac{Zfc \cdot Zbat}{Zfc + Zbat}} \quad (24)$$

$$IZLi = \frac{INp \cdot ZCi}{ZLi + ZCi + \frac{Zfc \cdot Zbat}{Zfc + Zbat}} \quad (25)$$

$$IZfc = \frac{Zbat}{Zfc + Zbat} \cdot IZLi \quad (26)$$

$$IZbat = \frac{Zfc}{Zfc + Zbat} \cdot IZLi \quad (27)$$

One method used to block this ripple is using a DC-DC converter operating with constant current control, as presented by [15]. Using this method, all the ripple current will circulate through the converter output capacitor, causing a ripple voltage, which can be easily controlled by increasing the capacitance value. In this case, the converter is operating like a low band pass filter. Another method to reduce the ripple is by using an active filter in parallel with the DC bus bar, as was cited in [5]. But, using a battery to perform this work, the ripple current will circulate through this component, reducing its life. A good way to solve this problem, if possible, is by using ultra-capacitors, which have large power and energy densities. Remembering that UC's support larger RMS current than batteries, with lower internal resistance, resulting in smaller reduced losses.

V. Experimental Results and Theoretical Validation

Using a system already built, which uses a push-pull converter and a single-phase inverter, the theoretical analysis was verified. The parameters utilized are presented as follows:

Co=1280 μF; Lo=470 μH; Li=1μH; Ci=7500μF; Zfc=126 μΩ; Zbat=180 μΩ; n=9; D=0.82; P=960 W.

The Fuel Cell and battery impedances include the resistance of the cables and connections, estimated experimentally. Figure 8 presents the sources' drained current. Note the presence of the ripple and the natural reduction caused by the source impedances.

In Fig. 9, the battery waveforms are presented. The ripple current is causing a distortion in the DC voltage due to the sources' internal resistances. Some battery manufacturers specify a limit for this ripple voltage. Another detail is that the battery current has a DC level because it is still being charged. Since batteries have different behaviors and efficiencies in the charge/discharge modes, this DC level is extremely necessary to maintain the battery charged. Without a DC level, the battery would discharge by itself. Figure 10 is showing the fuel cell voltage and current. Since the battery and fuel cell have an internal resistance close each other, the ripple current will circulate through both. This is an undesirable situation, mainly because this ripple current circulating through the fuel cell will waste fuel. Thus, some harmful chemical reactions can take place, because the ripple frequency is low.

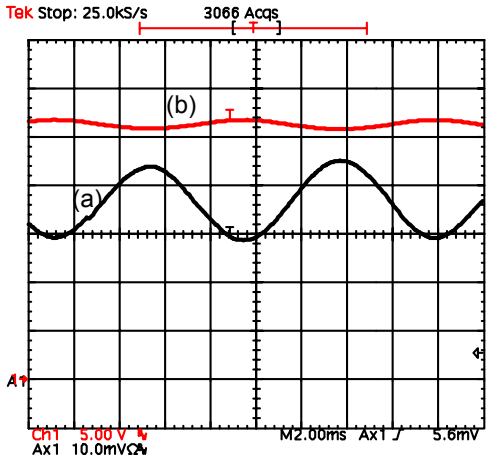

Fig. 8 - (a) DC-DC input current (10A/div), (b) DC-DC input voltage (5V/div).

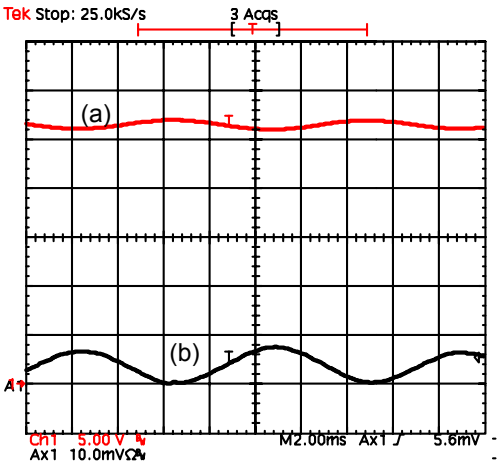

Fig. 9 - (a) Battery voltage (5V/div); (b) battery current (10A/div).

In the quantitative analysis, a simplification was made regarding the impedances of the sources. Only the resistive characteristic was considered, ignoring other capacitive or inductive elements like the capacitor originated by the charge double layer phenomenon. This simplification can be made at low frequencies because the internal resistance is predominant, therefore, the other parasitic elements can be neglected. This affirmation is proved in Fig. 11 where the fuel cell voltage and current are shown in phase. The same occurs with the battery current and voltage, shown in Fig. 12. With the objective of confirming the validity of the equations obtained previously, the main theoretical calculations and the experimental results are compared in Table 1.

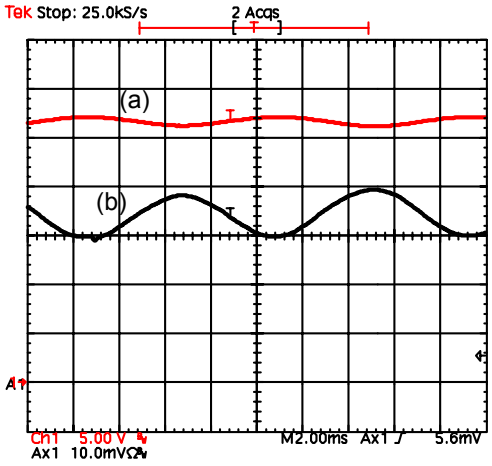

Fig. 10 - (a) Fuel Cell stack voltage (5V/div); (b) Fuel Cell current (10A/div).

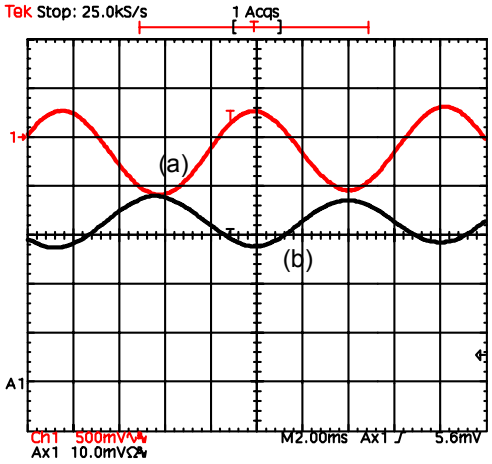

Fig. 11 - (a) Fuel cell voltage (500mV/div); (b)Fuel cell current (10A/div)

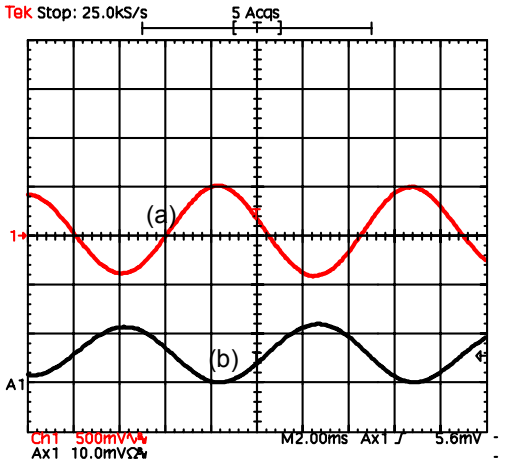

Fig. 12 - (a) Battery voltage (500mV/div); (b) Battery current (5A/div).

TABLE I
ANALYTICAL AND EXPERIMENTAL RESULTS COMPARISON

	Calculate	*Measured*
IZLi	5.992 A	6 A
IZfc	3.480 A	3.18 A
IZbat	2.438 A	2.82 A

VI. REDUCING THE RIPPLE CURRENT BY USING AN ACTIVE FILTER

As was said before, one solution to suppress the ripple from the main circuit is creating an alternative path for circulation. An active filter, using capacitors as the energy storage stage, can create this path. This active filter has to be bi-directional in current. Hence, the topology chosen to reach this objective is presented in Fig. 13. A boost converter drains the current from the sources during half of the period and during the other half, a buck converter reverses the current flow. Design and control considerations for the active filter were presented in [16].

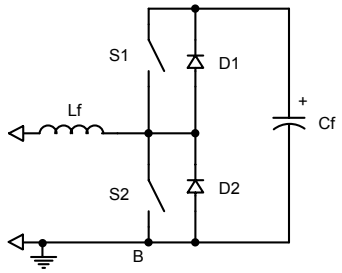

Fig. 13 – Topology of the active filter converter.

Chosen the topology, the point of connection of this filter can be decided. It can be connected between the DC-DC converter and the inverter. This place is quite attractive because the ripple will not circulate through the DC-DC converter. This solution would be excellent if ultra-capacitors were used as large energy storage components to compensate variations in the load demand and still suppress the ripple current. If this were possible, the power battery could be eliminated from the system. Since the main objective of this paper is to quantify and eliminate the ripple from the sources, a small active filter using common electrolytic capacitors was connected between the sources and the converters, as is shown in Fig. 14. If the objective of this work were to eliminate the ripple before the DC-DC converter, the filter's VA power would be at least the same value as the inverter's nominal output power instead of being smaller, which was implemented.

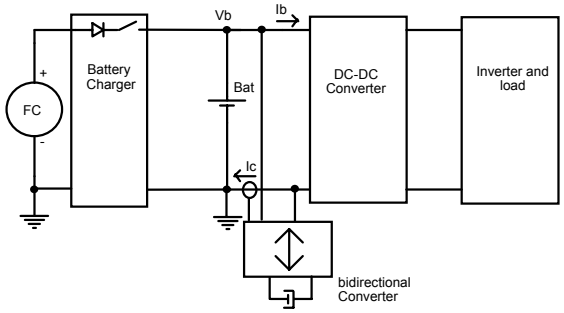

Fig. 14 – Fuel cell system using an active filter to suppress the low frequency ripple current.

The experimental results of the active filter are shown in Fig. 15. This figure is showing the inverter's current, the filter's current and the voltage VCf. Some control improvements must still be made to eliminate the

oscillations in the current waveform.

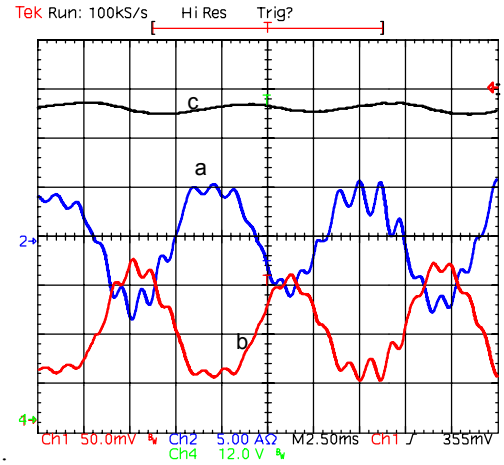

Fig. 15 - Active filter waveforms - (a) Current ILf; (b) Current Ib (10mV/A), (c) Voltage VCf (12V/div).

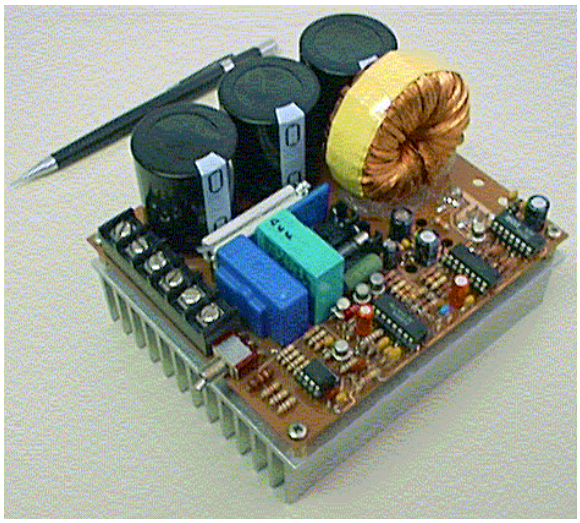

Fig. 16 - Picture of the active filter prototype.

VII. Conclusion

Nowadays, mainly in fuel cell systems, batteries are still being used as large capacitor banks, through which large ripple current circulates. This ripple will result in heating and maybe reduce their life. Thus, the ripple current should be avoided or reduced. The goal of this work was to reduce the ripple current generated by single-phase inverters in fuel cell systems when power batteries cannot be substituted by ultra-capacitors. To achieve this objective, an analysis of the ripple current distribution in a power conditioning architecture was performed. After quantifying how much ripple circulates through the sources, an active filter was applied to suppress this reactive energy. A theoretical analysis and experimental results were presented.

Acknowledgment

The authors gratefully acknowledge PHB Electronic Ltd for making the system's experimentation possible. We would like to thank LEM S/A and Intech Engineer Ltd, especially J. E. Antonio, for the Hall effect sensors supplied.

References

[1] K. Kordesch, R.F. Sproull, "Fuel Cells and Their Applications", VCH Verlagsgesellschaft, Weinheim, Federal Republic of Germany, 1996.

[2] J.E. Larminie, A. Dicks, “Fuel Cell Systems Explained, John Wily & Sons”, Chichester, England, 2000.

[3] J.H. Hirschenhofer, D.B. Stauffer, R.R Engleman, et. all., “Fuel Cell Handbook”, fifth edition, pub. under USDOE contract.

[4] P.T. Krein, "Fuel Cells: Electrical Energy Conversion Issues", Power Point presentation of the University of Illinois at Urbana-Champaign, nov 2002.

[5] E. Santi, et al., "A Fuel Cell Based Domestic Uninterruptible Power Supply", in Proc IEEE Applied Power Electronics Conf., 2002, pp. 605-613.

[6] T.A. Nergaard, et al "Design Considerations for a 48V Fuel Cell to Split Single Phase Inverter System with Ultra-capacitor Energy Storage", in Proc IEEE Power Electronics Specialist Conf., 2002, pp. 257-261.

[7] A.M. Tuckey, J.N. Krase, "A Low-Cost Inverter for Domestic Fuel Cell Applications", in Proc. IEEE Power Electronics Specialist Conf., 2002, pp 339-346.

[8] R. Gopinath, et al., "Development of a Low Cost Fuel Cell Inverter System with DSP Control", in Proc. IEEE Power Electronics Specialist Conf., 2002, pp. 309-314.

[9] A. Monti et al., "Fuel Cell Based Domestic Power Supply - A Student Projetc", in Proc. IEEE Power Electronics Specialist Conf., 2002, pp. 315-320.

[10] K. Wang et al., "Bi-directional DC to DC Converters for Fuel Cell Systems", in Proc. IEEE Power Electronics Specialist Conf. 2002, pp. 47-51.

[11] A.D. Napoli, et al., "Multiple Input DC-DC Power Converter for Fuel-Cell Powered Hybrid Vehicles", in Proc IEEE Power Electronics Specialist Conf., 2002, pp. 1685-1690.

[12] C. Liu et al., "Power Balance Control and Voltage Conditioning For Fuel Cell Converter With Multiple Sources", in Proc. IEEE Power Electronics Specialist Conf., 2002, pp. 2001-2006.

[13] S. Soter, S. Buchhold, "Adaptable Inverter for Injection of Fuel Cell and Photovoltaic Power", in Proc. IEE Power Conversion Conference, 2002, pp.1453-1455.

[14] P.T. Krein and R. Balog, "Low Cost Inverter Suitable for Medium-Power Fuel Cell Sources", in Proc IEEE Power Electronics Specialist Conference, 2002, pp. 321-326.

[15] A.M. Tuckey, J.N. Krase, "A Low-Cost Inverter for Domestic Fuel Cell Applications", in Proc. IEEE Power Electronics Specialist Conf., 2002, pp. 339-346.

[16] Y. R. Novaes, I. Barbi, “Design of an Active Filter for Fuel Cell Systems”, COBEP 2003 – to be published.

Development of a Low Cost Fuel Cell Inverter System with DSP Control for Residential Use

Maja Harfman Todorovic*, Leonardo Palma*, Woojin Choi*, Cody Dowling*, Daniel Humphrey, David Tarbell*, Prasad Enjeti**, Jo Howze**

*Student Members **Faculty Advisors

Power Electronics and Power Quality Laboratory
Department of Electrical Engineering
Texas A&M University
College Station, TX – 77843-3128
Tel: 979-845-7466; Fax: 979-845-6259
Email: enjeti@tamu.edu

***Abstract* – In this paper, the development of a fuel cell inverter system suitable for residential use is detailed. The approach consists of a two-terminal push-pull DC-DC converter to boost the fuel cell voltage (41-22V_{dc}) to 400VDC. A six-switch (IGBT) inverter is then employed to produce 120V/240V, 60Hz AC outputs. Highlights of the proposed design include protection, diagnostic features, and the control strategy used. The control strategy allows the inverter to adapt to the requirements of the load as well as the power source (fuel cell). A unique aspect of the design is the use of the TMS320LF2407 DSP to control the inverter. One set of lead-acid batteries is provided on the high voltage DC bus to supply sudden load demands. Efficient and smooth control of the power drawn from the fuel cell and the high voltage battery is achieved by controlling the front end DC-DC converter in current mode. The paper details experimental results of the proposed design on a fuel cell simulator, which mimics a SOFC fuel cell steady state V-I curve.**

I INTRODUCTION

The Department of Energy (DOE) has identified the fuel cell as a distributed energy technology that will soon be participating in the energy market. Despite its obstacles, fuel cells are being considered increasingly as a viable source of energy. One of the main barriers for fuel cell technology to penetrate the energy market is its manufacturing cost as well as the cost of the power conditioning system used in conjunction with the fuel cell. Fortunately, fuel cell system production costs are rapidly decreasing to the level of competition with other energy source technologies. To further assist the reduction of cost, the price of the power-conditioning portion of the fuel cell system must also decrease, while at the same time increasing its efficiency, reliability, and output power quality. Lower cost will enable the fuel cell systems to achieve a production cost at a more competitive rate than that offered by many local utility companies, thus triggering rapid penetration into the utility market.

One of the main components whose cost can be reduced in the fuel cell system is the power-conditioning unit, which converts direct current (DC) power from the fuel cell to consumer usable alternating current (AC). The inverter design should be small, efficient, and reliable at a low cost to promote small-scale fuel cell system commercialization and encourage the development of distributed power systems.

II POWER CONDITIONING TOPOLOGY

Figure 1 shows the block diagram for the proposed fuel cell power-conditioning unit. In general, as shown in the figure below, this system consists of a DC-DC boost converter cascaded with a single-phase inverter circuit. A filter is then connected to the inverter terminals to assure that the output voltage of the system meets power quality standards such as the IEEE 519.

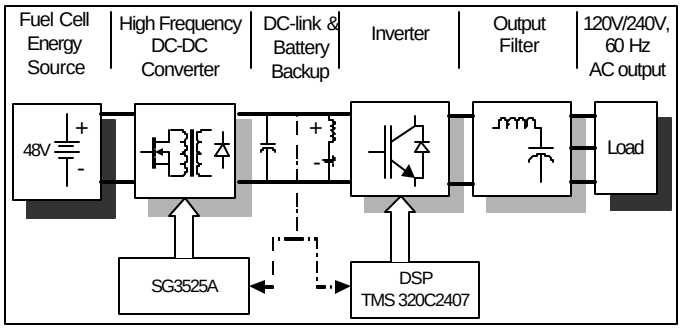

Figure 1: Block Diagram of the TAMU Fuel Cell Inverter

As shown in Figure 1, each system block is controlled independently. The dc-dc converter is controlled using a modified commercial analog control scheme. This is done to meet the slow dynamic response of the fuel cell. On the other hand, the control of the inverter is entrusted to a TMS 2407 DSP. The use of the DSP for the inverter control gives more

flexibility to the system [1],[2]. Further, the DSP code can be modified easily to add more features to the system.

A detailed description of the design and operation of each power stage within the power conditioning system is given in the following points.

2.1 DC-DC converter.

The design specifications for the power processing unit dictate that the DC-DC converter has to process 5kW. Therefore, designing one Dc-Dc converter to handle all this power is cumbersome and the resulting unit is less efficient for low power operation. To solve this issue the approach taken in this design employs three push-pull converters whose outputs are connected in parallel to suitably boost the fuel cell voltage from a range of 22-41V to 400V. Each push-pull converter is rated for an input voltage ranging from 22-48V with an output of 400V at 1.7kW. Figure 2 shows a schematic diagram of the converter topology used.

The output voltage is regulated by means of feedback control employing a low cost digital control scheme using a TMS2407 DSP from Texas Instruments [3],[4].

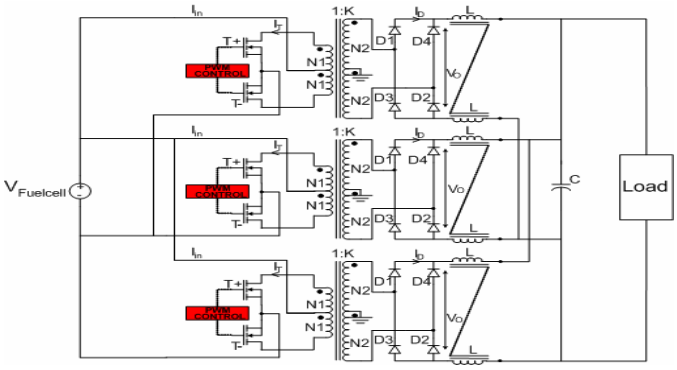

Figure 2: Parallel output push-pull converters used in the design

A challenge that arises with the push-pull topology is that the transformer core may saturate if the characteristics of the forward-voltage drop and conduction times of the transistors are not precisely matched. Small imbalances can cause the DC component of voltage applied to the transformer-primary to be nonzero. Consequently, during every switching period, there is a net increase in the magnetizing current. If this imbalance continues, then the magnetizing current can eventually become large enough to saturate the transformer. Core saturation results in rapid thermal runaway and destruction of the transistors. To ensure that there is no significant imbalance between the two switch currents a coupled inductor is employed on the secondary of the transformer. The coupled inductor balances the currents in the two halves of the center-tapped transformer. Additionally, the choke filters out the switching frequency components off the DC output current and balances the power output of each inverter phase, (which are specified to be capable of being loaded independently), and helps generate a clean 400VDC voltage for the inverter.

Component sizing for the DC-DC converter is done as follows [5],[6],[7].

Inverter power output= 5000W

Assuming an overall efficiency of 90%, we have an input power

$$P_{in} = \frac{5000\,W}{0.9} = 5555\,W \quad (1)$$

A nominal fuel cell input voltage, V_{in}= 42VDC-nom., is assumed.

Output voltage, V_o= 400VDC

Switching frequency= 40kHz (duty ratio control)

Designing for the maximum load condition (V_{in}=22VDC), input current from fuel cell can be calculated to be

$$I_{in} = \frac{5555\,W}{22\,V} = 252.5\,A \quad (2)$$

The push pull DC-DC converter shown in Figure 2. This comprises of two switches, T+ and T-. At the maximum duty ratio of 0.5, rms current rating I_T of the switches

$$I_T = \frac{I_{in}}{\sqrt{2}} = 179\,A \quad (3)$$

Therefore, MOSFET's rated 200V; 50A with three devices in parallel in each leg are selected for each DC-DC converter.

For obtaining an output voltage of 400VDC for each push-pull converter, a turns ratio of K=7.5 for the high frequency transformer is chosen. Center taps are available on both the primary and secondary sides of the transformers shown in Figure 2 at the beginning section 3.3. The VA rating of the transformer is defined as the sum of the total primary and secondary winding VA divided by two,

$$VA_{Tr} = \frac{1}{2}\left(\frac{V_{in}}{\sqrt{2}}\cdot\frac{I_{in}}{\sqrt{2}}\cdot 2 + V_{in}\cdot K\cdot\frac{I_{in}}{K}\cdot 2\right)$$
$$= 1.5\,V_{in}\cdot\frac{I_{in}}{3} = 1.5\cdot 42\cdot 84$$
$$= 5292\ W \cong 5.3\,kVA \quad (4)$$

Voltage ratings of the transformer are selected as:

Primary voltage=80V, Secondary voltage=400V

To specify the diode ratings, it was considered that the reverse blocking voltage is equal to the DC link voltage 400V. Also, the current rating is the rms current through the diode, I_D,

$$I_D = \frac{I_{in}}{K\cdot\sqrt{2}} = 24.43\,A \quad (5)$$

2.2 DC link and buffer battery

Due to the slow dynamic response of the fuel cell, a battery backup system is essential to manage sudden load changes at the inverter output terminals. As shown in Fig. 1, the battery backup is connected to the DC-link (400V) between the DC-DC converter and the inverter. A high voltage battery system was adopted to avoid another power processing stage and to minimize the cost of the power electronics. The employed battery bank is composed by a string of thirty-three (33), 12V, 18Ah Panasonic sealed rechargeable lead-acid batteries. In total, the batteries will provide 4kW for one hour or 6.9kW for ten minutes. An inductor is connected in series with the battery (Fig. 3) to block the inverter ripple current from flowing into the battery bank. Since the DC-DC converter stage regulates the inverter to 400V, the 396V battery bank will essentially float on the DC-bus.

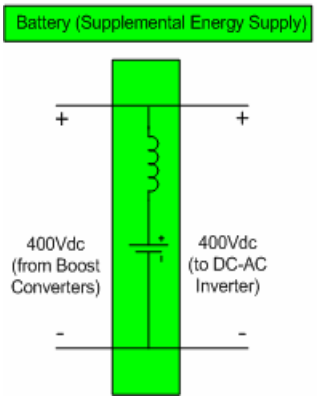

Figure 3: Backup battery used in the design

2.3 Inverter topology

Three inverter legs serve to generate the 120V/240Vac output as well as to establish a neutral point to the output of the system. This design is known as a solid DC link and is an improvement on the "split DC link" commonly used in this type of application. In this design, the neutral is established by the switching scheme implemented on the DSP rather than relying on series connection node of the two capacitors (or capacitor banks) that are attached to the DC link. Relying on this midpoint assumes that the two capacitors are precisely equal to each other, and that the currents being supplied by the two phases are identical. In contrast, using the DSP to establish the neutral point is more efficient and effective. Also, in the six switch configuration (Fig. 4) the dc-link current i_{dc} consists of higher order harmonics when the output load is unbalanced and/or nonlinear. This contributes to smaller size of the dc-link capacitor.

The 400V provided at the output of the DC-DC converter is used across three parallel switching legs. Each leg consists of two IGBT's connected in series across the 400V input. The IGBT's are controlled by the gating signals sent from the DSP. A cascaded fourth order LC filter is used to filter out high frequency harmonics components in the output voltage. The design of the LC filter is not trivial and must be optimized in order to maintain efficiency as well as the THD rating.

After the voltage is filtered by the LC filter, a voltage sensor measures the output voltage. This voltage is fed back into the DSP to ensure that the output voltage meets the power quality standards.

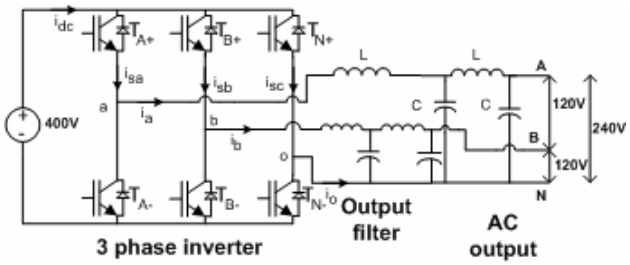

Figure 4: General schematic for DC-AC inverter used in the design.

Component sizing for the inverter is outlined as follows. Consider the case when Phase-B is not loaded and Phase-A is on full load (5000W). The peak amplitude of the fundamental frequency component is the product of m_a and ½ V_{DC}, where m_a is the modulation index. A modulation index of 0.9 is assumed for this example.

$$(V_{AO})_1 = m_a \cdot \frac{V_{DC}}{2}\sin(w_1 t) \quad 0 < m_a < 1 \tag{6}$$

The switching function sw_1 of the half bridge inverter is,

$$sw_1 = 0.5 + \frac{0.9}{2} + \sin w_1 t + \textit{higher order terms} \tag{7}$$

The Phase-A output current is assumed to contain fundamental and third harmonic component due to nonlinear load.

$$i_a = \sqrt{2} I_1 \sin(w_1 t - f_1) + \sqrt{3} I_3 \sin(3w_1 t - f_3) + \ldots \tag{8}$$

The current through the switch T_{A+} is given by

$$i_{SA} = sw_1 \cdot i_a = \frac{\sqrt{2}}{2} I_1 \sin(w_1 t - f_1) + \frac{\sqrt{3}}{2} I_3 \sin(w_3 t - f_3) + \ldots. +$$
$$+ \frac{0.9}{2}\sqrt{2} I_1 [\cos f_1 - \cos 2(w_1 - f_1]) + \frac{0.9}{2}\sqrt{2} I_3 [\cos f_3 - \cos 3(w_1 - f_3]) + \ldots \tag{9}$$

The dc-link current i_{dc} given by

$$i_{dc} = sw_1 i_a + sw_2 i_b + sw_3 i_c \tag{10}$$

If I_{rms} is the rms value of the Phase-a output current, neglecting higher frequency terms, we have

$$I_{rms} = \sqrt{I_1^2 + I_3^2} \tag{11}$$

Assuming I_3=0.7 I_1 which is typical of single phase rectifier type nonlinear loads,

$$I_{rms} = 1.22 \cdot I_1 \quad (12)$$

When supplying full load of 5000W at unity power factor,

$$I_{rms} = \frac{5000}{120} = 41.7A \quad (13)$$

which gives,

$$I_1 = \frac{41.7}{1.22} = 34A \quad (14)$$

To consider the inverter switch ratings, it is been shown that the rms current i_{sA} is 41.7A. Thus, rms current rating of each switch is

$$I_T = \frac{41.7}{\sqrt{2}} = 30A \quad (15)$$

Voltage should be above the DC link voltage of 400V, so the rating of the IGBT's is 600V.

2.4 DC-DC converter control strategy

The linear voltage-current characteristic from the fuel cell, as shown in Fig.5, allowed us to implement simple digital control algorithm for the DC-DC converter stage. This voltage-current relationship is used to calculate the proper current-limit setting for the DC-DC converter using the Power Available (PA) signal (analog) from the fuel cell. This ensures that the power drawn from the fuel cell does not exceed its capability at any given moment. The remaining power necessary to satisfy the load is provided by the battery backup system (Fig. 1). The inverter, on the other hand, determines the actual power drawn by the loads and communicates that information to the fuel cell to either increase or decrease its power output. This ensures that the fuel cell has sufficient time to adjust its power generation to meet changes in the load demand.

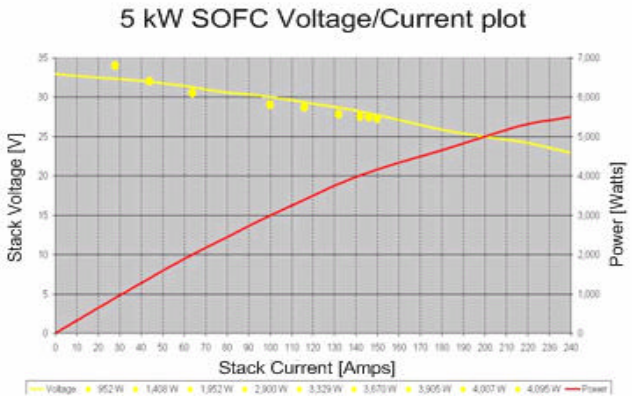

Figure 5: V-I and P-I curves

The control diagram for the DC-DC converter is illustrated in Fig. 6 Here a inner PI control loop controls the current being drawn from the fuel cell and the outer voltage PI control is used to regulate the output voltage to its reference value. The output of the outer control loop is limited by the value calculated from the fuel cell voltage current characteristic and from the power available signal. This limit is changed as more power is available at the fuel cell terminals. From the system operation three different scenarios are possible when the fuel cell system supplies the load. The first situation occurs when the fuel cell system is capable of fully supplying the load demand and the DC-DC converter maintains the constant battery voltage. In the second scenario, the fuel cell system is unable to accommodate the load, so the auxiliary device (battery) feeds one part of the load decreasing its state of charge. The last possibility refers to a situation when the fuel cell must supply not only the load but also charge the battery.

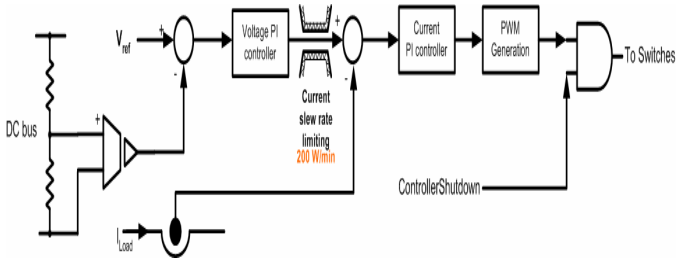

Figure 5: Control diagram of the DC-DC controller

The proposed control is able to compensate for load changes under these three conditions during the operation of the system.

III COST EVALUATION

The cost evaluation of the Fuel Cell Inverter considers two types of costs. First, the cost of the development process and second the cost evaluation based on a normalized system cost projection. The development budget helped guide the design team in organizing and prioritizing time and resources for optimum use. The working budget allowed team members to make the best cost-design decisions by showing the team actual costs of the specific components for the fuel cell inverter.

The cost of three different topologies was calculated. The topologies under study were:

a. Two stage DC-DC converter with a high-frequency isolation transformer followed by a six switch DC-link inverter, output filter for 120V/240V output. (see Fig 1A in Appendix A)
b. A boost converter, a low voltage four switch 1-phase inverter followed by a 60Hz line frequency transformer with two secondary windings to produce 120V/240V output. (Fig. 2A in appendix A)

c. The proposed converter in this paper: Push-pull converter and solid dc-link inverter. (described in Figs. 1, 2 and 4)

The cost evaluation considered the component and manufacturing cost of each unit, and it was performed using the cost analysis spreadsheet provided by the Future Energy Challenge organizing committee [3]. Appendix-A describes the usage of the cost analysis spreadsheet [3] for the above described three converter topologies. The results from this analysis are summarized in Table 1.

Topology	Cost [US$]
a	1040.26
b	357.40
c	652.34

Table 1. Cost evaluation comparison

From Table. 1, it can be concluded that the topology (b) shown in Fig. 2A (in Appendix-A) appears to be the most cost efficient. However this approach employs a bulky 60Hz transformer and may not meet the weight/volume specifications of a fuel cell converter in most applications. On the other hand the topology "c" presented in this paper has many advantages as described and has the potential to result in an efficient, compact design.

IV TEST RESULTS FOR DC-AC INVERTER

Figure 7 shows the output voltage and current measured in the prototype when feeding a 500W linear load. The AC_{RMS} waveform shown is the sinusoidal output voltage VAO after the filter stage. This voltage is below the required voltage for the final specification purposes. However, the point of this experiment was not necessarily to test the current and voltage output capabilities of the inverter, but instead served to verify the effectiveness of the switching scheme.

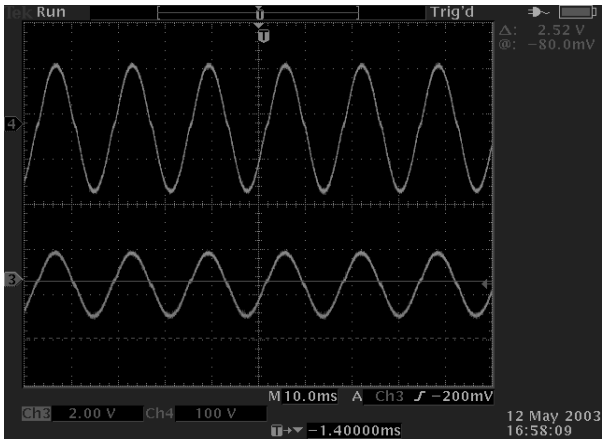

Figure 7: Output voltage for a 500W linear load.

Figure 8 shows experimental waveforms measured when feeding a 1000W non linear load.

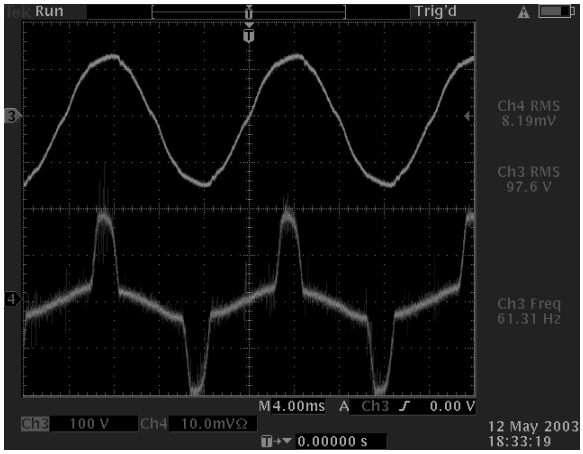

Figure 8: Output voltage for a 1000W non-linear load.

From this figure it can be seen that despite the severe non linear current being drawn by the load the inverter is capable of maintaining a good quality voltage signal.

V CONCLUSIONS

In this paper, a low cost high efficiency power conditioning system is presented and evaluated. This power conditioning unit incorporates an innovative dc-dc control strategy. This control strategy takes in to account the slow dynamic response of a typical fuel cell, thus limiting the amount of power it can deliver. Also an efficient three leg inverter topology is used to reduce loses and reliability issues typically found in a conventional bi-phase inverter with a split dc link.

Cost analysis showed that the proposed topology meets the targeted price per kilowatt, resulting in a more convenient approach than other alternative topologies.

VI REFERENCES

[1] Jiang, H.J., Qin, Y., Du, S.S., Yu, Z.Y., Choudhury, S., *DSP based Implementation of a Digitally-Controlled Single Phase PWM Inverter for UPS*, Telecommunications Energy Conference, 1998, INTELEC. Twentieth International, 1999, Page(s): 221 -224

[2] Shih-Liang Jung, Hsiang-Sung Huang, Meng-Yueh Chang, Ying-Yu Tzou,
DSP-based Muliple-Loop Control Strategy for Single-Phase Inverters Used in AC Power Sources, Power Electronics Specialists Conference, 1997. PESC '97 Record., 28th Annual IEEE
Volume: 1 , 1997 , Page(s): 706 -712 vol.1

[3] Abdel-Rahim, N., Quaicoe, J.E. *Multiple feedback loop control strategy for single-phase voltage source UPS inverter*, Power Electronics Specialists Conference, PESC '94 Record., 25th Annual IEEE , 1994 , Page(s): 958 -964 vol.2

[4] Abdel-Rahim, N.M., Quaicoe, J.E. *Analysis and Design of a Multiple Feedback Loop Control Strategy for Single-Phase Voltage-Source UPS Inverters*, Power Electronics, IEEE Transactions on
Volume: 11 4 , July 1996 , Page(s): 532 -541

[5] Robert W. Erickson, Dragan Maksimovic, *Fundamentals of Power Electronics*, Kluwer Academic Publishers, 2001

[6] Ned Mohan, Tore M. Undeland, William P. Robbins, *Power Electronics, Converter Applications and Design* John Wiley and Sons, 1995

[7] Gopinath, R., Sangsun Kim, Jae-Hong Hahn, Webster, M, Burghardt, J., Campbell, S., Becker, D., Enjeti, P., Yeary, M., Howze, J. *Development of a low cost fuel cell inverter system with DSP control*, Power Electronics Specialists Conference, Volume: 1 , 23-27 June 2002, Page(s): 309 -314 vol.1

[8] IEEE/DOE Sponsored "Future Energy Challenge", Website: http://www.energychallenge.org

APPENDIX

A1. Cost Evaluation topology "a", Figure 1A

	QTY	DESIG	MEASURE	UNIT	VOLT (Vpk)	VOLT (Vrms)	CUR (Avg)	CUR (Arms)	UNIT COST	EXTENDED COST
DIODE	4	D1,2,3,4			755		7		2.54	10.16
DIODE - DUAL MODUL	1	D5			50		85		2.45	2.45
IGBT	6	S1,2,3,4,5,6			400		23		3.75	22.52
TRANSISTOR	3	S7,8,9			50		50		1.25	3.74
MOSFET	2	T1,2			96		50		6.38	12.77
CAP (ALUM)	1	C5	10	uF	60				0.11	0.11
CAP (ALUM)	4	C1,2,3,4	280	uF	250				2.52	10.10
CAP (FILM)	4	C6,7,8,9	30	uF	180				5.09	20.38
CHOKE	2	L1,2	500	UH				13	45.29	90.58
CHOKE	1	L3	100	UH				212	295.64	295.64
CHOKE	4	L4,5,6,7	44	UH				66	51.38	205.50
TRANSFORMER	1	TR1				580		11	13.29	13.29
LOSSES			1000	W					83.33	83.33
CONTROL										154.11
PACKAGING										115.58
TOTAL										1040.26

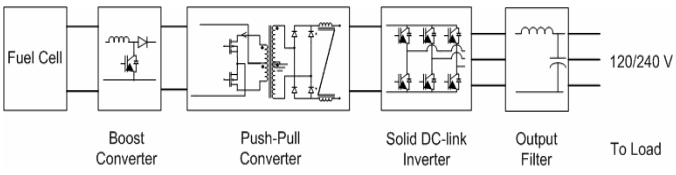

Figure 1A: Topology "a"

A2. Cost Evaluation topology "b", Figure 2A

	QTY	DESIG	MEASURE	UNIT	VOLT (Vpk)	VOLT (Vrms)	CUR (Avg)	CUR (Arms)	UNIT COST	EXTENDED COST
DIODE	4	D1,2,3,4			200		60		3.15	12.59
IGBT	4	S5,6,7,8			200		13		1.14	4.57
MOSFET	4	S1,2,3,4			200		52		9.40	37.60
CAP (ALUM)	1	C1	100	uF	50				0.14	0.14
CAP (ALUM)	2	C2,3	1000	uF	100				1.49	2.97
CAP (FILM)	2	C5,6	60	uF	170				8.59	17.19
CHOKE	2	L2	125	UH				22	43.93	87.86
TRANSFORMER	2	TR1				123		22	9.25	18.49
LOSSES			1000	W					83.33	83.33
CONTROL										52.95
PACKAGING										39.71
TOTAL										357.40

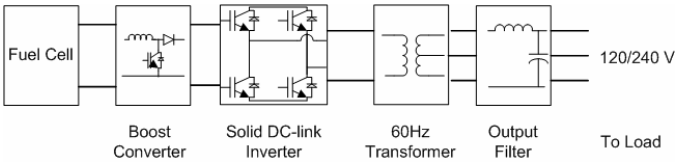

Figure 2A: Topology "b"

A3. Cost Evaluation topology "c"

	QTY	DESIG	MEASURE	UNIT	VOLT (Vpk)	VOLT (Vrms)	CUR (Avg)	CUR (Arms)	UNIT COST	EXTENDED COST
DIODE	4	D1,2,3,4			980		15		3.39	13.57
IGBT	6	S1,2,3,4,5,6			400		23		3.75	22.52
MOSFET	6	T1,2,3,4,5,6			43		50		4.96	29.75
CAP (ALUM)	1	C5,6	10	uF	30				0.10	0.10
CAP (ALUM)	4	C1,2,3,4	280	uF	250				2.52	10.10
CAP (FILM)	4	C7,8,9,10	30	uF	180				5.09	20.38
CHOKE	2	L1,2	500	UH				8.5	42.55	85.09
CHOKE	4	LI3,4,5,6,	44	UH				66	51.38	205.50
TRANSFORMEI	1	TR1				400		15	12.87	12.87
LOSSES			1000	W					83.33	83.33
CONTROL										96.64
PACKAGING										72.48
TOTAL										652.34

A 10KW SOFC-Low Voltage Battery Hybrid Power Processing Unit for Residential Use

Jinhee Lee, Jinsang Jo, Sewan Choi*
Department of Control & Instrumentation Eng.
Seoul National University of Technology
Seoul, Korea
*E-mail: schoi@snut.ac.kr

Soobin Han**
Electrics & Lighting research Center
Korea Institute of Energy research
Daejeon, Korea
**E-mail: sbhan@kier.re.kr

***Abstract*—This paper outlines a 10kW power processing unit for 5KW SOFC-low voltage battery hybrid power generation which has been developed for participation in the 2003 Future Energy Challenge Competition organized by U.S. Department of Energy and IEEE. The objective of the competition was to develop a fuel cell inverter with minimum requirement for cost of $40/KW and efficiency of 90%. The proposed power processing unit consists of the front-end DC-DC converter, the DC-AC inverter and the bi-directional DC-DC converter. Practical issues such as component rating calculation, high frequency transformer design, heat sink design, and protection are detailed aiming at the cost and efficiency targets. A low-cost controller design is discussed along with current-mode control, output voltage regulation with capacitor balancing and a SOC control for battery management. A 10kW hardware prototype was successfully built and tested in the steady-state as well as in the transient-state. Experimental performances are compared to minimum target requirements of the fuel cell inverter. The cost analysis is done based on the spreadsheets evaluation forms provided in the competition.**

1. INTRODUCTION

A Fuel cell power generation systems are expected to see increasing use in various applications such as stationary loads, automotive applications, and interfaces with electric utilities due to the several advantages over conventional generation systems. These advantages include 1) low environmental pollution 2) highly efficient power generation 3) diversity of fuels(natural gas, LPG, methanol and naphtha) 4) reusability of exhaust heat 5) modularity and 6) faster installation [1].

Fuel cells are generally characterized by the type of electrolyte that they use. Solid oxide fuel cells (SOFC) have grown in recognition as a viable high temperature fuel cell technology. The most striking quality of SOFCs is that the electrolyte is in solid state and is not a liquid electrolyte. The high operating temperature up to 1000°C allows internal reforming, promotes rapid kinetics with non-precious materials and produces high quality byproduct heat for cogeneration or for use in a bottoming cycle. A number of different fuels can be used from pure hydrogen to methane and carbon monoxide. The major advantage of SOFC lies in its efficiencies raging from 55 to 60% [2].

In general, the function of a power processing unit (PPU) in a fuel cell generation system is to convert the DC output power from the fuel cell to regulated AC power. The power conditioning unit that basically consists of an inverter is required to have the following characteristics: 1) allowable for wide output voltage regulation of fuel cell 2) controllability of output voltage 3) available for isolated operation and line parallel operation 4) fast reactive power dispatch 5) low output harmonics 6) high efficiency and 7) suitable for high power system [3]. Fuel cell production costs are currently decreasing and have nearly achieved energy costs that are competitive with local utility rates. The inverter cost must also decrease while at the same time increasing efficiency, reliability, and power quality levels. The cost reduction of a PPU will enable the fuel cell systems to penetrate rapidly into the utility market.

Table I. System Specification

Design item	Minimum Target Requirement	
Manufacturing cost	Less than US$40/kW in high volume protection	
Output Power	nominal	5kW continuous @ DPF 0.7
	overload	10kW overload for 1 minute @ DPF 0.7 5kW from fuel cell and 5kW from battery
Energy source	Primary source (SOFC)	29V nominal, 22~41 VDC, 275A max. from 5kW fuel cell
	Battery	48V nominal, +10% ~ -20%, 500Wh
Output voltage	Split single-phase 120V/240V, 60Hz	
	Voltage regulation	± 6%
	Frequency regulation	± 0.1Hz
	THD	Less than 5%
Acoustic noise	Less than 50dBA @ 1.5 m distance	
Overall efficiency	Higher than 90%	
Protection	Over current, over voltage, short circuit, over temperature, and under voltage	

2. PROPOSED POWER PROCESSING UNIT

Fig. 1 shows the block diagram of the SNUT fuel cell inverter system. The DC voltage from the fuel cell, $29V_{DC}$ nominal, is first converted to $400V_{DC}$ via an isolated high frequency DC-DC converter. The 400V DC-DC converter output is then converted to 120V/240V, 50/60 Hz, single-phase AC by means of a PWM inverter stage. The 48V battery bank is connected to the 400V DC link via a bi-directional DC-DC converter for charge and discharge modes of operation.

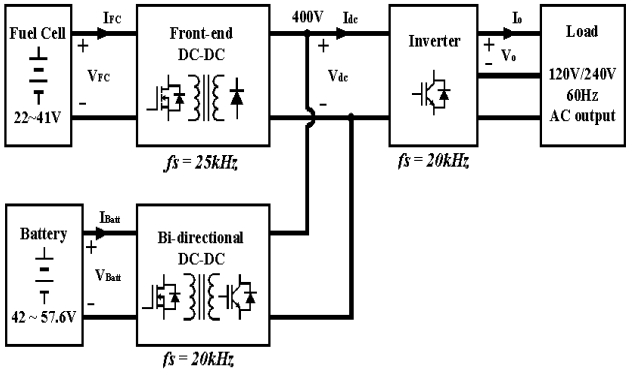

Fig. 1 Block Diagram of the SNUT Fuel Cell Inverter System

2.1 Front end DC-DC converter

A front end DC-DC converter is required to boost an unregulated fuel cell voltage of 29V nominal to a regulated 400V. As shown in Fig. 2, the full-bridge type with two diode bridges connected in series at the secondary is a topology of choice. High frequency transformers are employed to allow a low voltage to be boosted to two split $200V_{DC}$ buses for the DC link to the Inverter. The reason why two 2.5kW high frequency transformers are employed instead of using a 5kW high frequency transformer is to reduce the leakage inductances and therefore to reduce the duty loss. The reduced duty loss also reduces turns ratio of the transformer. This in turn reduces the voltage rating of diodes in the secondary side and the current rating of MOSFETs in the primary side. The voltage source type has been chosen because the inductor in the current source type should have a large peak current rating of 275A.

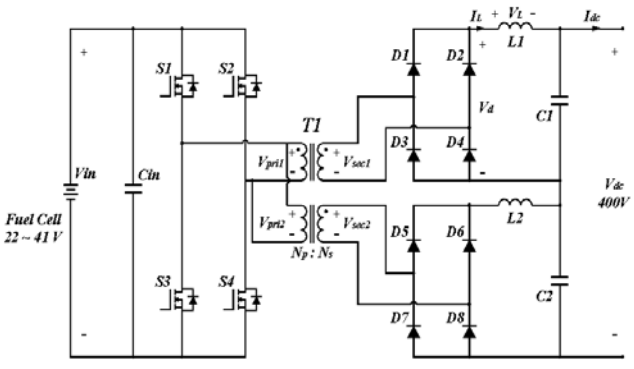

Fig. 2 Front-end DC-DC Converter

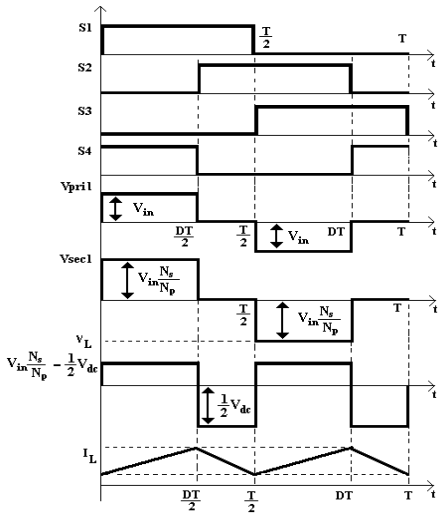

Fig. 3 Main waveforms of the front-end DC-DC converter

Fig. 3 shows the main waveforms of the front-end DC-DC converter. From the inductor voltage V_L an equation can be written as,

$$(V_{in} \cdot \frac{N_s}{N_p} - \frac{1}{2} \cdot V_{dc}) \cdot \frac{DT}{2} = \frac{1}{2} \cdot V_{dc} \cdot \left\{ \frac{T \cdot (1-D)}{2} \right\} \quad (1)$$

Therefore, the duty cycle of the proposed front-end DC-DC converter is obtained by,

$$D = \frac{N_p \cdot V_{dc}}{4 \cdot N_s \cdot V_{in}} \quad (2)$$

According to eqn.(2), the duty cycle ranges 0.24 to 0.45 to regulate the dc link voltage of 400V when the fuel cell voltage varies between 22V and 41V.

Fig. 4 shows the block diagram for feedback control of the front end DC-DC converter. The first goal of the control is to regulate the dc link voltage. A PI compensator is used for the voltage control. A current control is also implemented to improve the dynamic characteristic of the system and to reduce current ratings of the power components during load transient. The current reference is restricted by a current limiter whose value is adjusted by a command from the fuel cell controller so that the power drawn from the fuel cell does not exceed its capability. A low-cost phase-shift PWM controller, UC3895, is employed for control of the front-end DC-DC converter. It allows constant frequency PWM in conjunction with resonant zero-voltage switching to provide high efficiency at high frequency [9].

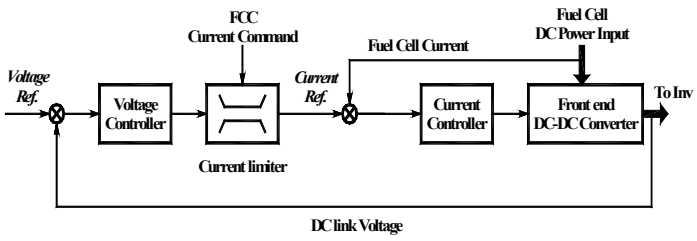

Fig. 4 Control block diagram for the front end DC-DC converter

2.2 DC-AC Inverter

The inverter system consists of two half-bridge inverters, utilizing center tapped dc link capacitors to generate a split single-phase 120/240V_{ac}, 60Hz output as shown in Fig. 5. An output L-C filter stage is employed to reduce the ripple component and to draw a low THD AC waveform.

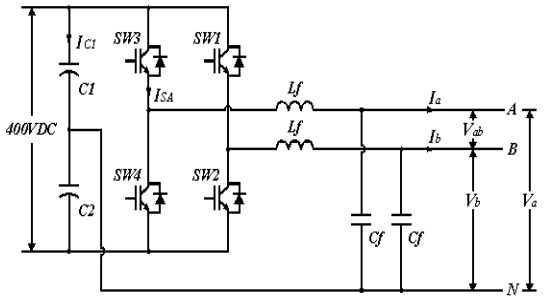

Fig. 5 DC-AC Inverter

A low cost DSP Texas Instrument TMS320LF2407 DSP is implemented to provide the control for the inverter system. The DSP control will offer increased flexibility and will minimize component cost. The goal of the DSP control is as follows: 1) Supervise the whole PPU. 2) Generate the PWM gating signals for IGBTs in the inverter stage. 3) Implement output voltage regulation under varying load conditions. 4) Send the bi-directional DC-DC converter a current reference. 5) Communicate with the fuel cell controller.

To meet the output voltage tolerance requirement the AC output voltage is sensed and a closed-loop control is implemented with a digital PI compensator in the DSP. In the meanwhile, unbalance in dc-link capacitor voltages causes generation of even harmonics in the inverter output voltages. A simple output voltage regulation method with capacitor voltage balancing function is implemented as shown in Fig. 6. Suppose output voltage V_a has a positive dc offset, which means that the upper capacitor voltage is greater than the lower capacitor voltage. The output voltage V_a is sensed and passed through a low pass filter to obtain a dc component of voltage V_a. This causes addition of a positive value to the reference output voltage V_b^* resulting in a decrease in upper capacitor voltage and an increase in lower capacitor voltage.

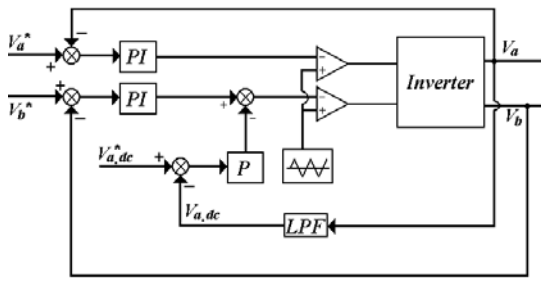

Fig. 6 Output voltage regulation and capacitor voltage balancing

2.3 Bi-directional DC-DC Converter

The fuel cell has a slow response, and therefore the power demand from the load and the power supply from the fuel cell does not coincide during a transient load. Therefore, a secondary energy source is required to match the power difference between the fuel cell and the load. High voltage batteries could be directly connected to the 400V dc link without any intermediate power converter, but the high voltage battery is relatively expensive and may have the battery cell unbalance problem in the long run. A 48V lead acid battery pack is connected to the 400V dc link via a bi-directional DC-DC converter shown in Fig. 7. A current-source push-pull converter employing MOSFETs is operated to discharge the battery whereas a voltage-source full-bridge converter employing IGBTs is operated to charge the battery.The control block diagram for the bi-directional DC-DC converter is shown in Fig. 8. The DSP in the inverter system determines the current reference for the bi-directional DC-DC converter by calculating the difference in real power between the PPU input and the load. The two PWM controllers, UC3825 and UC3895, are employed for charge and discharge modes of operation, respectively. One should be in idle state while the other is in operation. Fig. 9 shows the inductor voltage and current waveforms for charge and discharge modes, respectively. Let us define turns ratio n_2 of the high frequency transformer T_2 to be (See Fig. 7),

$$n_2 = \frac{N_s}{N_p} \tag{3}$$

During the charge mode, we have

$$-(V_{batt} - \frac{V_{dc}}{n_2}) \cdot DT_S = V_{batt} \cdot (\frac{1}{2} - D)T_S \tag{4}$$

which gives

$$\therefore \frac{V_{batt}}{V_{dc}} = \frac{2D}{n_2} \quad \text{(where, } 0 < D < 0.5\text{)} \tag{5}$$

During the discharge mode, we have

$$V_{batt} \cdot D_d T_S = -(V_{batt} - \frac{V_{dc}}{n_2}) \cdot (\frac{1}{2} - D_d)T_S \tag{6}$$

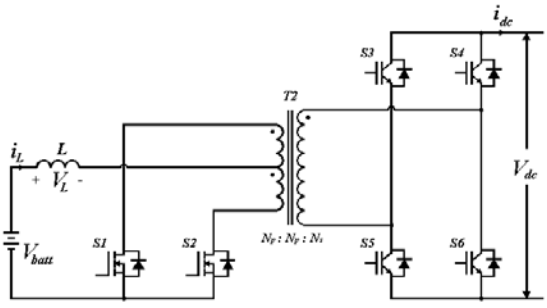

Fig. 7 Bi-directional DC-DC Converter

which gives

$$\therefore \frac{V_{dc}}{V_{batt}} = \frac{n_2}{(1-2D_d)} \quad (0<D_d<0.5) \tag{7}$$

$$\therefore \frac{V_{dc}}{V_{batt}} = \frac{n_2}{2(1-D)} \quad (0.5<D<1, \text{ where } D = 0.5+D_d) \tag{8}$$

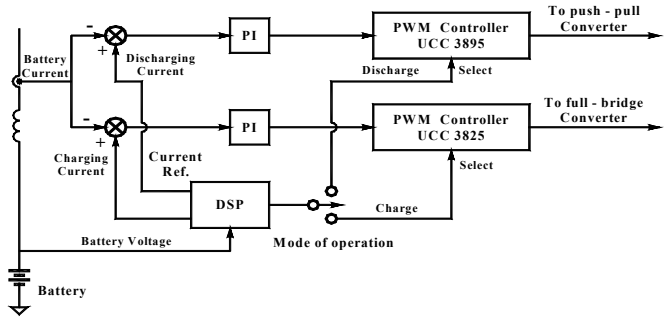

Fig. 8 Control block diagram for the bi-directional DC-DC converter

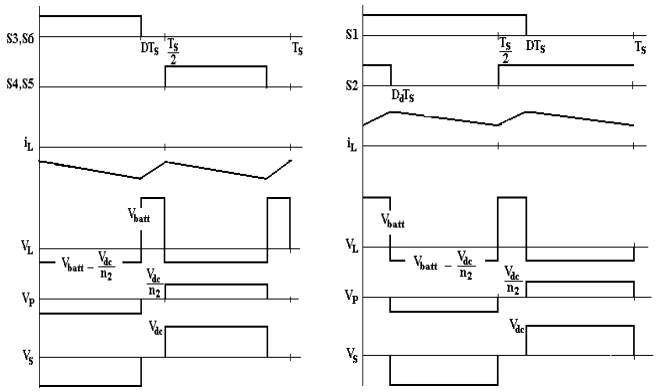

(a) Charge mode (b) Discharge mode

Fig. 9 Inductor voltage & current waveforms

2.4. Battery management

An optimum use of battery combined with fuel cell can reduce the cost of the fuel cell system, or improve the system performance such as reliability and lifetime. To cope with the slow dynamic response of the fuel cell(Maximum Slew Rate = 200 watts/minute), a 48 V battery pack is used as a secondary energy source to supply transient load since the fuel cell system including a reformer is sluggish even if the fuel cell stack has a fast response.

During an overload condition the PPU is supposed to draw 5kW from the fuel cell and 5kW from the battery for maximum 1 minute. Charging and charge management must be provided such that charge is unchanged at the end of a 24 hour test sequence [8]. The SNUT fuel cell inverter determines the mode of operation based on battery state of charge (SOC). The SOC could be measured simply by integrating the battery charging current I_{bat} as follows,

$$SOC = \frac{Q_0 - \int i_{bat}\, dt}{Q_n} \tag{9}$$

where Q_o is initial charge and Q_n is rated ampere-hour of battery. The initial charge Q_o is set to be Q_n when the system starts from full battery charge. More accurate measurement requires in-depth considerations of various parameters such as temperature, discharge rate, age and cumulative calculation errors [5,6]. But this research is out of paper's scope and it is the authors' intention to show the mode of operation determined by SOC as an index.

In hybrid electric vehicle system where regeneration braking is considered, the SOC is maintained between 0.4 and 0.8. However, the SOC is controlled to maintain 1 for residential use, which is the case of the competition. Detailed operational procedure is as follows. When the load power exceeds 5kW, which is the maximum output power of the fuel cell, battery discharges its energy to the load through a bi-direction converter until the overload condition is removed. When the load jumps, but not overloaded, the battery should also discharge until the fuel cell power increases and is able to supply the demanded load power. After the discharging mode ends, the fuel cell power continues to increase to charge the battery until the SOC reaches 1. In charging mode, the fuel cell charges the battery with a current proportional to depth of discharge, but limits the current to a maximum value recommended by manufacturer. The magnitude of the charging current in the SNUT fuel cell inverter system is determined as shown in Fig. 10.

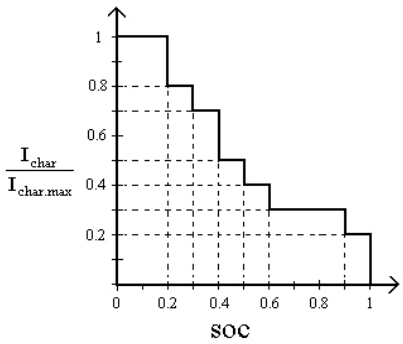

Fig. 10 Battery charging current

2.5. Protection and Diagnostic

The proposed PPU provides the protection capability of over current, short circuit, over/under voltage and over temperature in the circuit. Table II lists all the protection implemented in the proposed PPU. The PWM control IC such as UC3895 provides the capability to detect any fault signal through an input pin of the

chip and will shut down the chip by disabling all the gate signals to the switches. Temperature protection is implemented by using a bimetal as a temperature sensor that is mounted on the heat sink. If the temperature of the sensor rises over 60°C a fan on the heat sink starts to operate. If the temperature of the sensor rises over 80°C a signal is sent to the gate drive for immediate shutdown. A PC is connected to the inverter system so that the output phase voltage, the output phase current, the output power, the frequency of the output voltage and some inverter status including faults, etc. could be monitored. All the data monitored are also recorded in the PC and updated every two minutes so that inverter status could be interpreted after the fault has occurred.

Table II. Protection

Fuel Cell	OV (over 41V), UV (under 22V), OC (over 275A)
DC-link	OV (over 500V), UV (under 300V)
Load	OC (100%~110%, 1min.), SC (over 110%)
Battery	OV (over 56.7V), UV (under 42V)
Heatsink	Over 60°C → Fan Start, Over 80°C → Shutdown

3. POWER COMPONENT DESIGN

The power components of the proposed PPU are designed with the following system parameters.

- Switching frequency for the front-end DC-DC converter : 25kHz
- Switching frequency for the DC-AC converter : 20kHz
- Switching frequency for the bi-directional DC-DC converter : 20kHz
- DC link voltage V_{dc} : 400V
- Transformer turns ratio N_{p1}: N_{s1} = 1 : 10
- Permissible ripple current ΔI_{L1} = 50% of maximum dc link current
- Permissible ripple voltage ΔV_{c1} = 10% of the dc link voltage

Power switches

The ratings of the power switching devices used in each section of the converters are listed in Table III. A safety margin for MOSFETs and diodes in the front-end DC-DC section should be considered due to voltage spikes originated from the leakage inductance and/or the ringing phenomenon at the secondary winding of the high frequency transformer. A ultra-fast recovery diode is chosen to lower the switching loss due to the high switching frequency operation. Since the maximum battery discharge current is much larger than the maximum battery charge current, the switch ratings of the bi-directional DC-DC converter should also be determined based on the discharge mode of operation at full load (5KW, 1min.).

Table III. Ratings of the Power Switching Services

Section	Component	Designed value		Actual device Selection
Front-end DC-DC converter	MOSFET (S1~S4)	V_{peak} (V)	41	IXFN180N10 (100V, 180A, 8mΩ)
		I_{rms} (A)	177.4	
	Diode (D1~D8)	V_{peak} (V)	410	DSEI2X31-10B (1000V, 30A, trr = 35ns)
		I_{rms} (A)	8.8	
DC-AC Inverter	IGBT (SW1~SW4)	V_{peak} (V)	420	2MBI200N-060 (600V, 200A, $V_{CE(sat)}$ 1.5V)
		I_{rms} (A)	50	
Bi-directional DC-DC converter	MOSFET (S1,S2)	V_{peak} (V)	140	IXFN180N20 (200V, 180A, 10mΩ)
		I_{rms} (A)	88.4	
	IGBT (S3~S6)	V_{peak} (V)	420	MG50J2YS50 (600V, 50A, $V_{CE(sat)}$ 2.1V)
		I_{rms} (A)	11.9	

High Frequency Transformer

Ferrite core is chosen as a material of a high frequency transformer. The power handling capacity of a transformer core can be determined by its area product $W_a A_c$, where W_a is the available core window area, and A_c is the effective core cross-sectional area.
The area product $W_a A_c$ is given by[9],

$$W_a A_c = \frac{P_{dc} \cdot C \cdot 10^8}{4 \cdot e \cdot B \cdot f_s \cdot K} = 23.47\, cm^4 \qquad (10)$$

where P_{dc} is output power, C is current capacity which is $5.07 \times 10^{-3} cm^2 / Amp$ for '**EER**' core, e is transformer efficiency which is assumed to be 90%, B is flux density which is assumed be 2000(gauss), f_s is switching frequency and K is winding factor which is 0.3 for primary side only. Using the core selection table by area product distribution, the core of 47054-EC was selected. Once a core is chosen, the calculation of primary and secondary turns and their wire sizes are readily accomplished. The number of primary turns is given by [9],

$$N_p = \frac{V_P \cdot 10^8}{4 \cdot B \cdot A \cdot f_s} = \frac{41 \cdot 10^8}{4 \cdot 2000 \cdot 3.39 \cdot 25000} = 3.18 turns \qquad (11)$$

Here, V_p is the peak primary voltage and A is the cross-sectional area of the core. Considering duty loss of 20% at the secondary winding of the transformer originated from the leakage inductance, the final number of turns for primary and secondary windings are determined to be N_p : N_s = 6 : 90. The wire sizes AWG 0 and AWG 12 are selected from AWG table for the primary and secondary wires whose circular mil requirements are 93,500 and 5,900, respectively. Ritz wires were used to reduce the copper loss due to skin effect.

DC Link Inductor and Capacitors

From eqn.(1), the inductance can be obtained by,

$$L = \frac{(1-2D) \cdot (\frac{N_s}{N_p}) \cdot V_{in} \cdot D}{\Delta I \cdot f_s} = 100\ \mu H \qquad (12)$$

At displacement factor of 0.7 the maximum output VA becomes,

$$VA_{out} = \frac{10000}{0.7} = 14280 \ VA \tag{13}$$

The full load current of each phase is given by,

$$I_{a,rms} = \frac{14280}{2 \cdot 120} = 59.5 \ A \tag{14}$$

For the sake of simplicity, the output current i_a is assumed to consist of only fundamental ($I_{a,1}$) and third harmonic ($I_{a,3}$). Further, assuming $I_{a,3} = 0.7 I_{a,1}$ since this is a typical case of a single phase rectifier type nonlinear load [4],

$$I_{a.rms} \cong \sqrt{I_{a,1}^{\ 2} + I_{a,3}^{\ 2}} = 1.22 I_{a,1} \tag{15}$$

The most dominant component of the DC-link capacitor current i_{c1} is the fundamental frequency current, the rms value of which equals,

$$I_{c1,1} \cong \frac{1}{2} \cdot I_{a,1} = 24.3 \ A \tag{16}$$

Capacitance can be obtained by,

$$C_1 = \frac{I_{c1,1}}{\omega \Delta V_{c1}} = \frac{24.3}{2\pi \cdot 60 \cdot 20} = 3222 \ \mu F \tag{17}$$

Output filter

Based on the design procedure in [4], the filter inductance and capacitance become,

$$L_f = \frac{X_L}{2\pi f_1} = \frac{0.035}{2\pi \cdot 60} = 92.84 \ \mu H \tag{18}$$

$$C_f = \frac{1}{2\pi \cdot f_1 \cdot X_c} = 16 \ \mu F \tag{19}$$

Battery Inductor

The ripple component in the charging current should be restricted by an inductor on the battery side. The magnitude of the charging current depends on the capacity of the battery. The maximum charging current is assumed to be 45A for battery of 48V, 155Ah. We allow the ripple current to be 20% of the maximum charging current, that is, $\Delta i_L = 9$A.

During the charge mode, the duty ratio D lies between $0.33 < D < 0.5$.

When the switches S3 and S6 are turned on during the charge mode we have (See Fig. 9),

$$\frac{(V_{dc} / n_2) - V_{batt}}{L} = \frac{\Delta i_L}{DT_S} \tag{20}$$

Then, the worst case inductance is obtained by,

$$\therefore L = \frac{(1-2D) \cdot D}{n_2 \cdot \Delta i_L \cdot f_s} \cdot V_{dc} = 39 \ \mu H \tag{21}$$

The current rating of the inductor is dominated by discharge mode of operation. The rms inductor current at a maximum discharge becomes $I_L = 113$ (A).

Heat sink

The heat sink is a crucial and a costly component of the PPU. The first step is to calculate the power dissipation of switching devices. Then, a thermal equivalent circuit for analyzing thermal characteristic of the heat sink is defined as shown in Fig. 11, where two different power devices are mounted on a heat sink. Given power loss P_l (where, l = 1 or 2) of a switching device, junction to case thermal resistance $R_{jc,l}$ case to heat sink thermal resistance $R_{ch,l} = 0.3$°C/W, ambient temperature $T_a = 40$°C, and juntion temperature $T_{j,l}$, heat sink to ambient thermal resistance R_{ha} can be obtained in the following procedure. The case temperature $T_{c,l}$ can be given as,

$$T_{c,l} = T_{j,l} - P_l \cdot R_{jc,l} \tag{22}$$

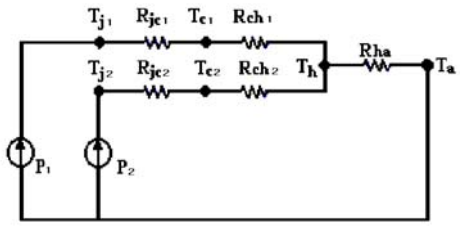

Fig. 11 Thermal equivalent circuit

Then, heat sink temperature $T_{h,l}$ can be given as,

$$T_{h,l} = T_{c,l} - P_l \cdot R_{ch,l} \tag{23}$$

Then, the total heat sink temperature T_h is,

$$T_h = T_{h,1} + T_{h,2} \tag{24}$$

Finally, heat sink to ambient thermal resistance R_{ha} is obtained by,

$$R_{ha} = \frac{T_h - T_a}{P_1 + P_2} \tag{25}$$

Table IV summarizes the thermal calculation required for the heat sink design. Using the heat sink to ambient thermal resistance, the area of the heat sink required can be calculated or the heat sink can directly be selected from a manufacture by the heat sink to ambient thermal resistance obtained.

Table IV. Thermal Characteristics for the Heat Sink Design

Section	Device	Power loss per unit (W)	R_{jc} (°C/W)	T_j (°C)	T_{c-} (°C)	T_h (°C)	R_{ha} (°C/W)
Front-end DC-DC	MOSFET	48.9	0.21	70.26	60	45.4	0.11
	Diode	13.2	1.25	65.85	49.3		
Inverter	IGBT	120.9	0.22	112.5	85.9	49.7	0.08
Bi-directional DC-DC	MOSFET	107.7	0.18	103.3	80.9		
	IGBT	39.9	0.31	67.5	55.2		

4. EXPERIMENTS AND PERFORMANCE EVALUATION

The output voltage and current waveforms for a steady state condition at 4.4KW load level are shown in Fig. 12. The experimental waveforms were also obtained for a discharge mode of operation, that is, a load increase from 2kW to 2.7kW. In this experiment a DC power supply emulates the fuel cell. The lower trace in Fig. 13(a) shows an increase of the output phase current, and the upper trace in Fig. 13(a) shows the output phase voltage, which is well regulated during the load increase. The upper trace in Fig. 13(b) shows the output current of the front end DC-DC converter whose average value did not change after the transient even if the ripple was slightly increased due to operation of bi-directional DC-DC converter. The lower trace in Fig. 13(b) shows the dc link voltage, which undergoes an overshoot and is stabilized. Fig. 13(c) shows the PWM current waveform on the dc link side of the bi-directional DC-DC converter. Fig. 13(d) shows the current waveform on the battery side of the bi-directional DC-DC. This demonstrates that for a sudden load increase the output voltage is well regulated while the bi-directional DC-DC converter would quickly draw the power difference from battery. Fig. 14 shows variations in SOC and in real power of the PPU input, load and battery sides. Initially, the fuel cell is supplying a load of 600W, and the SOC is being kept at 1. The load power jumps to 2000W at t = 2.13 min., and the battery immediately starts to discharge with a current corresponding to the power difference. The SOC starts to decrease from this moment. As the PPU input power increases at a rate of 200W/minute, the battery power decreases at the same rate until it reaches the demanded load power plus losses. Since the SOC is supposed to be maintained at 1 in the SNUT system, the PPU input power continues increasing to charge the battery until a charging current is set up. The PPU keeps charging with the constant charging current and finishes the battery charge mode when the SOC reaches 1. Photograph of the SNUT fuel cell inverter system is shown in Fig. 15. Experimental performances of some important design items have been obtained and listed in Table V. As shown in Table V, the SNUT prototype inverter met the minimum target requirements for most of the design items such as frequency regulation, THD of the output voltage, output voltage regulation and input current ripple. The cost analysis is based on the spreadsheets evaluation forms provided in the competition. The values in the table indicate only preliminary, relative cost estimates, not dollars.

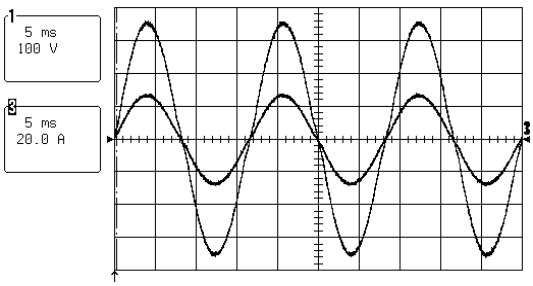

Fig. 12 Experimental waveforms (4.4kW load): output voltage and current : phase AB

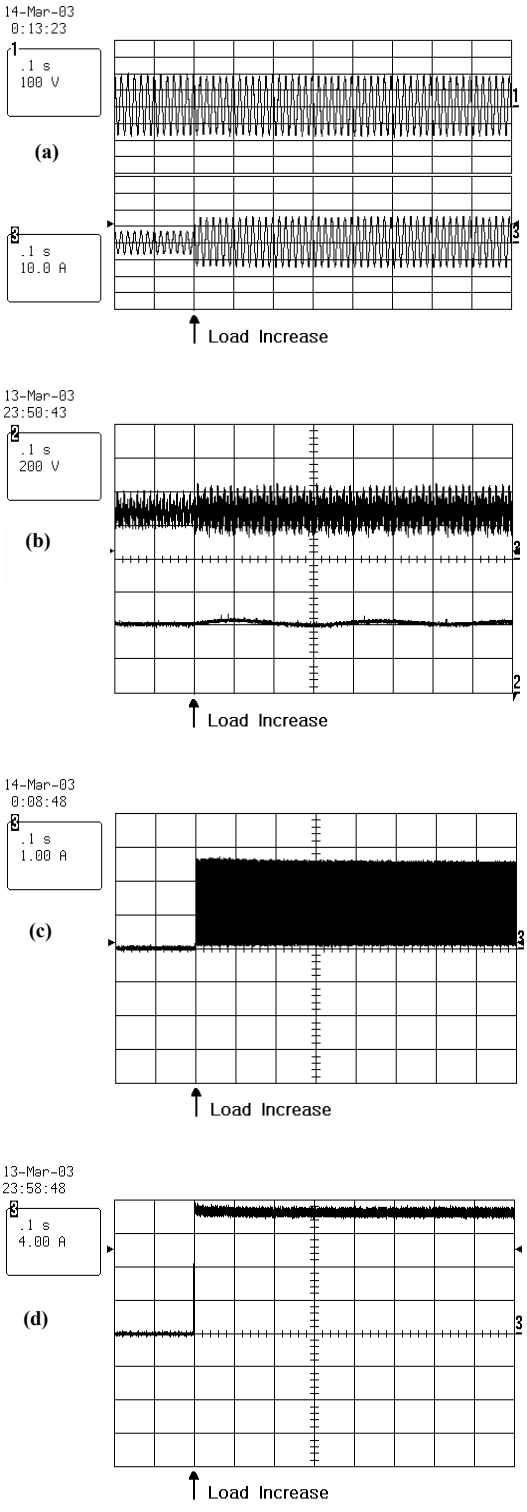

Fig. 13 Experimental waveforms (2KW→ 2.7KW), (a) output phase voltage and current (b) upper : output current of the front end converter ; lower: dc link voltage, (c) output current of the bi-directional converter, (d) battery current

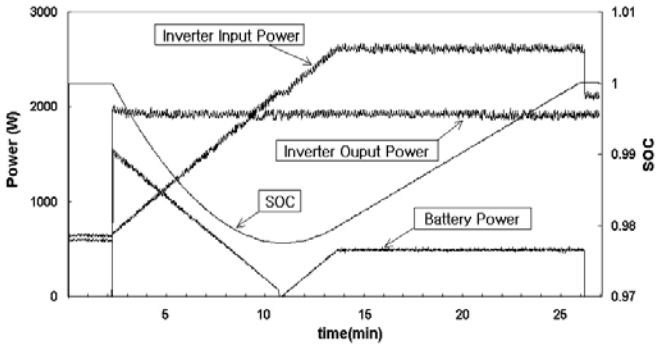

Fig. 14 SOC control for battery management

Fig. 15 Photograph of the SNUT fuel cell inverter

Table V. Experimental performance (no load to 4.4kW load)

Design Item	2003 FEC Specification performance	SNUT team Experimental performance
Frequency	60Hz ±0.1Hz	59.95Hz ~ 60.09Hz
THD (Output voltage harmonic)	5%	Lower than 1.94%
Regulation	±6%	-2.4% ~ +0.2%
Input current ripple	3%	Lower than 2.2%
Efficiency	Higher than 90%	Total 88% at 4.4kW load (DC-DC:90%, INV:97%)
Cost	$40/KW	$45.18/KW

5. CONCULSION

In this paper a 10kW power processing unit for 5KW SOFC-low voltage battery hybrid power generation has been proposed for the 2003 Future Energy Challenge Competition organized by U.S. Department of Energy and IEEE. The objective of the competition was to develop a fuel cell inverter with minimum requirement for cost of $40/KW and efficiency of 90%. Many practical issues such as component rating calculation, high frequency transformer design, heat sink design, and protection have been detailed. Battery management has been performed by a SOC control. The SNUT prototype inverter met the minimum target requirements and demonstrated a good performance in most of the design items.

REFERENCES

[1] R. Anahara, S. Yokokawa and M. Sakurai, "Present Status and Future Prospects for Fuel Cell Power Systems", Proceedings of the IEEE, March 1993, vol 81, no. 3, pp399-407

[2] M.W. Ellis, M.R. Von Spakovsky, D.J. Nelson, "Fuel cell systems: efficient, flexible energy conversion for the 21st century", Proceedings of the IEEE, vol. 39, no. 12, pp. 1808-1818,2001

[3] N. Azli, A. Yatim, "DSP-based Online Optimal PWM Multilevel Control for Fuel Cell Power Conditioning Systems", IEEE IECON 2001 conf. Rec., 29 Nov-2 Dec.2001, vol. 2, pp.921-926

[4] R. Gopinath, D. Kim, J. H. Hahn, M. Webster, J. Burghardt, S. Campbell, D. Becker, P. N. Enjeti, M. Yeary, J. Howze, "Development of a Low Cost Fuel Cell Inverter System with DSP Control", IEEE PESC 2002 Conf. Rec. , June 2002, vol. 1, pp. 309-314

[5] A. H. Anbuky and P. E. Pascoe, "VRLA Battery State-of-Charge Estimation in Telecommunication Power Systems", IEEE Trans. on Indus. Elec., vol. 47, no3, , pp. 565-573, 2000

[6] X. Wang and T. Stuart, "Charge Measurement Circuit for Electric Vehicle Batteries", IEEE Trans. on Aerospace and Electronic systems, vol. 38, no. 4, pp. 1201-1209, 2002

[7] K. Wang, C.Y. Lin, L. Zhu, D. Qu, F.C. Lee, J.S. Lai, "Bi-directional DC to DC Converters for Fuel Cell Systems",in Conf. Rec. 1998 IEEE Workshop on Power Electronics In Transportation, pp.47-51

[8] The 2003 International Future Energy Challenge Web Site; http://www.energychallenge.org/

[9] Texas Instruments, http://www.ti.com/

[10] Design application note MAGNETICS. INC.

[11] A. I. Pressman, Switching Power Supply Design.McGRAW-HILL INTERNATIONAL, 1999.

A Low-Cost Inverter for Domestic Fuel Cell Applications

T. P. Bohn
Department of Electrical and Computer Engineering
University of Wisconsin -Madison
Madison, WI 53706, USA
bohn@cae.wisc.edu

Dr. R.D. Lorenz
Department of Electrical and Computer Engineering
University of Wisconsin-Madison
Madison, WI 53706, USA
lorenz@engr.wisc.edu

Abstract – **The development of a low cost fuel cell inverter is described in this paper. The design is an optimized version of the successful unit built for the FEC2001 competition, based on an H-bridge/transformer/rectifier boost stage and a conventional dual ½ bridge output inverter stage. The 5kW DC input from the solid oxide fuel cell is boosted from 22vdc (@full load) to 400VDC where an additional 5kW of power from the 400VDC transient energy storage battery provides a maximum of 10kW to the inverter output stage (120/240vac split phase 60Hz). The UW-Madison team focused on using the fewest parts possible in the power processing path to keep the overall cost beneath the $400 target ($40/kW for 100,000 unit volumes). Planar magnetics, low inductance power planes in the 80kHz section, integrated power electronic modules, aggressive heatsink integration and a modular architecture resulted in a package that meets the target cost, is under 15 kg, and 30 liter volume. The control system is modular as well, decoupling the boost stage from the output inverter load transients by incorporating an observer on the output filter capacitor voltage to infer output current. The UW-Madison team finished in the top 5 of 12 participating teams.**

Keywords—**Fuel cell, Renewable Energy, Distributed Generation.**

I. Introduction

In the near future it is anticipated that smaller sized, distributed power generation resources will play a greater role in meeting total electrical power demand in the US. Fuel cells are a solid state energy conversion device that can use a renewable fuel (hydrogen) with no regulated emissions and can be located in the utility area of a home much like other conventional appliances. Developing technologies to drive down production cost barriers in the power conditioning electronics associated with fuel cells is critical in deploying these distributed resources.

II. The 2003 Future Energy Challenge

The 2003 International Future Energy Challenge involved 12 university teams from three countries. Sponsored by DOE, IEEE, DOD and other entities, these students have been challenged to design, build and test a 10kW fuel cell inverter for $40/kW, or $400 total production cost in 100,000 units per year volume. The $40/kW inverter target is based on the Solid State Energy Conversion Alliance(SECA) $400/kW fuel cell cost target.

The top 5 designs were selected and these prototypes were tested on a fuel cell simulator at the National Energy Technology Lab in Morgantown WV, May 19-22nd, 2003. It should be noted that the original goal was to test on an actual 5kW solid oxide fuel cell unit from Siemens-Fuel Cell Technologies Canada, but the unit was not available at the time of the competition so a back-up power supply based fuel cell simulator from MagnaPower/TAMU was used instead.

The UW-Madison FEC team is a multi-disciplined group of traditional engineering undergraduates (ME, ECE, CE, ChE, EMA, etc) as well as members from the School of Education, Journalism School and Political Science majors. Two electrical engineering master's students acted as team mentors to facilitate the weekly meetings and manage the progress of the project.

This paper describes the system architecture, circuit topology, energy management, interfaces, and design aspects of the inverter designed by the UW-Madison team. It uses new technology devices with a conventional topology based on detailed analysis to optimize component size, cost, and efficiency. Selection of topology, component sizing, and packaging issues are discussed as part of this optimization process.

III. Background

The estimated fuel-to-electrical conversion efficiency of fuel cells is about 50%. A system that recovers 35% more as heat energy, shown in Fig 1, can bring the system efficiency up to 85%. The FEC competition goal is to design and build the DC-to-AC 'power conditioner', or inverter, shown in this diagram. The system architecture is mainly governed by the performance and input/output specifications set forth in the IFEC competition guidelines. Taken from the 2003 FEC RFP, summarized in Table I.

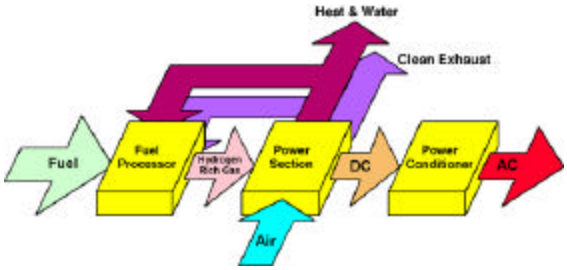

Fig. 1 Combined Heat and Power Residential Power Generation

Table I: FEC Inverter Specifications

Characteristic	Goal
Cost	$400 production cost; 100,000 volumes
Mass	< 30kg w/o SOFC or batteries
Volume	< 88.5 Liters
Input Power	5kW from SOFC, (5kW batteries)
Input Voltage	22-41vdc, 29v nominal
Input Current	275 amp max, <3% ripple
SOFC response	SOFC changes output at ~200 watt/min
Output Power	5kW cont, 10kW for 1 min. @ 0.7d.f.
Output	120/240 v_{rms} ±6%, 60 Hz ± 0.1 Hz.
Efficiency	Greater than 90% (5kW resistive load)
Communication	RS232/RS485- status and control info
Cooling	Air cooled
Ambient Temp	0-40 °C
Lifetime	16 years w/routine maintenance

The UWFEC team concluded that the $400 system cost was the primary constraint when comparing system architectures. The system with the fewest parts and acceptable performance will likely have the lowest cost. The first architecture considered was a simplistic 29vdc to 60Hz inverter with center tapped output transformer. The cost and mass of a 10kW low frequency transformer was unacceptable as well as lacking a means of adjusting output voltage independent of input limitations.

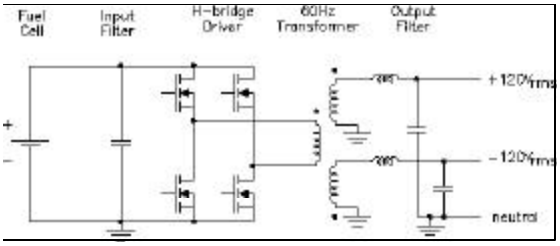

Fig 2 Simplistic H-Bridge Driven 60 Hz Transformer Topology

IV. Design Rationale

The inverter input specifications reflect the need for the DC/DC converter block to compensate for the Solid Oxide Fuel Cell (SOFC) as a poorly regulated power source. The V-I curve shown fig. 3 is taken from the 2003 FEC RFP. The Solid Oxide Fuel Cell considered for this competition also does partial fuel reformation and as a result has a very slow (200 watt/minute) power slew rate. The DC/DC converter block is responsible for tracking this power limit. As seen in fig 4 the transient energy storage element (384 vdc battery) is directly connected to the DC link to reduce parts count. The inverter block control system regulates output voltage by compensating for changes due to change in load, change in input power availability, and changes in DC link voltage from varying battery state of charge.

A.1 Boost Stage Topology Selection

The boost converter needs to track input power availability as well as transient energy storage battery state of charge (SOC). The maximum boost ratio (V_o/V_i) is 450/22, or 20X. Minimum boost ratio is 340/41, or 8.3X. This is a dynamic control range of ~240% min boost ratio.

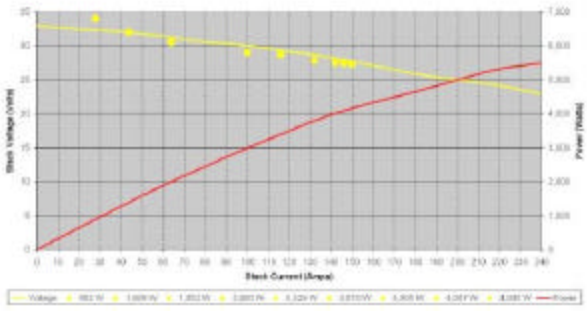

Fig 3 5kW Siemens/FTC Solid Oxide Fuel Cell Power Delivery

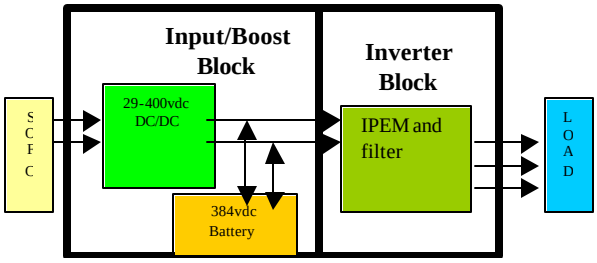

Fig 4 UWFEC Fuel Cell System Block Diagram

The topology selection process started with two classes of converters; isolated, and non-isolated. The simplest non-isolated topology is the flyback converter. This class of non-isolated converter was rejected for lack of sufficient boost ratio, high device stresses and lossy reset circuitry.

Looking at isolated topologies, a transformer based single ended forward converter, shown in fig 5, has a low component count, but high device stress.

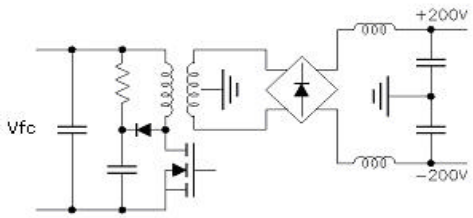

Fig 5 Single Switch isolated DC/DC Converter Topology

The current fed push-pull converter, shown in fig 6, is also a low part count, simple to implement topology. The main limitation comes at high power (5 kW in this case) where leakage inductance of the transformer is a problem unless soft switching is used. The limited available range of switch duty cycle also makes it difficult to track input voltage changes (29 vdc nominal, with ~±30% variation).

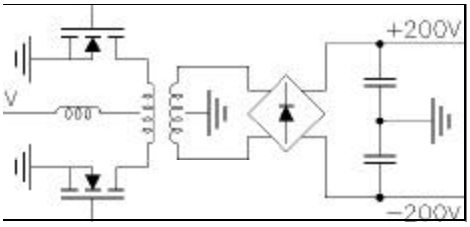

Fig 6 Current Fed Push-Pull Converter Topology

The full bridge topology, shown in fig 7, was chosen for the UWFEC team design because it offers the best distribution of switch stress, good controllability of duty cycle/boost ratio, and is a well known robust design that scales well to high power.

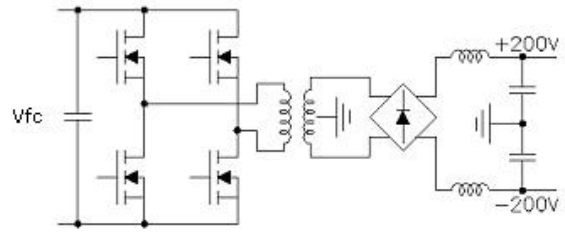

Fig 7 Full Bridge Converter Topology

One of the goals of the FEC competition is to introduce technologies that will reduce cost barriers in power conditioning electronics for fuel cells. A novel the three-phase DC/DC converter was considered. The converter described in a paper by DeDonker, Divan and Kheraluwala[1] has great appeal for reducing ripple current, dividing switch stress more evenly and reducing the filter components. The drawback is that it requires an active rectifier to maintain control of output voltage. A symmetric 3-phase transformer for such a converter is shown in Fig 8. The design is more novel than practical.

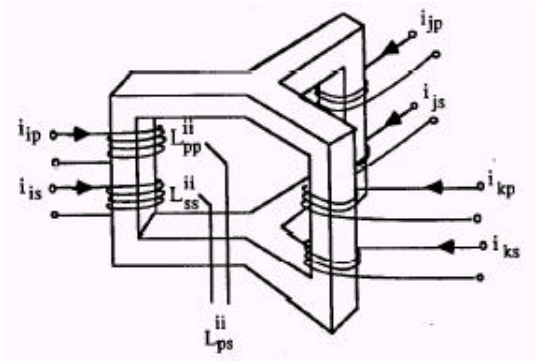

Fig 8 Symmetric 3 Phase Transformer for 3ϕ DC/DC Converter

The loss budget for the boost section is 300 W. Table II shows a comparison of switch power for each topology described above. The total switch power, rms switch current multiplied by peak switch voltage multiplied by the number of switches, is equivalent for all topologies.

Table II Topology vs Switch Requirement Comparison

Topology	$\#_{switch}$	Device Voltage	Device Current	Pwr per switch	Rqd R_{DS_on}
Forward	1	60v	275 A	16.5 kW	4.0 mΩ
Push-pull	2	60v	137 A	8.25kW	8.0 mΩ
H-Bridge	4	30v	137 A	4.11kW	4.0 mΩ

A.2 Boost Converter Switching Device Selection

The selection of devices available to populate the DC/DC converter is aided by the wide variety of MOSFETs designed for automotive applications. Table III compares various packages and devices. With new, low thermal impedance packages comes a new tradeoff; isolation built into the package vs lower performance associated with thermal/isolation pads and assembly cost.

Table III Power MOSFET Package Comparison

Part #	Package	V_{ds} Max	I_{ds} (A)	R_{Dson} mΩ	C_{iss} (nF)	R_{thJH} C/W
IRFP2907	TO247	75	209	4.5	1.3	0.56
IXFN280N085	SOT-227B	85	280	4.4	1.6	0.23
IXFN340N06	SOT-227B	60	340	3	1.68	0.23
FMM150-0075P	ISOi4PAC	75	150	4.7	1.2	0.51
VWM350-0075P	ECONO2	75	350	2.3	1.8	0.26

The TO-247 (or Super247) package gives the best performance-cost ratio. New materials and processes have greatly reduced the SOT227 package cost. Fig 9 shows the various MOSFET packages considered by the UWFEC team. The most basic is the non-isolated TO-247 package. Even though the IRFP2907 is rated at 209 amps, the package lead limit is 90 amps which typically means parallel devices are required. An isolation pad is also required which reduces the package thermal properties.

Fig 9 TO-247, ISOi4 (1/2 Bridge), SOT227, ECONO2 (6pack) Devices

The next step up in integration is the ISOi4 package from IXYS which is a low cost isolated ½ bridge module. These are both solder lead devices which requires a high current capacity circuit board. The SOT227 package uses mechanical fasteners that work well with formed/ laminated bus work (200 amp bus bar thickness limited by skin effect at high frequencies). A result of a new demand for low voltage 3 phase AC drives in forklift traction applications, IXYS packaged all 6 MOSFET devices in an isolated ECONO2 package (75v/350A). With cost as a main design constraint, the UW FEC team declined to use a device that costs 10 times a TO-247.

A.3 Boost Converter Rectifier Selection

The UWFEC fuel cell inverter schematic is shown below in fig. 10. The rectifier section of the boost converter is a full bridge to reduce the voltage rating of the diodes and lower voltage transformer secondary winding. The FEC cost analysis spreadsheet (Table V) indicates that it costs less to

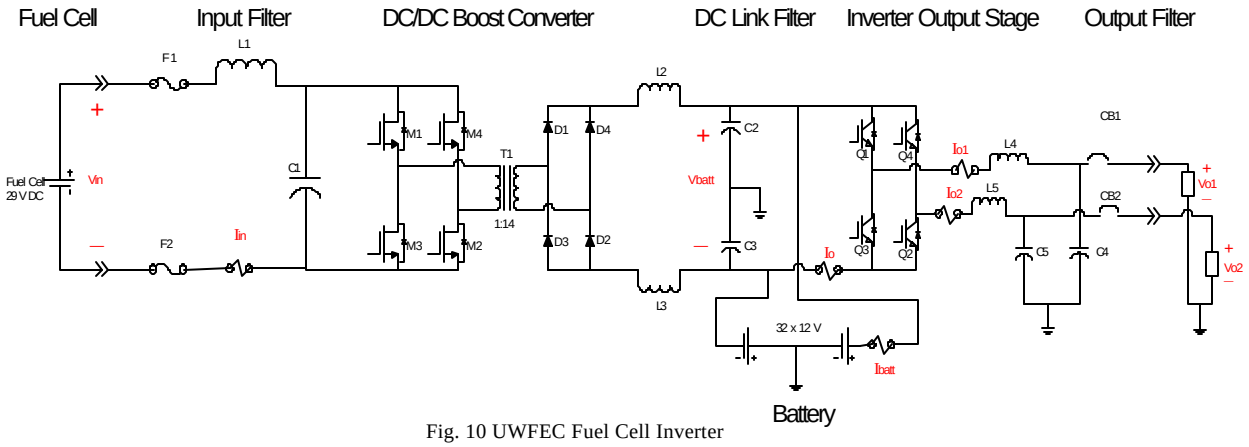

Fig. 10 UWFEC Fuel Cell Inverter

use a full bridge rectifier reduce ripple, and as a result, reduce filter size/cost than to use only 2 diodes in a ½ bridge configuration.

Table IV Comparison of Candidate Rectifiers

Config.	**Part #**	**Pkg**	**I_{favm} (A)**	**V_{rrm}(V)**	**t_{rr}(ns)**
Single	30EPH06	TO-247	30	600	40
	DSEI120-06A	TO-247	60	600	40
	DSEI60-10A	TO-247	60	1000	35
	DSEI60-12A	TO-247	52	1200	40
1/2 Bridge	DSEP 2x35-06C	SOT-227B	2 x 35	600	20
H-Bridge	VBE26-06NO7	Eco-pac	44	600	35
	VBE55-12NO7	Eco-pac	59	1200	40
	VBE55-06NO7	Eco-pac	68	600	35

Like the MOSFET package comparison, table IV shows ratings of several rectifier candidates. The total rectifier cost is about the same for discrete vs modular when assembly costs and thermal performance issues are considered. Since this is a high frequency design, an IXYS fast recovery epitaxial diode VBE55-12N07 (1200v/44A) was selected in the Eco-pac bridge module. The Eco-pac is a low cost isolated package molded onto metalized alumina. Low diode reverse recovery time (T_{rr}) is important for reducing switching losses in high frequency power converters. Unlike an ideal diode, the stored charge in a real diode needs to be dissipated before current stops flowing after it is reverse biased.

A.4 Inverter Output Stage Topology and Devices

The split DC bus and dual ½ bridge switches shown in the schematic, fig. 10, is one of two inverter stage topologies investigated by the UWFEC team. The output specification of the FEC inverter is rated for full imbalance (5kW on one phase, 0kW on the other). The DC bus capacitors need to be rated to handle full load current since they are the neutral return path for this configuration.

The other alternative investigated is a 2-leg/3-wire topology. This requires a 3d ½-bridge that provides a 'virtual neutral' which allows the DC link capacitors to be sized in terms of energy storage instead of current capability. A very simple control scheme consisting of a fixed duty cycle was used to generate this virtual neutral. This trades silicon for capacitor cost. Since the goal is to have a 16 year product service life this is a fair trade.

Inverter control, thermal and packaging considerations were heavily weighted when an integrated power module was chosen for the inverter output stage switching device. More detail is provided in those respective sections of this paper. The International Rectifier IPPIM50P12B004 'iNTERO' module (1200v/100A @20ºC) was selected because it is rated to provide the entire output while incorporating all the necessary controls/sensors in an ECONO2 footprint. At maximum load (10 kW, 240 V_{rms}, 0.8 pf), the inverter devices require 57 A_{rms} current capability and 400 V blocking.

B.1 Input Filter

In order to minimize filter component cost a tradeoff analysis was performed between increased heatsink cost and reduced filter component size/cost with respect to switching frequency. The boost converter switching frequency (80 kHz) was chosen to optimize the planar technology boost transformer performance while keeping H-bridge MOSFET device switching loss reasonable.

The FEC 2001 cost analysis spreadsheet had an error in the data points used to calculate inductor cost (a $40 offset). Once that was corrected, the assessed cost of the input filter inductor (L_1) dropped to $6 for the 200amp, .46µH part. Fig 11 shows a Solidworks model of the assembled converter, the input bus bars are on the left. Micrometals was able to source the .46 µH input inductor as a split-core bus inductor, $0.96 in 100,000 unit volumes. The inductor is sized to limit input current ripple due to the 80 kHz component <3%, or 6 amps. The 120Hz component is eliminated via input current control in the boost converter feedback loop.

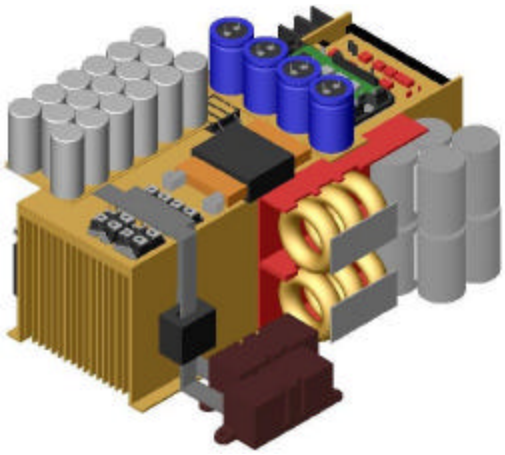

Fig 11 Solidworks Model of Assembled UWFEC Prototype

The higher boost stage switching frequency (80kHz) significantly reduced the size and cost of the input inductor, but caused problems with leakage inductance on input capacitor (C_1-Fig. 12). The problem was solved by using parallel conductor planes and axial lead metalized polypropylene capacitors. The inductive loop of the leads was minimized by crossing the top end lead of the capacitor through the conductive plane of the bottom lead. The stray inductance was reduced by a factor of 10. A hybrid combination of electrolytic and polystyrene capacitors is a lower cost solution for the 450μF value.

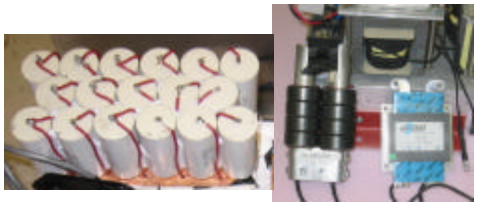

Fig 12 Input Capacitor Bank and Various High Frequency Transformers

B.2 High Frequency Transformer

Fig. 12 shows three low cost high frequency transformers; E-core (left), Coaxial wound (center), and planar (right). The E-core transformer needs to be wound with Litz wire for the rated currents and 80 kHz operation (skin effect), which increases unit production cost.

The coaxially wound transformer is elegantly simple; conventional ferrite torroidal cores slide over a copper tube (primary turn), with the secondary Litz wire passed through the center. The coaxial construction couples all the primary flux the secondary. This example is a 5kW design, but not available as a production part.

The planar transformer could be built into the layers of the circuit board itself for reduced cost. The problem is that the PC board needs to carry 275 amps on the primary side- not cost effective. Payton Planar was able to quote a production price of $18 (100k volumes) for the 5kW (1:22) used in the UWFEC prototype. The primary side leads are made of laminated copper foil to maximize conduction with the limits of skin effect. The transformer has a calculated loss of 20 W at full load.

B.3 Intermediate DC-Link Filter

The two 100 μH, 25 A inductors between the rectifier and the batteries completed the boost design. The same planar technology from the transformer can also reduce the cost of this inductor, $9 each, for 100k quantities. The UWFEC prototype used student made Litz wire wound torroidal inductors due to lead time for the planar parts.

The DC link capacitors (C_2, C_3) protect the transient energy storage batteries by providing a lower impedance path for the ripple current (switching di/dt). The capacitors chosen were Cornell Dubilier type 330, 470 μF capacitors with an ESR of 85 mΩ. In this case two capacitors had to be paralleled across each bus handle the switching frequency ripple current.

B.4 Output Filter

The output filter needs to be large enough to passively filter the inverter PWM voltage ripple and small enough to allow the controller to regulate the output voltage under closed loop feedback conditions. The LC filter (L_4/C_4, L_5/C_5) is made of a wound torroid inductor and metalized polypropylene capacitors (100 μH and 80 μF). The peak output current was calculated to be 80 A. Three parallel inductors were used to distribute the heat load (air cooled). The lowest cost approach is powdered iron torroidal inductors since planar types are not appropriate here.

C. Transient Energy Storage (Batteries vs Capacitors)

The sluggish response of the fuel cell to load changes means that an additional energy buffer is needed to handle load transients typical of unpredictable residential use patterns. This buffer cannot reasonably be applied directly across the terminals of the fuel cell since the power drawn from the SOFC needs to be precisely regulated to prevent damage to the SOFC.

Ultracapacitors have great appeal as a long life, low maintenance transient energy source. The specifications given in table I show that the transient energy required is 5kW (plus losses) for up to 1 minute, or 83 watt-hrs ($3*10^6$ Joules). The energy stored in a capacitor is given by $W=1/2*C*V^2$. If the nominal loaded to unloaded voltage of the SOFC was used (41v-29v=12v) without losses that would require a $4.2*10^3$ Farad capacitor.

As stated in the previous paragraph, fuel cell current needs to be stringently regulated, precluding direct connection of the ultracapacitor to the SOFC without power conditioning. A 5kW bi-directional power conditioner is needed, about the same cost as the 29v/400vdc boost stage (about 30%). Even though the transient energy storage system is not part of the system cost, the extra circuit is.

A bi-directional converter would allow a higher voltage capacitor, reducing the capacitor size. A lower cost solution, typically used in UPS systems is lead acid batteries. A low voltage (48v/100 ahr) telecom rated sealed lead acid battery was offered as the standard solution at the

NETL/FEC test site in May 2003. This consisted of 4 modules, 12v each. The low number of batteries made pack equalization easier, but required large bus currents at 5kW (5000w/48v=104A). This approach also requires a 5kW bi-directional DC/DC converter.

Fig 13 10kW UPS Battery Pack Built by APC; use by UWFEC Team

Fig 13 shows the UPS battery pack used by the UWFEC team. Built by APC, it consists of 32 series connected (12v/7ahr) units. At a nominal voltage of 384v, current draw at 5 kW is only 13A. The rate of discharge is a very important figure of merit when sizing batteries for periodic discharge applications (i.e. 1 minute rate vs 20 hr rate typically given on data sheets- < 2C in this case).

One of the requirements of the FEC competition was a comparison of energy storage system approaches, and in particular a differential cost comparison based on the 48v solution. Dr. E. Landsman at APC was consulted for a UPS industry perspective. His opinion is that all systems over 3 kW are high side connected (384v vs 48v). A similar inquiry was made to battery industry experts. Kenneth James, CEO of Sunbelt Battery, generated high volume (100k unit) cost estimates of the price per energy of the top 5 UPS/telecom battery manufacturers. The price per energy ratio was the same for 4 large modules (48v/100ahr) as 32 smaller modules (384v/7A hr). The difference being shipping costs and packaging, which varied by supplier. The big difference in system price comes down to the cost of the 5kW bi-directional power conditioning circuit. System losses relative to this converter must also be considered since the processed energy must pass through this converter twice before being delivered to the load.

Similar to UPS industry standard practice, the UWFEC team connected the transient energy batteries directly to the split dc bus, as shown in fig 10. This required no extra components, allows the input DC/DC converter to manage battery state of charge while regulating power flow from the SOFT. The Powersonic PS-1282L 12v/8ahr batteries have an ESR of 20 mΩ, or 1.4Ω total resistance, plus conductor and fuse series resistance. The 120 Hz load current ripple seen by the DC bus is sourced by the lowest impedance path, the bus capacitors, directly connected to the output switching devices. This stresses the capacitors more but shields the batteries from the current ripple.

D. Circuit Protection and Auxiliary Power Supply

As seen in fig 10-11, the 200 amp input leads are protected by a set of 200A Littelfuse MEGA series fuses that also serve as input terminals for connection to the SOFC leads. The DC link is fused at both sources (inverter side and in the battery pack), with 10A fuses. This is less than the peak current (1 minute) rating since the I^2t curve shows the time to clear is not reasonable for a higher rating. The AC output leads to the load are protected by a 40A circuit breaker on each leg, residential grade units.

A 300W auxiliary power supply for logic and startup of the SOFC is part of the FEC specification. The simplest approach is a flyback converter connected to the DC bus (400v/48v). The battery pack has a soft start resistor to bring up the DC bus slowly. The 48v aux power supply automatically cuts in at 300vdc and powers up controls. A Vicor backup was used when the student version failed.

E. Heatsink and Packaging

As seen in the FEC cost analysis breakdown, Table V, packaging and control components are assessed at 26% of the total design or $100 of the $400 limit. The UWFEC design is optimized for cost with acceptable performance. Fig 14 shows a Solidworks exploded view of the inverter assembly. The heatsink is used as the mechanical support structure rather than the enclosure. There are no power PC boards used, only solid copper bus bars on the input. Due to skin depth at 80 kHz, 3" long laminated conductors are used in that part of the boost converter (MOSFET-to-transformer, C_1-to-MOSFET). The inverter stage is based on the iNTERO module that already includes interconnects and embedded sensors.

Fig 14 Solidworks Exploded View of UWFEC Inverter Assembly

Several heatsink fabrication styles were examined; extruded, bonded fin, folded fin, pin fin, and carbon foam. The extruded type had the best cost advantage, but not best thermal performance. Extruded heatsinks are limited to a 10:1 fin length to opening ratio. The bonded fin style heatsink had the best compromise of cost, performance, mechanical strength and ability to use only one 5" blower to extract the necessary heat load. The thermal coefficient is 0.06C/W. A Microchip TC642 adjustable speed fan control chip was used to conserve parasitic load on the auxiliary power system by reducing fan speed proportionally with temperature (<$1.00). Fig 15 shows the thermal simulation of heat loads on the heatsink.

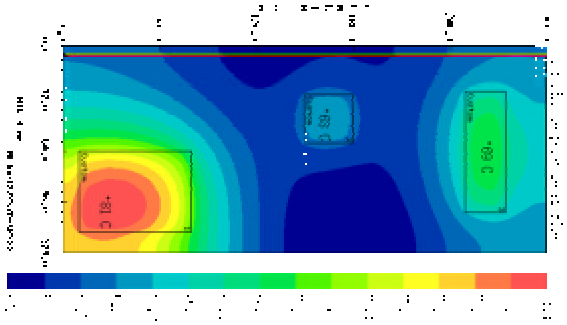

Fig 15 Thermal Simulation of UWFEC Heatsink Assembly

Fig 16 shows the finished UWFEC prototype. Except for fuses, circuit breakers and I/O connectors, all components are mounted on the heatsink assembly. The finished

Fig 16 Finished UWFEC 10kW SOFC Inverter Prototype

dimensions are 33cm x 33cm x 24cm; 15kg. Low volume package allowed for a simple 'double-C' shaped enclosure made of two folds of symmetric metal pieces.

F. Communication and Controls

The SOFC has its own control system that communicates with the FEC fuel cell inverter via an RS485 serial link. Power demand, power availability and system status information are exchanged. The UWFEC modular design uses the I.R. iNTERO module as the basis for both boost and inverter blocks. Each block runs its own closed loop regulation software and decouples disturbances from other blocks. As such the iNTERO module built in RS485 port (as well as CAN bus) exchange information with the SOFC and other controls.

Shown in fig 17, the iNTERO module contains both control and power processing functions. A TI 320F2406 40 Mips DSP, along with gate drive and sensors are integrated into a single power module, ECONO2 sized.

Fig 17 iNTERO Integrated Power Module

F.1 DC/DC Converter Control

The DC/DC converter is also based on the iNTERO module, but a 200 amp version was not available in 2003 so hybrid was created using SOT227 MOSFETs and external sensors, tied to the sensor/ gate leads.

Switching frequency current is passively filtered and the dc/dc controller actively decouples the 120 Hz current generated by the load. Fig. 18 shows the control block diagram. It generates an output current command, I_o^* then multiplies I_o by the bus voltage to yield P_o, the requested power. This provides a bus-voltage independent gain term.

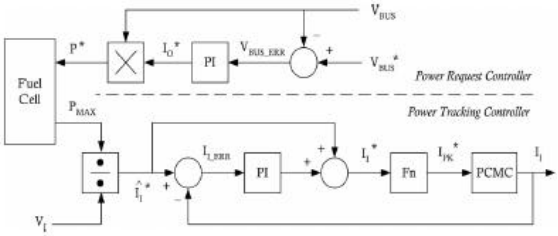

Fig 18 DC/DC Converter Control Block Diagram

The power tracking controller accurately regulates average current drawn from the fuel cell via ramp-compensated, peak-switch-current turn-off, clocked turn-on Peak Current Mode Control (PCMC).

F.2 Inverter Control

An observer-based single-phase-inverter controller is used in the UWFEC design for higher performance and requires no current sensors, shown in fig 19. Bus voltage decoupling was further developed to include decoupling of voltage imbalance between the two halves of the DC bus.

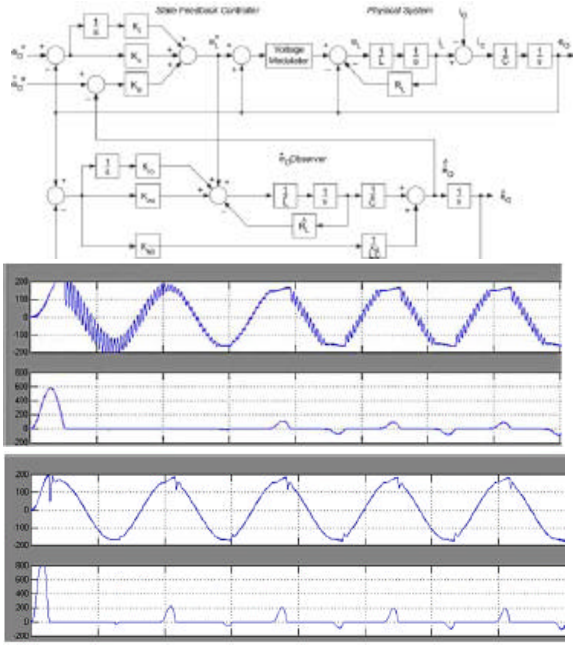

Fig 19 Observer Based Inverter Block Diagram, Open Loop/Closed Loop

Table V Cost Analysis Spreadsheet for UWFEC Prototype

2003 FUTURE ENERGY CHALLENGE

19-May-03	UW-Madison												
DEVICE	QTY	DESIG	UNIT	MEASURE	VOLT (Vpk)	VOLT (Vrms)	CUR (Avg)	CUR (Arms)	UNIT COST	EXTENDED COST	Cost %		
DIODE	4	D1 to D4			1200		13		3.47	13.89	3.874%	Silicon	36.295%
IGBT	4	Q1 to Q4			450		42		7.59	30.35	8.465%		
MOSFET - SINGLE MOD	4	M1 to M4			50		100		21.47	85.90	23.956%		
CAP (FILM)	1	C1	470	uF	50				6.03	6.03	1.681%	Capacitors	12.870%
CAP (ALUM)	2	C2, C3	500	uF	450				14.12	28.24	7.876%		
CAP (FILM)	2	C4, C5	40	uF	170				5.94	11.88	3.313%		
CHOKE	1	L1	0.46	UH				200	6.10	6.10	1.702%	Inductors	14.653%
CHOKE	2	L2, L3	93	UH				13	5.93	11.87	3.310%		
CHOKE	2	L4, L5	110	UH				42	17.28	34.57	9.641%		
TRANSFORMER	1	T1				25		200	11.77	11.77	3.283%	Xformer	3.283%
LOSSES			300	W					25.00	25.00	6.972%		
CONTROL										53.12	14.815%	Pkg+Ctrl	25.926%
PACKAGING										39.84	11.111%		
OTHER (EXPLAIN)													
TOTAL										358.57	100.000%		

Actual Components Used in UW Prototype

Part	Quantity	Description	Rating	Package style	Part Number	MFG	Unit Cost(100k
M1-M4	4	MOSFET 1/2 bridge switches	280Amp/85Volt	SOT227	IXFN280NO85	IXYS	$9.50
D1-D4	1	FRED Rectifier Bridge	1200Volt/19Amp	ISOPLUS227	VB17-12N07	IXYS	$4.50
Q1-Q4	1	Inverter Intero IPEM w/ DSP Control Card	1200Volt/50Amp	ECONO2	PIIPM50P12B004	IR	less than $100
C1	17	Input Metal Film Capacitor Bank (parallel 17 * 30uF)	100Volt/6.5Amp	Axial Lead	935W1K30	CDE	$6.00
C2,C3	4	Electrolytic Capacitor (parallel)	450Volt/450uF	Can Type		EC	$10.00
C4,C5	8	Input Metal Film Capacitor Bank (parallel 4 * 10uF)	400Volt/6.5Amp	Axial Lead	935W4K10	CDE	$4.00
L1	3	Input Bus Bar Inductor (3 in parallel)	200Amp/.14uH	C-Core	HS300-26C	MicroM	$0.32
L2,L3	2	DC Link Inductor	14Amp/150uH	Planar	50817	Payton	$9.00
L4,L5	2	Output Filter Torroid	42Amp/110uH	Torroid		SCHOTT	
T1	1	22:1 boost/isolation transformer	200Amp/25Volt	Planar	50797	Payton	$18.00
H1	1	Bonded Fin Heatsink	5" * 5" * 14	Cold Plate		Aavid	$35.00
AUX1	1	DC-DC converter 300:15 Volt	300Volt/150Watt	Gen2		Vicor	$20.00

Handling nonlinear loads was the most challenging inverter control issue. Loads such as diode-bridge rectifiers used in computers and most other household electronics draw large current spikes that excite a resonance in the inverter output filter. Matlab/Simulink simulation results shown in Fig. 19 show the performance of the inverter with open and closed loop control. The load used for this simulation was a 3 kW diode bridge rectifier, equivalent to 20 computer power supplies (CPS) in parallel. While this is an unrealistically difficult load, the voltage THD was still under the required value of 5% given in the specifications shown in Table I.

V. Cost Analysis

Production cost is the core challenge in meeting the specifications for the FEC competition. To assist in the analysis, teams were given the spreadsheet shown in Table V. The UWFEC design met the cost point by using high frequency magnetics, aggressive modular packaging, and integrated controls.

VI. Conclusions

Cost is the toughest design constraint for the FEC competition. UW students used synergies in packaging, controls and careful analysis of peak vs rms loading to optimize the design of their 10 kW SOFC inverter prototype. This paper presented the system architecture, circuit topology, energy management, interfaces, and control aspects of their design.

[1] "Three-Phase Soft-Switched High Power Density DC-DC Converter for High Power Applications"; R.W. De Donker, D.M. Divan, M.H. Kheraluwala WEMPEC research report #88-26, June 1988

[2] Phillip T. Krein, *Elements of Power Electronics*, Oxford University Press, Inc., 1998.